Master's Thesis Internship

Master Water Science and Management

Assessment of P retention dynamics in tile drainage upon exfiltration of nutrient-rich groundwater in a marine clay polder

Erica Caverzam Barbosa
Student number: 5831555

University and Internship supervisor:
Prof. dr. Jasper Griffioen

10th July, 2018

Summary

The majority of the studies on phosphorus (P) immobilization in lowland catchments focus on the final mechanisms and pathway of phosphorus retention in surface water bodies, with little or no attention given to tile drainage and, mostly, regardless the effects of the landscape heterogeneity and the geochemical processes associated to it. Based on that, the aim of this research was to assess the P retention in the drains of a marine clay polder dominated by agricultural practices, by taking into account the heterogeneity of the surroundings. To do so, several components of the soil and water system of the study area were collected and analyzed for the main elements, including sequential chemical extraction procedures for iron (Fe) and P speciation of the sediment samples. Drain and ditch particulate material were also collected and analyzed in the same form. Furthermore, a temporal data set for drain and ditch water was obtained for a period of approximately 5 months. The second part of this research consisted of geochemical modeling based on the fieldwork data in order to get a better insight into the potential degree of P immobilization in the drains. The main findings of this study are as follow.

The triweekly water sampling showed that Fe and phosphate (PO_4) concentrations were not only detectable but sometimes high in the drains, which can be attributed to the unfinished Fe oxidation as a result of the short residence time of drain water. Furthermore, Fe and PO_4 concentrations seemed to follow a large scale spatial pattern, mainly governed by the exfiltrating groundwater. Phosphate leaching from the surface as, i.e., manure application, seemed to be of minor importance during the research period. Nevertheless, concentrations in the drains were sometimes larger than those found in groundwater and showed large spatial variability. Such discrepancies may be ascribed to the heterogeneity of the parcel area and the subsequent geochemical transformations occurring in the shallow subsurface (i.e. pyrite oxidation), which are likely to be responsible for additional mobilization of Fe and PO_4 to the drains. Iron and phosphate concentrations also showed an inverse correlation with discharge and temperature, suggesting a possible effect of seasonality. However, these correlations were weak, indicating that temporal trends in drain water composition may be overshadowed by the large spatial variability resulting from the heterogeneity of the parcel and tillage practices.

The sediment analysis pointed out that the ditch and drains particulate material holds nearly 20 to 80 times more phosphorus than in the geological sediment throughout the soil domain. The average P content in the drains sediments was 22.6 mg/g, being higher than the references found in literature for suspended particulate matter (SPM). From this particulate P (PP) content, nearly 81% was P bound to ferric iron particles (Fe-P) in the ditch, and more than 95% was Fe-P in the drains sediments. The Fe-P fraction was also the prevailing form among the PP found in the shallow soil samples. The calcium-bound P (Ca-P) fraction was of minor importance in the P sequestered for both drains and ditch sediment material, presumably due to the small extent of CO_2 degassing in the water samples analyzed.

Last but not least, the outcome from the geochemical modeling reinforced the hypothesis that, although groundwater exfiltration is responsible for the large-scale distribution of P and Fe in the drains, the geochemical processes occurring in the shallow subsurface are likely to exert major influence in individual drain water composition. Besides, the results revealed that P could be completely immobilized in nearly all the drains analyzed, for the two most extreme conditions, when the highest and lowest P and Fe were found in solution. Opposite to the drains, the aeration of the groundwater samples resulted in incomplete immobilization of phosphate for both the simulation scenarios, which is attributable to the excess of PO_4 in the groundwater exfiltrating in the parcel. In this sense, even though the potential of P immobilization in the drains is significantly high, the complete phosphate retention in the ditch – which has a larger contribution of exfiltrating groundwater – is unlikely to occur. As such, this research highlights the importance of subsurface tile drainage networks as a major sink of P in lowland catchments. Lastly, the results of the modelling simulations also showed that, thermodynamically, Fe hydroxyphosphate is preferably formed upon the oxidation of Fe(II) in presence of PO_4 instead of Fe oxyhydroxides, which is in accordance with the findings of Van der Grift et al. (2016b).

Table of Contents

1. Introduction

1.1. Phosphorus as a nutrient and pollutant

Phosphorus (P) is a macronutrient essential to all forms of life. Together with nitrogen (N) and water, P tends to be the dominant yield-limiting factors for agricultural crop growth (Merrington et al., 2002) and, thereafter, global food production is dependent on the constant input of phosphorus. Currently, P is mainly extracted from phosphate rock, which is a non-renewable source (Neset & Cordell, 2011). Predictions regarding phosphate rock depletion are extremely contrasting due to the uncertainties involving demand and resource base estimates (Van Vuuren et al., 2010), and may vary from 50-100 years (Cordell, 2010) to beyond the 23rd century (Koppelaar & Weikard, 2013). Despite its benefits, the over-enrichment of P (and N) in water bodies induces the occurrence of the eutrophication phenomena, which leads to oxygen depletion and ultimately the death of aquatic biota (Carpenter, 2008).

In the Netherlands, the concentration of P in soils and surface waters is high, compromising the water quality status of the regional water bodies and posing a risk of eutrophication (Schoumans & Chardon, 2015; Van Grinsven et al., 2016; Van Puijenbroek et al., 2014). Agriculture, which comprises 60% of the total surface area of the country, is pointed out as the major source, as discharges from industry and WWTP have decreased from the 1980's (Oenema et al., 2005). In the past three decades, however, Dutch policies aiming to reduce losses of N and P from agriculture were established. These policies include the implementation of common directives instigated by the European Commission such as the Water Framework Directive (WFD). The WFD requires essentially that all EU Member States achieve 'good' ecological and chemical status of all regional surface water bodies (Van Grinsven et al., 2016). As a result of the environmental legislation, the total consumption of phosphate fertilizer has decreased by 85% since 1990, reducing the phosphate surpluses (Van Grinsven et al., 2016).

The present context reveals a conflict: whilst researchers recommend the need for more strict regulations over the use of P in agriculture-dominated areas in order to achieve the targets of the WFD (Van Grinsven et al., 2016; Ligtvoet et al., 2008), the farmers claim that the use of more fertilizers is essential for the cost-benefit of the productivity, and risk avoidance seems to be the decisive factor for pursuing soil P status above the agronomical optimal range (Reijneveld & Oenema, 2012). Currently, however, it is unclear to what extent the current P loads of water bodies in agricultural areas are attributable to present day farming practices (Baken, 2015) and the precise role of agriculture in eutrophication still remains poorly understood (Withers & Haygarth, 2007) and sometimes overestimated (Withers et al., 2014).

The proper assessment of the contribution of agriculture in the P loads to surface water is indispensable for the establishment of effective mitigation practices. In order to address this issue, it is necessary to understand the mechanisms involved in the mobilization and transport of P in soils and aquatic system. In the Netherlands, the past fertilization loads have lead to large areas in agricultural lands with P-saturated soil (Schoumans & Chardon, 2015). Despite the decrease in the national P surplus, P still accumulates in the soil (Smit et al., 2015), due to the strong adsorption capacity of P to soil and sediment particles (Merrington et al., 2002). These legacy stores of P can provide a continuous long-term supply of phosphorus into groundwater through leakage (Withers et al., 2014), which ultimately may end up in surface water through subsurface groundwater flow (Baken et al., 2015b). However, only a small fraction of the phosphorus accumulated in the soil or the P load applied annually to the soil leaches to surface water (Van der Grift, 2017). In flat lowland catchments with shallow groundwater table, as in most of the Dutch polders, P loads to surface waters mostly occur via subsurface flow through groundwater (Schoumans and Groenendijk, 2000 cited in Van der Grift et al., 2018). Additionally, phosphate concentrations in groundwater in the coastal area of the Netherlands may be particularly high, due to the extensive degradation of subterranean organic matter (OM) (Griffioen, 2006). This is presumably the main reason for inorganic P concentrations in deep groundwater (>13 m) where it is assumed that, due to the high phosphate sorption capacity of the overlying soil, P at those depths is not influenced by agricultural practices (Schoumans & Chardon, 2015). The highest ortho-P concentrations in deep groundwater are found in the west of the country (Schoumans & Chardon, 2015), which is covered by marine sediments, with higher pyrite, OM and Ca-carbonate contents (Griffioen et al., 2013).

1.2. Phosphorus retention

During the transport in the drainage system and surface waters, phosphorus is subject to various processes of transformation or removal from the water system (De Klein, 2008; Nguyen & Sukias, 2002), which can affect P speciation and consequent mobilization and bioavailability (see Figure 1.1). Among these processes, the interactions between iron (Fe) and P at the surface-groundwater interface upon the exfiltration of Fe-rich anoxic groundwater is known to be a major mechanism controlling the mobilization of P in natural environments (Baken, 2015). In a simplified way, when Fe-rich anoxic groundwater exfiltrates, strong redox and pH gradients in the interface surface-groundwater are created (Dahm et al., 1998) and, as a result, Fe^{2+} is oxidized and Fe^{3+} precipitates (Baken et al., 2013). If phosphate (PO_4) – originating either from leaching or from the decomposition of OM in the subsoil – is present during the oxidation of Fe^{2+}, the exfiltration of groundwater is expected to be followed by the immobilization of aqueous PO_4 as a result of its association with Fe precipitates (Griffioen, 1994). Accordingly, the transfer of PO_4 from groundwater to surface water will not be necessarily conservative and phosphate concentrations in surface water are expected to be much lower than in groundwater (Baken et al., 2015a). The resulting particulate Fe-P form has limited bioavailability if compared to dissolved PO_4 or P bound to degradable OM, and the effect of P loads on the ecological status of water bodies is expected to be reduced in the occurrence of exfiltration of Fe-bearing groundwater. In this sense, the Fe-P interactions resultant of redox transformations of iron strongly influence not only the mobility of P but also its bioavailability, alleviating the environmental risk with P in receiving systems (Baken, 2015).

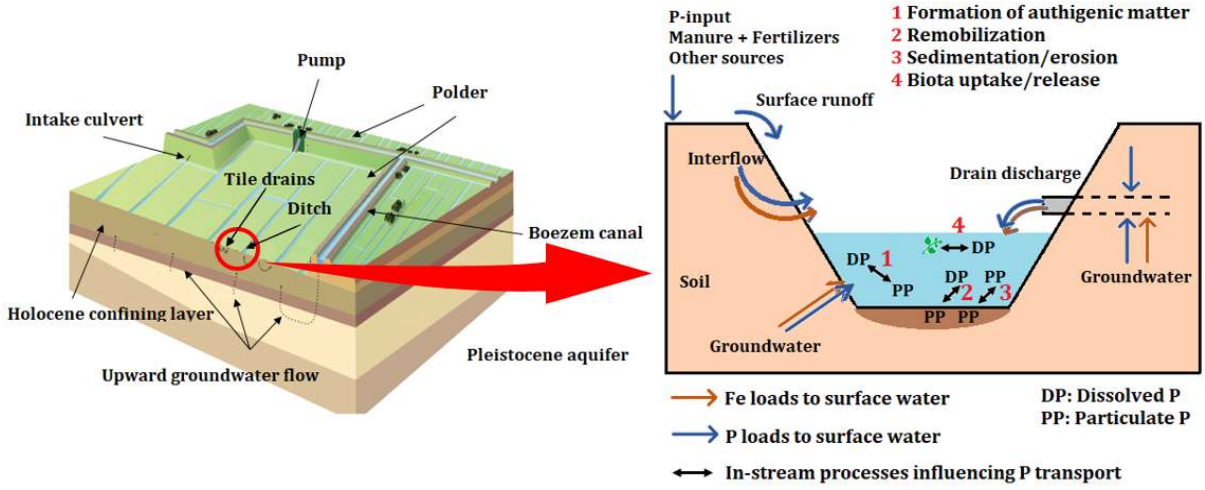

Figure 1.1: Left: Schematic overview of a polder-boezem system. Adapted from Delsman, 2015. Right: Main processes controlling P retention in ditches and streams in lowland catchments fed by groundwater. Adapted from Van der Grift, 2017.

These Fe-P interactions are more evident in lowlands deltaic areas, such as the Dutch polders, where both flow aspects and groundwater composition provide suitable conditions for the occurrence of this process. The low elevation areas of the polders lead to hydraulic gradients that ensure the upward flow of groundwater, and consequent exfiltration to the surface water, which occurs mainly by the subsurface flow drains and ditches (Delsman, 2015). Additionally, the groundwater in these areas, especially in the western part of the country, is mostly anoxic, rich in Fe and PO_4 (Griffioen et al., 2013).

Besides the immobilization of aqueous P by Fe precipitates, P loading to the regional water bodies also depends on the retention capacity of this drainage network (Reddy et al., 1999). Loads of P from agricultural sources in polder areas need to be transported through several drains, ditches, and channels before it can actually affect the water quality of downstream regional surface water bodies (see Figure 1.1). This dense drainage network buffers flow velocities in polder catchments, increasing storage capacity and residence time of surface water, suggesting that, aside from the chemical immobilization, polders have

enhanced potential for P retention and can be considered to attenuate P export loads from agriculture. In this sense, the combination of Fe-bearing groundwater and the limited water flow in polder areas reduces the environmental risk of eutrophication due to P loads from agricultural practices (Van der Grift, 2017).

1.3. Previous researches

Recently published, the study of Van der Grift et al. (2014) investigated how the transformation processes upon exfiltration of Fe(II)-bearing anoxic groundwater affect the immobilization of dissolved phosphorus in a lowland catchment in the Eastern of the Netherlands. This region is located in the Pleistocene part of the country, where groundwater is usually rich in Fe and low in nutrients as PO_4 (Griffioen et al., 2013). Similarly, Baken et al. (2015a) studied the immobilization of P upon exfiltration of Fe-rich groundwater in two lowland catchments in Belgium. In both studies, P was rapidly and almost totally immobilized upon exfiltration of Fe-rich anoxic groundwater and P is depleted before Fe(II) is completely depleted. Previously to that, Griffioen (2006) also studied the extent of immobilization of phosphate upon experimental aeration of groundwater from the Western Netherlands, which is naturally nutrient-rich. His results demonstrated that uptake of PO_4 by Ca phosphates and/or carbonates may play an additional role in PO_4 immobilization in lowland catchments. Despite the significant contribution of these researches to the knowledge of P retention mechanisms in lowland catchments, little attention has been paid to the influence of the landscape heterogeneity in the phosphorus retention capacity in agriculture-dominated areas. The majority of these researches focused on the final mechanisms and pathway of phosphorus retention in surface water bodies, generally regardless of the effects of the surrounding processes in the landscape. Furthermore, ditches and other surface water bodies are usually the emphasized means of phosphorus immobilization, whereas drains sediment and water composition are mostly left behind. In addition to that, with except of the experimental study of Griffioen (2006), the aforementioned researches were majorly performed in areas with Fe-rich and nutrient-poor groundwater. Hence, a deeper understanding on the heterogeneity of phosphorus dynamics in drains upon the exfiltration of nutrient-rich groundwater is still lacking.

1.4. Objectives

In face of the current situation, this thesis aims to contribute to a better understanding of the phosphorus and iron retention dynamics in tile drains taking into account the heterogeneity of the landscape in agriculture-dominated lowlands. The main research question that will be addressed in the thesis is:

What is the phosphorus retention in tile drains in a marine clay polder and how does it spatially and temporarily vary at the parcel scale?

The hypotheses made for this study hold as follows:

1. A great part of P retention occurs upon mixing of rainwater and groundwater in the drains.
2. The Fe-P fraction is the largest among the particulate P (PP), due to the high binding potential of P with ferric particles.
3. Calcium-bound P is the second major fraction among PP.
4. The heterogeneity of the parcel affects the sources of P and Fe and, thereby, has an indirect effect on the immobilization of P in the drains.
5. Drain water quality varies with drain discharge and season, including temperature.

This study took place in an agriculture-dominated marine clay catchment located in Schermer Polder, in the Western Netherlands. The parcel was recently also the study area of Delsman et al. (2014), who characterized the hydrology of the area.

This research was carried out as an internship at the Geological Survey of the Netherlands TNO (Nederlandse Organisatie voor Toegepast Natuurwetenschappelijk Onderzoek).

2. Theory

The theory that will be used in this study relies mainly on the P speciation, cycling and transport mechanisms in clay polders. The P cycling includes the main chemical reactions responsible for the release and uptake of P in aqueous media, whilst the transport mechanisms are related to the hydrological features of the polder area and the means of displacement and mobilization of P. Among the chemical interactions, the Fe-P binding mechanisms are of main interest, once they are a major factor determining the mobilization of P. In this sense, processes affecting the availability of Fe are also of interest, as well as externalities that might influence the Fe-P mechanisms. The following sections present a more detailed overview of the theory that will be used in this research.

2.1. P speciation and bioavailability

The fate and environmental effects of P are highly determined by its chemical speciation (Baken, 2015). In nature phosphorus occurs almost exclusively in the form of phosphate, in all known minerals more specifically as orthophosphate with an ionic form of PO_4^{3-}. The distribution of orthophosphate species ($H_2PO_4^-, HPO_4^{2-}, PO_4^{3-}$) due to dissociation of orthophosphoric acid is pH-dependent (Holtan et al., 1988). Phosphorus is present in waters either in dissolved or particulate forms and as inorganic or organic bound species (Robards et al., 1994). The dissolved phosphorus (DP) forms comprise orthophosphates, inorganic condensed P (pyro-, meta- and polyphosphates), and organic phosphates such as nucleic acids and proteins. The particulate P (PP) may include clay and silt-associated organic and inorganic P, precipitates of authigenic origin, metal binding P and P-containing biological matter (Worsfold et al., 2016). Particulate P exists in many forms, mostly in association with Al, Fe, Ca and Si (Poulenard et al., 2008). Both particulate and dissolved P fractions might also contain P under colloidal form, which is referred to as the P fraction in the 1nm - 1µm size range (Worsfold et al., 2016). Among the fractions, dissolved inorganic phosphorus (DIP) is considered bioavailable, whilst organic and PP forms normally must be transformed to inorganic forms before being considered bioavailable (Reddy et al., 1999).

2.2. P sources and sink

The availability and mobilization of P in soil and water phases is related to a number of chemical and biological processes.

2.2.1. Mineralization of organic matter

The decay of organic matter is an oxidation reaction which may occur in the soil but also within aquifers, where fossil OM can be present, e.g. peat and lignite. Organic matter molecules might contain humic and fulvic acids and other constituents, as P, K, N and S, which are released upon degradation (Appelo & Postma, 2005). Organic matter can be degraded by a series of electron acceptors and the overall process can be synthesized as follows (Sinke, 1992; Burdige, 1993).

Electron Acceptor	Donor	Products
$O_2/NO_3^-/MnO_2/Fe^{3+}/SO_4^{2-}/CO_2$	Organic matter	$\rightarrow CO_2 + N_2/Mn^{2+}/Fe^{2+}/S^{2-}/CH_4 + \text{biomass} + NH_4^+ + PO_4^{3-}$

The mineralization of organic matter is accompanied by CO_2 production, with a subsequent release of protons, which may result in the dissolution of iron oxides and calcium-bearing carbonates (Appelo & Postma, 2005; Sinke, 1992).

2.2.2. Dissolution/Precipitation

Dissolution and precipitation are reactions responsible for the release and uptake of PO_4 to and from solution, respectively. The dissolution and precipitation of minerals containing PO_4 are determined by the solubility products of these minerals. When the concentration of P in solution and relevant cations exceed the solubility product of the mineral, a precipitation reaction can be expected (Sinke, 1992). The concentration of phosphate is, therefore, associated with the solubility of sparingly soluble soil phosphate minerals which, in turn, depends on the concentration of H^+, P ions and either Ca, Fe or Al ions that can co-precipitate (Sas et al., 2001). Ca-phosphates are generally formed in neutral-alkaline soils, and show increasing solubility with decreasing pH. Oppositely, Al and Fe(III)-phosphates dominate in slightly acid soils, and show pH dependent solubility as well (Sas et al., 2001).

Under anaerobic conditions, reductive dissolution of ferric hydroxides carrying P is an important mechanism of PO_4 release (Shenker et al., 2005). Conversely, the co-precipitation of Fe^{3+} and P is proven to be an essential mechanism of retention of P at the surface-groundwater interface in lowland catchments (Van der Grift, 2017). As indicated before, phosphate might also co-precipitate, to a lesser extent, with Ca-precipitates upon oxygenation and degassing of groundwater, which can be reflected by the saturation state for hydroxyapatite in groundwater (Griffioen, 2006). However, the potential uptake of PO_4 by calcium carbonates is considered to be negligible since the precipitation of Fe hydroxides is a fast kinetic process in natural aqueous systems (Griffioen, 1994).

2.2.3. Adsorption-desorption & ion exchange

Phosphorus in the soil solution, either as orthophosphate or dispersed colloidal P, can be adsorbed on inorganic colloids, such as clay and Ca-precipitates and Fe/Al hydroxides, or bound to dissolved organic matter (DOC) (Chardon & Schoumans, 2002). The chemical composition of the sediments determines the P retention: while oxide-hydroxide binding capacity in the surface sediments persists, P will be retained. In these conditions, sediments rich in iron and clay perform better than calcareous sediments (Reynolds & Davies, 2001). Adsorption is a fast process and can be accompanied by diffusion into aggregates and sorption on internal surfaces. This process is particularly important with amorphous hydroxides (Chardon & Schoumans, 2002). Adsorption of phosphate to aluminum and iron oxides is expected to be more effective at low pH (Goldberg & Sposito, 1984). The pH dependence of phosphate in solution, however, is slightly more complicated than that: as the pH increases, the concentration of phosphate in solution decreases, pass through a minimum and increases again (Haynes, 1982). Murrmann & Peech (1969) showed that this minimum is about 5.5 to 6, and once the pH reaches 8 – 9, the solubility of PO_4 decreases again due to precipitation of Ca-P minerals.

2.3. Main processes affecting Fe availability

2.3.1. Pyrite oxidation

The oxidation of pyrite (FeS_2) can be an important source of iron and sulfate (SO_4) in groundwater and plays a role in the formation of acid-sulfate soils resulting from drainage of lowlands. The initial step is oxidation of the disulfide to sulfate by O_2, followed by the subsequent oxidation of Fe^{2+} to Fe^{3+}. The oxidation of disulfide proceeds at a lower redox potential than Fe^{2+} oxidation. In the absence of sufficient supply of electron acceptor, incomplete pyrite oxidation is likely to happen, resulting in a solution enriched with Fe^{2+} and SO_4^{2-}. Overall, the complete pyrite oxidation follows as described in Equation 2.1. The reaction is accompanied by a decrease in pH, which may lead to calcite ($CaCO_3$) dissolution (Equation 2.2) (Appelo & Postma, 2005).

$$FeS_2 + {}^{15}/_{4}\,O_2 + {}^{7}/_{2}\,H_2O \rightarrow Fe(OH)_3 + 2SO_4^{2-} + 4H^+ \quad (2.1)$$

$$CaCO_3 + 2H^+ \rightarrow Ca^{2+} + CO_2 + H_2O \quad (2.2)$$

Pyrite oxidation may also occur with nitrate (NO_3) reduction via microbial activity. The process involves both the oxidation of sulfur and Fe^{2+} (Equations 2.3 and 2.4). Since the energy gains for sulfide oxidation is larger than for Fe^{2+} oxidation, in the presence of excess pyrite Fe^{2+} remains unoxidized (Appelo & Postma, 2005).

Upon extensive pyrite oxidation and pH buffering by Ca carbonate dissolution, gypsum ($CaSO_4 \cdot 2H_2O$) may be formed. Authigenic gypsum formation can be found at shallow depth in the northern and western polders in the Netherlands, where calcareous, marine soils are present (Griffioen et al., 2016).

$$5FeS_2 + 14NO_3^- + 4H^+ \rightarrow 7N_2 + 5Fe^{2+} + 10SO_4^{2-} + 2H_2O \quad (2.3)$$

$$5Fe^{2+} + NO_3^- + 7H_2O \rightarrow 5FeOOH + {}^1/_2\,N_2 + 9H^+ \quad (2.4)$$

2.3.2. Formation of iron sulfides

In aquifers where mixing of freshwater and seawater occurs, a molar ratio of Cl^-/SO_4^{2-} above 19 (seawater ratio) points out to sulfate reduction conditions. Sulfate reduction through decomposition of organic matter results in H_2S, which may react with Fe-oxides present in the sediment, forming iron sulfide minerals. Amorphous iron sulfide (FeS) is rapidly precipitated, whereas pyrite has a more sluggish precipitation kinetics and usually is formed upon continuous sulfurization of FeS in completely anoxic environments (Appelo & Postma, 2005).

2.3.3. Dissolution of Fe(II) minerals

In anoxic environments, the dissolution of Fe(II)-bearing silicates, such as amphiboles and pyroxenes, and magnetite may release Fe^{2+} to the groundwater. However, these minerals have very low dissolution rates, and their contribution to the Fe^{2+} in solution will be equally low (Appelo & Postma, 2005).

2.3.4. Reductive dissolution of iron oxides

The reduction of ferric iron [Fe(III)] to ferrous iron [(Fe(II)] via microbial decomposition of organic carbon may be an important source of Fe^{2+} in aquatic environments. The content of Fe(III) in sediments often exceeds the concentration of other electron acceptors such as oxygen, nitrate and sulfate, resulting in a significant potential of organic matter mineralization with Fe(III) as the electron acceptor (Lovley & Phillips, 1986). The overall reaction of Fe(III) reduction by organic carbon is (Schwertmann, 1991):

$$CH_2O + 4FeOOH + 8H^+ \rightarrow 4Fe^{2+} + CO_2 + 7H_2O \quad (2.5)$$

2.4. Fe and P interactions

Iron plays a key role in phosphate transport in coastal lowlands, where streams are mainly fed by groundwater (Baken et al., 2015a). Shallow groundwater in these areas is often anoxic, rich in iron and pH-neutral (Griffioen et al., 2013). In the normal pH range of most groundwaters (pH=5-8), dissolved iron is present as Fe^{2+}, as Fe^{3+}under these conditions is insoluble (Appelo & Postma, 2005). In contrast, surface water is oxic, and usually presents a neutral to slightly alkaline pH, with a reduced concentration of dissolved phosphate and iron. The distinctive chemical composition between the waters enables strong redox and pH gradients at the interface between groundwater and surface water (Dahm et al., 1998; Van der Grift et al., 2014). The strong redox and pH gradients created at the interface of the ground- and surface water turns PO_4 reactive (Griffioen, 2006) and enables the oxidation of Fe^{2+} and the formation of particulate authigenic hydrous ferric oxides (Baken et al., 2013) as described in Equation 2.6.

$$Fe^{2+} + {}^1/_4\,O_2 + {}^5/_2\,H_2O \rightarrow Fe(OH)_3 + 2H^+ \quad (2.6)$$

The oxidation rate of Fe^{2+}increases with increasing pH (Appelo & Postma, 2005) and the formed Fe oxyhydroxide presents high specific surface area with high affinity for oxyanions (Dzombak & Morel, 1990). As a result, the Fe oxide type phases may bind PO_4 by adsorption or co-precipitation (Baken et al., 2015b). Overall, the main binding mechanisms are via surface complexation to amorphous iron oxyhydroxide (ferrihydrite or hydrous ferric oxide, $Fe(OH)_3$) or co-precipitation as Fe-hydroxyphosphate (Griffioen, 2006). More crystalline forms of iron oxyhydroxides, such as goethite, also enable phosphate adsorption (Torrent et al., 1990). However, the higher crystallization form of goethite implies a lower surface area, resulting in fewer sorption sites per unit weight (Appelo & Postma, 2005).

The mechanism responsible for the immobilization – adsorption or co-precipitation – is determined by the sequence of Fe^{2+} and P loading of the surface water, usually represented as the initial P/Fe molar ratio in solution. If PO_4 is present during the oxidation of Fe^{2+} to Fe^{3+}, Fe hydroxyphosphate will form, whereas in the case of Fe^{3+} formation in the absence of PO_4 – e.g. P advent from a source downstream the groundwater exfiltration site – surface adsorption of PO_4 by Fe oxyhydroxides is the likely main P binding mechanism. The latter condition is less favorable for the binding capacity of P, implying that the immobilization of P arising from diffuse sources can be more effective (Van der Grift, 2017). Recently, Van der Grift et al. (2016b) showed that dissolved PO_4 can be effectively immobilized upon aeration of pH-neutral groundwater with an initial molar P/Fe ratio up to 1.5 in the form of a homogeneous Fe hydroxyphosphate with a stoichiometry of $Fe_{1.67}PO_4(OH)_{2.01}$ and a molar P/Fe ratio of 0.6. The general precipitation reaction is shown in Equation 2.7, where 1/r is the stoichiometric molar P/Fe ratio of the Fe hydroxyphosphate (Van der Grift et al., 2016b).

$$rFe^{3+} + PO_4^{3-} + (3r-3)OH^- \rightarrow Fe_rPO_4(OH)_{3r-3}(s) \quad (2.7)$$

The uptake of PO_4 in iron hydroxides during seepage is determined by the aqueous Fe^{2+}/PO_4 ratio, the PO_4 concentration in groundwater, and the pH of the solution (Griffioen, 1994). Furthermore, other factors such as redox potential, ionic strength/cations, organic acids, and temperature play a role in governing the P mobilization reactions (Chardon & Schoumans, 2002).

2.4.1. Processes affecting Fe-bind P

2.4.1.1. pH and temperature

Lower pH and temperature conditions, usually found in winter time, are responsible for slower oxidation of Fe(II) and subsequent formation of authigenic particles which may bind phosphate (Baken, 2015). Additionally, pH also determines the surface charge of the Fe hydroxides (Chardon & Schoumans, 2002): the more alkaline the pH, the less sorption of anion will occur in case of surface complexation or ferrihydrite becomes more stable over strengite in case of a solid-solution precipitate (Griffioen, 2006).

2.4.1.2. Redox potential

Phosphate sorption tends to decrease with decreasing redox potential (Holtan et al., 1988). Reducing conditions may occur upon rising groundwater table, resulting in the reduction of iron compounds. In the case P is bound on Fe-oxides, P will be mobilized. If oxic conditions are re-established, precipitation of Fe^{3+} will occur, and P will re-adsorb (Chardon & Schoumans, 2002).

2.4.1.3. Residence Time

Lower discharge conditions in water bodies are usually associated with larger residence times, which reflect the exposure time of water to oxic environments. At such conditions, pH is expected to be higher due to greater CO_2 degassing and more Fe^{3+} is expected to become oxidized (Baken et al., 2015a).

2.4.1.4. Nitrate

Nitrate is a highly soluble compound and it can only be removed from groundwater by reduction (Equation 2.8), which mostly occurs through oxidation of organic matter but can also occur with pyrite (see Section 2.3.1). Opposite to ammonia, NO_3 is only stable under highly oxidizing conditions (Appelo & Postma, 2005).

$$2NO_3^- + 12H^+ + 10e^- \rightarrow N_2 + 6H_2O \quad (2.8)$$

As a strong oxidizing agent, NO_3 can maintain a high redox potential at the sediment-water interface, preventing the release of iron-bound phosphates (Sinke, 1992). However, NO_3 leaching into the groundwater may increase PO_4 mobilization by mobilizing sulfate through the oxidation of iron sulfides. Nevertheless, if NO_3 concentrations are sufficiently high, nitrate acts as a redox buffer, reducing the mobilization of PO_4 (Lucassen et al., 2004).

2.4.1.5. Sulfate

The origin of sulfate may vary from mixing of fresh water with seawater, decomposition of organic matter, dissolution of gypsum or pyrite oxidation (Boyd, 2015; Appelo and Postma, 2005). The redox couple sulfate/sulfide has an indirect effect on phosphorus dynamics. The reduction of sulfate to sulfide in anaerobic zones results in the formation of iron sulfides (see Section 2.3.2), which prevents the upward flux of Fe^{2+} and further oxidation to Fe^{3+}, reducing phosphate immobilization by ferric iron-bound particles (Sinke, 1992; Hyacinthe & Van Cappellen, 2004). Besides, iron sulfides have a much lower solubility when compared to Fe(II) phosphate minerals. As a result of iron sulfide formation, the equilibrium concentration of Fe^{2+} is lowered. At lower Fe^{2+} concentrations, higher PO_4^{3-} concentrations are required to exceed the solubility product of vivianite ($Fe_3(PO_4)_2 \cdot 8H_2O$). When phosphate concentrations are insufficient and vivianite is undersaturated, Fe(II) phosphate minerals may dissolve, increasing the phosphate efflux out of the sediment. If siderite ($FeCO_3$) is present, however, it may prevent vivianite dissolution, since it has a higher Fe(II) solubility (Gächter & Müller, 2003). Nevertheless, in Dutch catchments this process is unlikely to occur, since vivianite is often found supersaturated in groundwater in the Netherlands (Griffioen, 1994; Griffioen et al., 2013), avoiding its dissolution.

2.4.1.6. Dissolved Organic Carbon (DOC)

The presence of DOC is associated with higher stability of iron-rich colloids, which might influence the overall transport of iron in water systems and increase the exposure time of these particles for later surface adsorption of phosphate particles (Gunnars et al., 2002). Van der Grift et al. (2016b) reported the formation of stable PO_4- rich iron colloids, which was attributed to the high DOC content present in groundwater. In a similar experiment with synthetic solutions, the precipitates formed upon Fe(II) oxidation agglomerated and flocculated. The effect of DOC on the stability of Fe-rich colloids, however, seems to be less pronounced in seawater than freshwater, since salinity appears to enhance the aggregation rate of the colloids formed (Gunnars et al., 2002).

2.5. Transport of P

In lowland flat catchments, PP comprises up to 70% of the P transferred from agricultural grassland to drainage systems (Van der Salm et al., 2012). The transport of the dissolved, colloidal or fine-particulate P from the topsoil may occur via three main hydrological pathways: surface runoff (overland flow), subsurface runoff (leachate, throughflow that remains separate from local groundwater tables), or subsurface groundwater flow (Reynolds & Davies, 2001). In more flat areas, the main P losses pathways to surface waters are: subsurface runoff and leaching through the soil and/or bypasses via artificial drainage systems, whereas surface runoff is considered negligible (Schoumans, 2015; Van der Salm et al., 2012). In well-drained soils, with little P sorption capacity, the P leaching to groundwater and consequent seepage to surface waters plays an important role in the P transfer to surface water bodies (Baken et al., 2015b; Van der Zee, 1988). Van der Grift et al. (2016a) showed that, in polder catchments, the P transport mechanisms can be characterized as less incidental and more controlled by biogeochemical remobilization from bed

sediments. Additionally, groundwater in the Netherlands naturally contains high P concentrations (Griffioen, 2006) and, therefore, it is also an important contributor to the load of P in surface waters (Holman et al., 2008; Griffioen et al., 2003).

2.6. Study area

The Schermer Polder

The study area is an agricultural field located in the Schermer Polder, near the city of Alkmaar, in The Netherlands (52.599° N, 4.778° E). The study area within the field comprises a terrain of about 120 x 500 m with a flat relief at a surface elevation of 4.0 ± 0.14 m below NAP[1], drained by tile drains installed at 1 m below the surface at 5 m intervals, and by two ditches located at each side of the field. The drains discharge in the northern ditch, which is also a dead-end ditch, meaning that it solely drains the adjacent field (see Figure 2.1). The surface water level in this ditch is maintained at a constant 5.0 m – NAP, whilst in the southern ditch, the water level is kept at 4.7 m -NAP. The area is used for the cultivation of vegetables including celery, potatoes, and pumpkins (Delsman et al., 2014). The Schermer Polder is a result of the reclamation of a lake in 1635 AD (Oude Essink, 2001), becoming one of the deepest polders in The Netherlands. The average annual precipitation and Makkink reference evaporation amount to 880 mm and 590 mm, respectively (Delsman et al., 2014).

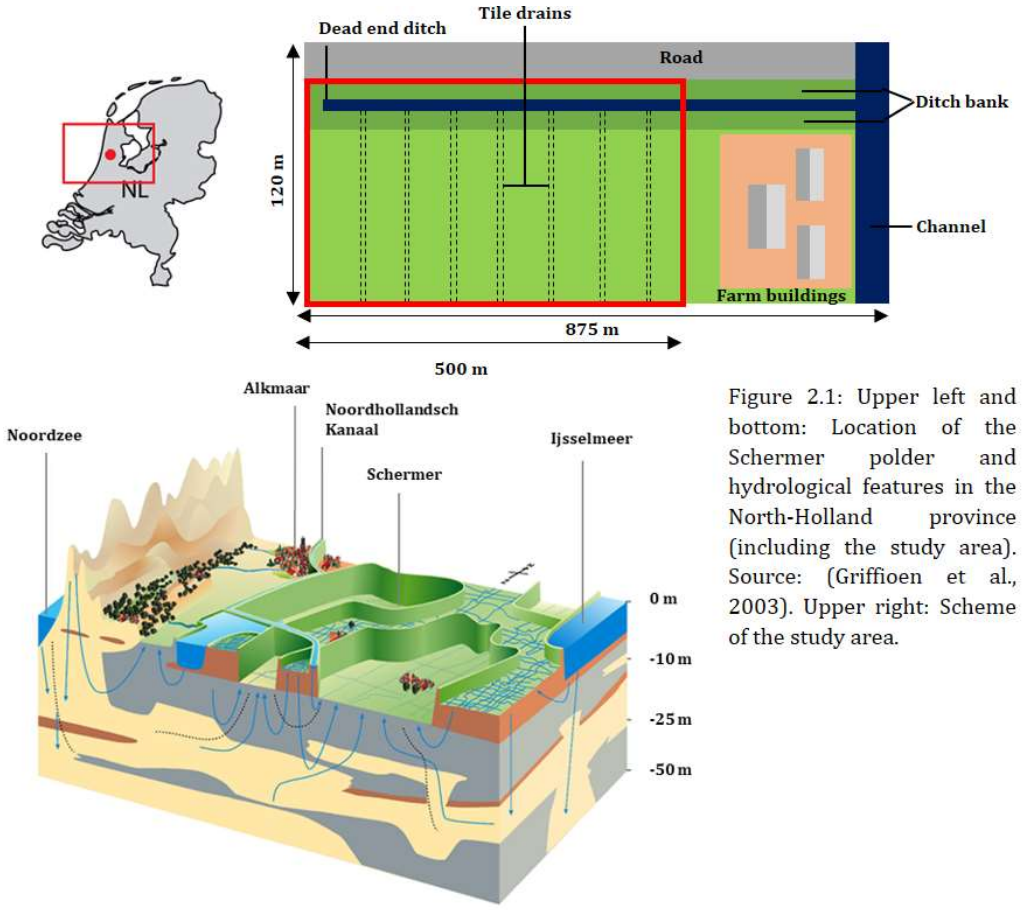

Figure 2.1: Upper left and bottom: Location of the Schermer polder and hydrological features in the North-Holland province (including the study area). Source: (Griffioen et al., 2003). Upper right: Scheme of the study area.

[1] NAP (*Normaal Amsterdams Peil)* is the reference level for height used in The Netherlands. The NAP height of 0 m is approximately equal to the mean sea level of the North Sea (Rijkswaterstaat, 2018).

The Schermer Polder is located in the Western Netherlands, where the Holocene layer serves as a confined, semi-permeable cover overlying Pleistocene coarser-grained deposits (Griffioen et al., 2016). The Holocene confining layer consists of alternating sandy channel deposits, clayey flood-plain and tidal-flat sediments and organic swamp deposits. It reaches a maximum thickness of 25 m near the coast, and the main part of this coastal lowland is situated below sea level (De Vries, 2007). This can be seen in Figure 2.2, which shows the geological cross-section of the study area. Down to 7.5 meters below ground level, clay and sand-clay deposits predominate, with some layers of coarse sand, and very little peat. According to Delsman et al. (2014), who performed a study in the same area, this Holocene cover layer is characterized by a 20-40 cm thick tillage clay layer on top of fairly homogeneous loamy sand, which possibly reaches a depth of at least 17 m. In terms of hydrology, the groundwater seems to be originated from infiltration in the coastal dune area and flows in a west-east direction (Delsman et al., 2014), exfiltrating in the polder area with an estimated upward flow of 0.5 mm/day in the summer and 0.3 mm/day in the winter time (Griffioen et al., 2002) (see Figure 2.1).

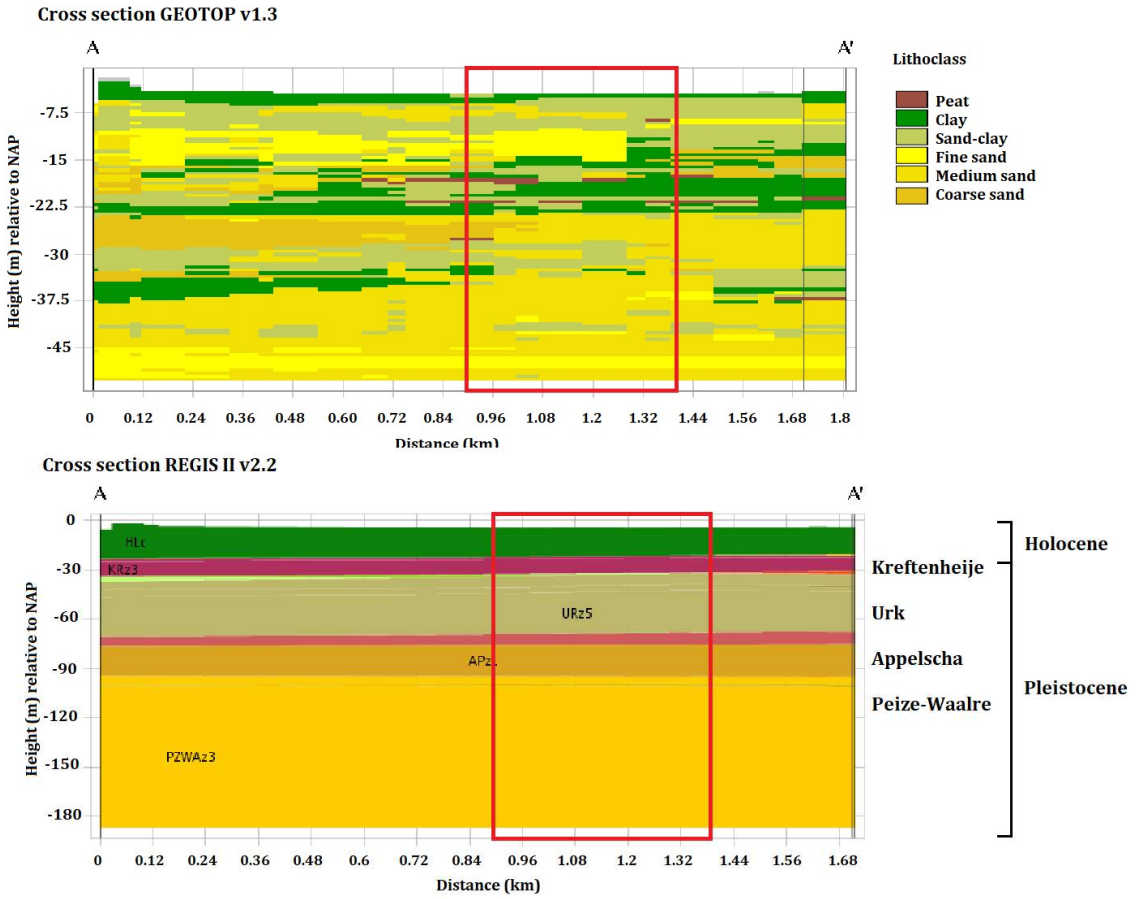

Figure 2.2: Cross section of area of interest. The parcel representing the study area is identified by the red contour. Images from the models GEOTOP v1.3 (top), which shows the lithological cross-section; and REGIS II v2.2 (bottom), which shows the stratigraphic units. Both images were obtained from DINOloket (2017).

3. Methods

3.1. Fieldwork

In order to understand the phosphorus retention dynamics in the drains taking into account the heterogeneity of the landscape, an extensive fieldwork campaign was performed in the parcel, which comprised the sampling of several components of the soil and water system. The data obtained with the fieldwork campaign was also necessary as an input for the modeling simulations, which was the second part of this thesis. The samples collected and their respective analytical procedure are described below.

3.1.1. Water samples

3.1.1.1. Ditch and drains water

Ditch and drain water samples were collected approximately every three weeks, from December to May, in order to obtain a time series data set. Roughly estimating, the parcel contains around 100 drains, distributed every 5 meters. For the drain water sampling, 10 drains with an average distance of approximately 40 m were selected, in order to cover most of the parcel area. Preferably the same drains were always sampled, but due to certain constraints, i.e., high ditch water level, some drains could not be sampled[2]. The drains were numbered from 1 to 10, in which drain 1 is located at the beginning of the ditch, and drain number 10 at the end of it (see Figure 3.1). The drains coordinates are found in Appendix I. Ditch water was also collected from two locations: one in the middle of its length and another at the end of it.

The water samples were collected with a bucket, which was also used to measure the discharge of the drains. First, 500 mL of sample was stored in plastic bottles, where pH, oxygen content, electrical conductivity (EC) and temperature were measured *in situ*, by using Hach HQD portable meters. This volume was stored in a cool box and used to measure alkalinity (also *in situ*) after all the samples were collected. Alkalinity was tested with a Hach field titrator set. In the second step, sampling water was filtered with 0.45 µm membrane filters and stored in bottles that were either neutral or pre-acidified, depending on the analysis to be performed in the laboratory. This sampling procedure was applied to all the water types sampled for this research.

Extra samples were collected in February to be analyzed regarding the concentration of Fe(II). Approximately 10 mL of sample was filtrated into 15 mL Greiner tubes, previously acidified with 0.5 mL of 1 M HCl. In the laboratory, they were analyzed with the ferrozine method described in Viollier et al. (2000).

After collected, all the water samples were stored in a cool box and transported to the laboratory, where they were analyzed mostly within one or two days after sampling. Table 3.1 summarizes the sampling procedure and laboratory analyses applied to all the water types sampled for this research.

3.1.1.2. Groundwater

Deep groundwater

In a single field campaign in the month of February, deep groundwater samples were collected from the well located near the end of the parcel, northwest of the farm (see Figure 3.1). The well is identified by the code B19B0237 and has the coordinates of 113465 (x) and 512729 (y) [3], according to the RD coordinates (Dutch coordinates system). The water was sampled by using a peristaltic pump and was purged enough to flush around three times the total volume of water in the tube. In total, groundwater from four different

[2] This was more evident in May when only one drain could be sampled without mixing with ditch water, due to high water levels in the ditch.
[3] Data obtained with DINOloket.

depths was sampled: 9 m, 25 m, 46 m, and 60 m below surface[4]. Samples were only collected after temperature, pH, and EC of the water had stabilized.

Shallow groundwater

Also in a single field campaign in May, shallow groundwater was sampled from the same locations were the soil sampling was performed (see Figure 3.1). First, an Edelman drill was used to dig a hole down to 1.5 – 2.0 m depth. Next, a perforated PVC tube was placed into the hole, in order to avoid the flow of associated clay with the groundwater. After waiting some time for sufficient flow into the hole, groundwater was pumped with a peristaltic pump and sampled as described for the other water samples.

Table 3.1: Summary of the laboratory analysis procedures applied to all water samples. The ferrozine method, however, was only applied to one batch of drain and ditch water samples.

Acidification	Volume	Filtration	Elements Analyzed	Laboratory analysis
1.88 mL 22% w/w HNO3	250 mL	Yes	Na K Fe Ca Mg Mn Al P	Inductively Coupled Plasma Mass Spectrometry (ICP-MS)
0.84 mL 2 M H2SO4	100 mL	Yes	PO_4 NH_4	Continuous Flow Analysis (CFA) with spectrophotometric detection
			DOC	Detection via infrared (IR)
Neutral	100 mL	Yes	SO_4 NO_3 Cl	Ion Chromatography (IC)
Neutral	500 mL	No	Alkalinity as HCO_3^-	Hach Field titration set
			pH, Temperature,O_2 , EC	Hach HQD portable meters
0.5 mL 1 M HCl	10 mL	Yes	Fe(II) and Fe total	Ferrozine method (Viollier et al., 2000)

3.1.2. Solid Samples

3.1.2.1. Shallow soil samples

Shallow soil material was collected during a single field campaign in January. The procedure was based on the mixed samples method, which consists of the collection of sub-samples from a central location and from 4 other symmetrically distributed around the central one. The five sub-samples were mixed, resulting in an average sample that represents a certain location. In total 8 locations were chosen and named from B1 to B8, as represented in Figure 3.1. The coordinates of the boreholes are found in Appendix I. These locations were also used for the sampling of deep sediment and groundwater. In order to collect the shallow soil samples, an Edelman drill was used to drill holes down to the depth of 20 – 30 cm below ground level. The average distance between the central hole and the surrounding ones was about 0.5 m. The soil samples were stored in regular plastic bags inside cool boxes during the transport to the laboratory, where they were stored at 4^0C until analysis.

[4] These depths are the approximated average values between the top and the bottom of each screen sampled.

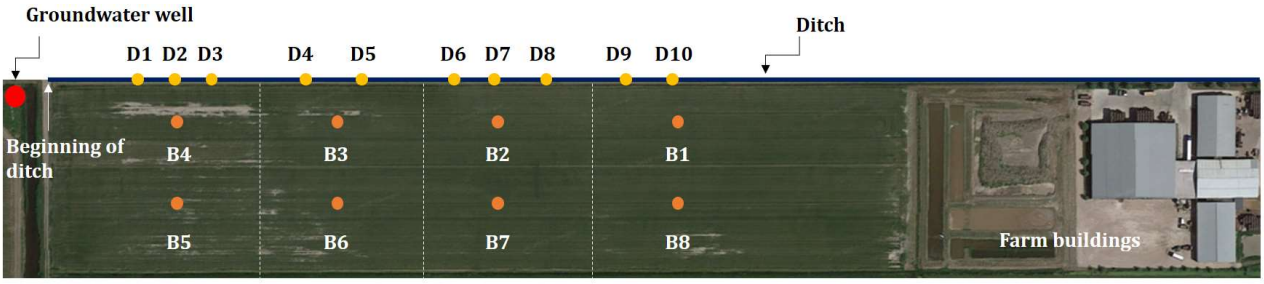

Figure 3.1: Scheme with the arrangement of boreholes (B1-B8) and drains (D1-D10) in the study area. The white dashed lines determine the limit of influence of the boreholes and their respective drains. This arrangement was used to create the mixing lines shown in the results section.

3.1.2.2. Deep sediment samples

Deep sediment cores were sampled one week after the shallow soil sampling, in the end of January. These samples were collected from the same 8 locations where topsoil was sampled (see Figure 3.1). Sediment was collected from the approximate depths of 0.75, 1.25, 2, 3 and 4 meters below surface, totalizing 5 samples for each borehole. The boreholes maintained the identification as B1 to B8, and each layer of the soil column was represented with a letter from A to E, in which A is 0.75 m and E is 4 m. The boreholes were initially drilled with an Edelman drill and the sediment extracted was placed in a half cylindric tube for visualization of the sediment column. In order to reach larger depths in the borehole, mud was removed by using the pulse method. After the desired depth was achieved, the Akkerman core sampler was immediately inserted in the hole, in order to avoid the sampling of mud which would not hold in the core. The equipment used is shown in Figure 3.2. Once the cores were pulled out of the borehole, they were directly closed with a plastic lid and PVC electrical insulation tape to minimize as much as possible the oxidation of the samples. The cores were further sealed inside aluminum bags containing Microbiology Anaerocult A mini pads to further reduce the chances of oxidation. The bags were kept inside cool boxes with cooling elements during transport to the lab, where they were stored at 4^0C until analysis.

Figure 3.2: Equipment used for the soil sampling. (A): Edelman drill. (B) and (C): Akkerman core sampler and Akkerman tube, respectively. (D) and (E): Equipment used to remove the mud and achieve greater depths.

3.1.2.3. Ditch settled particles

Settled suspended matter of the ditch was collected twice, once in January and another time in February. The samples were collected through two shallow trenches of approximately 1.2 meters long deployed for 3 weeks at two locations: in the beginning (upper) and at the end (down) of the ditch (see Figure 3.3). The samples were named according to the location where they were collected and the month of sampling, i.e., Upper January. The material deposited in the bottom of the trench was collected and stored in plastic containers at 4^0C until analysis (see Figure 3.3).

3.1.2.4. Drain particulates

Drain slurry was also sampled in February. The material was scraped from the interior of the drains and stored into plastic containers at 4^0C (see Figure 3.3). Samples from 4 drains relatively distant from each other in the parcel area were selected for analysis: drains 2, 4, 7 and 10.

Figure 3.3: (A): Ditch settled material. (B): Drain slurry. (C): Trench used to collect ditch sediments.

3.2. Laboratory analysis

The analytical activities performed are described as follows, according to the order that they were executed.

3.2.1. Deep soil samples – centrifuging and pore water extraction

All the 40 soil samples obtained with the Akkerman cores were centrifuged for the pore water extraction. The preparation of the samples was done inside a glovebox, in order to avoid the oxidation of the material. The first 1.5 – 2 cm of the Akkerman core content – usually the portion that had more contact with the air during the sampling – was placed into aluminum cups, weighed and oven dried at 60^0C for the lithological characterization, which was performed according to Bosch (2000). The sediment located in the center of

the core was scooped into 50 mL centrifuge tubes coupled with 0.45 µm nylon filters inlay. The tubes were centrifuged at 2300 rpm for 20 minutes. After centrifuging, pore water was filtered inside the glovebox, using 0.45 µm filters and stored into 50 mL Greiner tubes, in the glovebox. The centrifuged sediment was scooped into 50 mL tubes, which were sealed into plastic bags still in the glovebox. Once out, these plastic bags were sealed inside aluminum bags flushed 3 times with nitrogen gas. These bags were stored at -25^{0}C during the weekend, before being freeze-dried for the posterior extraction procedures.

3.2.2. Pore water analysis

The volume of pore water obtained from the samples varied considerably among the layers, being very little at 0.75 m and increasing with depth. Ideally, all the 40 samples would have a full water analysis, but due to constraints in the pore water volume, certain analyses were not performed for some samples. All the samples were diluted in order to obtain enough volume for the analysis and to guarantee that the results of the elements other than, i.e., Na and Cl, would be within the detection range of the analytical instruments. The dilution of the samples was determined based on the composition of the ditch and drain waters and varied according to the volume of pore water obtained. For the samples with high volume content, the dilution made is represented in Table 3.2. For samples with smaller volumes, a different dilution was applied. All the samples were also analyzed for pH. Alkalinity was not measured due to constraints with sample volume. Instead, it was calculated based on the difference between the sum of cations and anions present in the samples, in meq/L.

Table 3.2: Dilution applied for the majority of the pore water samples.

Analysis	Sample volume (mL)	UHQ (mL)*	Final volume (mL)	Dilution	Acidifcation
IC	1.0	2.0	3.0	3.0	-
PO_4	2.0	3.0	5.0	2.5	16.7 µL 1.8 M H_2SO_4
NH_4	2.0	3.0	5.0	2.5	16.7 µL 1.8 M H_2SO_4
ICP-MS	2.5	4.5	7.0	2.8	49 µL 65-67% HNO_3
DOC	2.0	6.0	8.0	4.0	26.6 µL 1.8 M H_2SO_4

*UHQ stands for ultrapure water.

3.2.3. Shallow soil samples

The shallow soil samples were prepared according to the aforementioned mixing sample procedure. For each of the 8 locations, 5 sub-samples were collected, totalizing 40 sub-samples. From each sub-sample, approximately 5 grams was scooped into aluminum cups and oven-dried at 60^{0}C for 2 days. Once dried, the 5 sub-samples from a certain location were mixed and ground using an agate mortar.

3.2.4. Ditch settled material and drain particulates

The solid material collected from the ditch and drains was scooped into 50 mL Greiner tubes and centrifuged at 2800 rpm for 15 minutes to remove the excess water. The centrifuged material was spread into plastic petri dishes and placed open inside the glovebox to dry for 4 days.

3.2.5. Fe extraction

Once all the solid samples were dried, approximately 1 gram of each sample was ground using an agate mortar to increase the surface area of the grains. With exception of the topsoil samples, all the others were ground inside the glovebox. From this ground material, 0.1 g was used for the Fe extraction.

The Fe extraction procedure followed a modified version of Claff et al. (2010). Since we were only interested in the Fe fractions in which P could be sorbed (Fe-oxides), solely steps 1, 2 and 4 from the original paper were executed. The volume of extractant used in all the steps was 10 mL. The extraction started with readily soluble salts and exchangeable Fe (1M $MgCl_2$, 1 h). The second step consisted of the dissolution of minerals sensitive to low pH, which includes carbonates and poorly ordered sulfides and oxides (1M HCl, 4 h). In order to avoid remains of HCl in the next step, a rinse of 3 mL of 1M $MgCl_2$ was applied before the next extractant was added. In the final step, the samples were treated with a 0.35 M acetic acid/0.2 M sodium citrate buffer with 50 g/L sodium dithionite solution (CBD, 4 h). The CBD dissolves the broadest range of crystalline iron oxide minerals (Claff et al., 2010). With exception of the CBD, all the other extractants were added inside the glovebox to avoid oxidation of the samples. All the samples – except the $MgCl_2$ rinse previous to the CBD – were shaken at 170 rpm at a platform shaker and centrifuged at 3000 rpm for 15 minutes, at 20^0C.

After centrifuging, all the solutions were filtered by 0.45 μm filters. The $MgCl_2$ solution was stored inside the glovebox, whilst HCl at 4^0C and the CBD at -25^0C. The Fe concentrations were determined according to the ferrozine method described at Viollier et al. (2000). The analysis included two duplicate samples for error estimation, resulting in 10 values. The average error obtained for these values was 5.9%.

3.2.6. P extraction

The P extraction followed the SEDEX method developed by Ruttenberg et al. (1992). Similarly to the Fe extraction, 0.1 gram of sediment was used, previously ground to increase the surface area of the grains and 10 mL of extractant in each step. The first step of the extraction targeted exchangeable or loosely sorbed P (Exch-P) (1M $MgCl_2$, pH = 8, 0.5 h). In the second day, the samples were treated with citrate dithionite bicarbonate buffer for the extraction of easily reducible or reactive ferric Fe-bound (Fe-P) (CDB, pH = 7.6, 8 h). Given the nature of the P species to be extracted, the first two extractants were added inside the glovebox, to avoid oxidation. The following extractants were added in a fume hood, instead of inside the glovebox. Next to CDB, a rinse of $MgCl_2$ (1M $MgCl_2$, 0.5 h) was applied to the samples. On the third day of extraction, calcium-bound P (Ca-P) was targeted and the samples were prepared with 1 M sodium acetate buffer (pH =4, 6 h). This fraction is constituted essentially by authigenic carbonate fluorapatite, biogenic apatite, and $CaCO_3$-associated P. This step was followed by a third rinse of $MgCl_2$ (1M $MgCl_2$, 0.5 h). The remaining inorganic P, referred to as detrital apatite P (Detr-P), was dissolved by the addition of hydrochloric acid (1M HCl, 24 h). Following this step, the samples were washed three times with ultrapure water and placed into ceramic crucibles. The crucibles were oven-dried for 1 day at 60^0C and ashed for 2 hours at 550^0C. The ashed material was treated with HCl (1M HCl, 24 h), for the extraction of the organic P (Org-P). In all the steps, the samples were shaken at 170 rpm at a platform shaker and centrifuged at 3000 rpm for 15 minutes, at 20^0C.

Once centrifuged, all the solutions were filtered by 0.45 μm filters. The CDB solution was diluted and P concentrations were determined via ICP-OES. For the remaining solutions, P content was determined using colorimetric analysis based on the ammonium heptamolybdate method. The analysis included two duplicate samples for error estimation, resulting in 14 values. The average error obtained for the method was 7.5%. For very low extracted contents (<0.01 mg/g), this error went up to 28% and was not included in the average error calculation.

3.2.7. Aqua regia

The solid contents of the main elements were determined via the aqua regia method. Between 0.3 g and 0.5 g of dried and ground sample was placed into Teflon PFA vessels. These vessels were filled with 9 mL of 12 M HCl and 3 mL of 14.4 M HNO_3. The closed vessels were placed inside a microwave, where the digestion took place for 25 minutes at 150^0C and a maximum pressure of 200 psi, according to the NEN-EN-ISO 15587-1. The extract was diluted with ultrapure water and analyzed via ICP-OES for the main elements, including Fe, Mn, Al, K, Ca, Mg, Na, Si, S, P and As. The analysis included six duplicate samples for error estimation. The average error obtained for the method was 9.9%. For Si, this error went up to 53.3%, which is expected, since Si is not entirely extracted via aqua regia.

3.3. Geochemical modelling

The second phase of this research comprised the determination of phosphorus retention in the drains by running modelling simulations with PHREEQC (Parkhurst & Appelo, 2013). The first simulation started with the mixing between rainwater and groundwater, using as a reference the proportion of each water type found in the drains calculated based on their chloride concentration. These mixed solutions would be an attempt to represent the initial solution composition entering the drains, prior to any oxidation. Data from the shallow groundwater samples were applied as an input for the rainwater, and groundwater from 9 m and 25 m depth was used as a reference for exfiltration composition, resulting in two simulations for each borehole sample. The mixing of solutions was followed by aeration given by an imposed constant oxygen pressure (Log P_{O_2}= -0.7) and CO_2 pressure, computed as the average obtained by SI calculations with the drains solutions composition. The estimation of the redox potential of each solution (pe) was done by initially classifying the water composition into a redox class (i.e. oxic, sub-oxic, Mn-anoxic), and further calculated based on the redox class and the pH using the functions for pe estimation reported in Griffioen et al. (1994). Next, the mixture was set in equilibrium with ferrihydrite and Fe hydroxyphosphate. For describing the precipitation of Fe hydroxyphosphate, the solubility constant of $Fe_{1.67}PO_4(OH)_{2.01}$ was used, which has a Log K value of (Van der Grift et al., 2016b):

$$\mathrm{LogK}_{Fe_{1.67}PO_4(OH)_{2.01}} = 1.67\ \log[Fe^{3+}] + \log[PO_4^{3-}] + 4.5\ \log[OH^-] = -63$$

The previously described aeration procedure was also applied for the solution composition of drain water from two sampling days. For these simulations, pe was assumed to be equal to 0, in order to obtain all Fe present as Fe(II). The data series with the highest and lowest PO_4 and Fe concentrations were chosen in order to assess P immobilization after drain water leaves the drain tubes under two extreme scenarios. Finally, the same procedure was also applied for the groundwater compositions of 9 m and 25 m depth, in order to address the P immobilization in the ditch, in which groundwater exfiltration is assumed to play a major role. PHREEQC was also used to calculate the geochemical speciation of all the water samples, including the Saturation Index (SI) for the main minerals: calcite, siderite, dolomite, gypsum, OH-apatite, and vivianite. Likewise, CO_2 and O_2 partial pressures in solution were also computed.

4. Results

The results from all the analytical procedures are summarized in this chapter. More detailed information is found in Appendix I-III.

4.1. Soil composition

Figure 4.1 shows the sediment profile down to 1.25 m depth for borehole B8. The first 0.5 m of the soil is characterized by a dense clay layer, also described by Delsman et al. (2014). The next layer is characterized by a grayish material with a sandy texture, much drier than the initial moist dense clay coverage, which is followed by a brownish sandy-clay material.

Table 4.1 shows the lithological classification of the soil samples regarding their percentage of clay, silt, and sand, according to Bosch (2000). More detailed information is found in the Appendix I. All the samples from 2 m to 4 m depth are classified as sand. From 0.75 m to 1.25 m, some differences can be pointed out. In B5, B6, B7, and B8, the first two layers of the sediment column are characterized as loam. In B3 and B4, the first layer is loam, but the second is already classified as sand. For B2, the soil at 0.75 m depth is classified as sand, and become loam at 1.25 m depth. Different from all the other boreholes, the soil type in B1 at 0.75 m depth was the only one to be characterized as clay.

Figure 4.1: Sediment profile down to 1.25 m depth for borehole B8.

Table 4.1: Lithological classification of soil layers based on their % of sand, silt and clay, according to Bosch (2000).

		Soil type							
Soil Layer	Depth (m)	B1	B2	B3	B4	B5	B6	B7	B8
A	0.75	Clay	Sand	Loam	Loam	Loam	Loam	Loam	Loam
B	1.25	Sand	Loam	Sand	Sand	Loam	Loam	Loam	Loam
C	2.0	Sand	Sand	Sand	Sand	Sand	Sand	Sand	Sand
D	3.0	Sand	Sand	Sand	Sand	Sand	Sand	Sand	Sand
E	4.0	Sand	Sand	Sand	Sand	Sand	Sand	Sand	Sand

4.2. Water analysis

Several components of the water system of the parcel were analyzed for various elements. The results of this section will be presented according to the element analyzed, instead of the origin water sample.

4.2.1. Physical parameters

4.2.1.1. Chloride, flow pattern and fresh-saline groundwater interface

Chloride is a conservative element and, as such, its concentration can provide an estimate of the origin of the water and the possible flow routes, making it convenient to be the first element analyzed. The classification of the water regarding the chloride concentration is based on the values described in Table 4.2. Chloride concentrations were the highest in the ditch water (see Figure 4.2), varying from 854.5 mg/L to 1838.3 mg/L for the samples collected in the middle of the ditch and from 1271.1 mg/L to 2415.0 mg/L for the samples collected at the end of it. Overall, the average chloride concentration found at the end of the ditch was 23% higher than in the middle of it. The range of chloride in drain water varied considerably: from 196.0 mg/L to 2198.9 mg/L. The average, however, is 945.8 mg/L, almost half of that found in the ditch water, 1715.0 mg/L. Analog to the ditch results, chloride concentrations increased towards the drains located near the farm (drains 7 – 10), which registered an average concentration 2.3 times higher than the other drains.

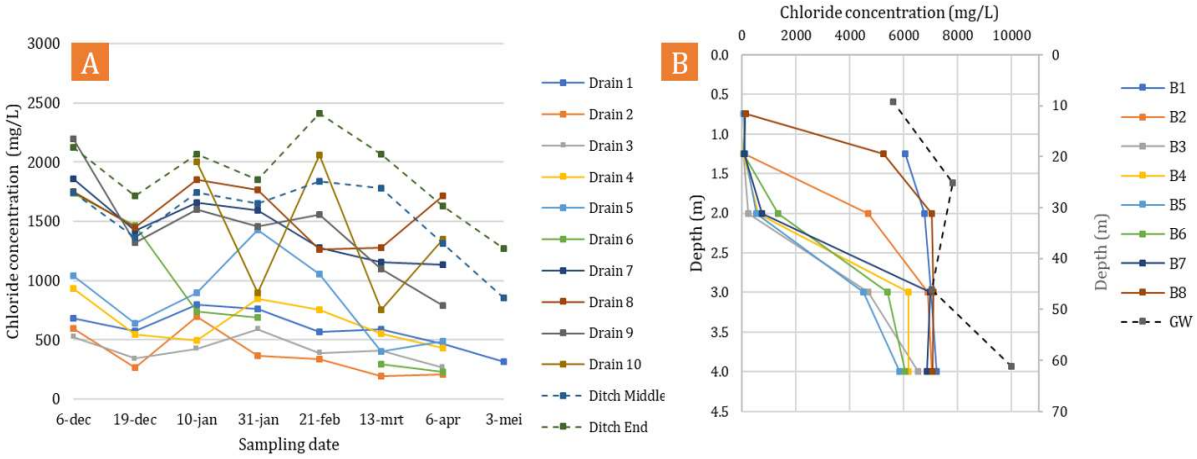

Figure 4.2: Temporal data set of chloride concentration in drains and ditch water. Right (B): Depth profile of chloride concentrations in pore water and groundwater.

Table 4.2: Classification of water by chloride concentration. Source: Griffioen et al. (2013).

Class	Cl concentration
Dilute	<50 mg/L
Fresh	50-100 mg/L
Contaminated fresh	100-300 mg/L
Brackish	300-1000 mg/L
Brackish-saline	1000-5000 mg/L
Saline	>5000 mg/L

Among the shallow groundwater samples, B1, B2, and B7 showed chloride concentrations above 1000 mg/L, indicating a mix between freshwater with deeper groundwater. For the remaining boreholes, concentrations of chloride varied between 41.3 mg/L and 81.3 mg/L.

In the groundwater samples, chloride concentrations were 5605 mg/L at 9 m and increased with depth, achieving 10000 mg/L at 60 m. For pore water, as expected, chloride concentrations also increased with depth (see Figure 4.2). In boreholes B1 and B8, saline conditions were found already at 1.25 m depth, where chloride concentrations were 6059 mg/L and 5252 mg/L, respectively. For boreholes B2 and B6 brackish-saline water was present at 2 m depth, with 4674 mg/L and 1339 mg/L. For the remaining boreholes, brackish conditions appeared at 2 m, and brackish-saline and saline, at 3 m depth. These results indicate that a shallower fresh-saline groundwater boundary occurs at the end of the ditch, near the region where boreholes B1 and B8 are located.

Equation 4.1 was used to estimate the composition of the water transported via drains. Each drain was compared with the pore water from the two boreholes expected to exert a major influence on the drain water composition, as depicted in Figure 3.1.

$$Cl_{drain} = \alpha(Cl_{shallow}) + (1 - \alpha)Cl_{deep} \qquad (4.1)$$

In the equation, Cl_{drain} is the average chloride concentration in a certain drain, $Cl_{shallow}$ is the average chloride in the shallow pore water (0.75 m depth) from the two boreholes exerting influence on the drain, and Cl_{deep} is the average between the concentrations of the deep pore water (4 m depth) from these boreholes and the groundwater samples from 9 m and 25 m depth. The results are presented in Table 4.3.

Table 4.3: Drain water composition based on average chloride concentrations from drains, shallow and deep pore water, and groundwater at 9 m and 25 m depth.

	% of rainwater in the drains	% of groundwater in the drains
Drain 1	91.1%	8.9%
Drain 2	95.1%	4.9%
Drain 3	94.4%	5.6%
Drain 4	91.5%	8.5%
Drain 5	88.4%	11.6%
Drain 6	88.6%	11.4%
Drain 7	79.9%	20.1%
Drain 8	77.8%	22.2%
Drain 9	80.8%	19.2%
Drain 10	81.1%	18.9%
AVERAGE	87.5%	12.5%

On average, drain water composition consists of 87.5% rainwater and 12.5% groundwater. As expected, chloride concentrations seem to be inversely related to the discharge of the drains (see Figure 4.3). This is in line with the findings of Delsman et al. (2014), who recently investigated summer flow paths in the parcel area. His results showed that tile drains were fed by a shallow flow system, and preferential discharge of meteoric water during peak discharge, whilst groundwater flows to and from the ditch indicated a deep flow system. Nevertheless, the percentage of rainwater transported by the drains decreases when approaching the end of the ditch, and the proportion of groundwater increases. In drain 8, for instance, nearly 5 times more groundwater is transported via tile drainage than in drain 2. This reinforces the suspect of a shallower fresh-saline groundwater interface near the end of the ditch. These results were used as a reference for the modelling simulation with PHREEQC.

Besides, when we compare the chloride found in the groundwater with the deepest pore water samples, we observe that the concentrations are very similar for the boreholes located in parallel, which are indicated by the same colors in Figure 4.3 (e.g. B1 and B8, B2 and B7). Furthermore, the concentrations of chloride at 4 m depth in boreholes B4 and B5 are very similar to those found at the 9 m depth screen. These boreholes are the ones closest to the groundwater well, in the beginning of the ditch. For the remaining boreholes, chloride concentrations seem to be an intermediate between the concentrations found at 9 and 25 m depth, and increase for the boreholes near the farm. These results suggest that B4 and B5 are fed primarily with groundwater from 9 m depth, whereas the remaining boreholes are fed with groundwater intermediate between that at 9 m and 25 m depth.

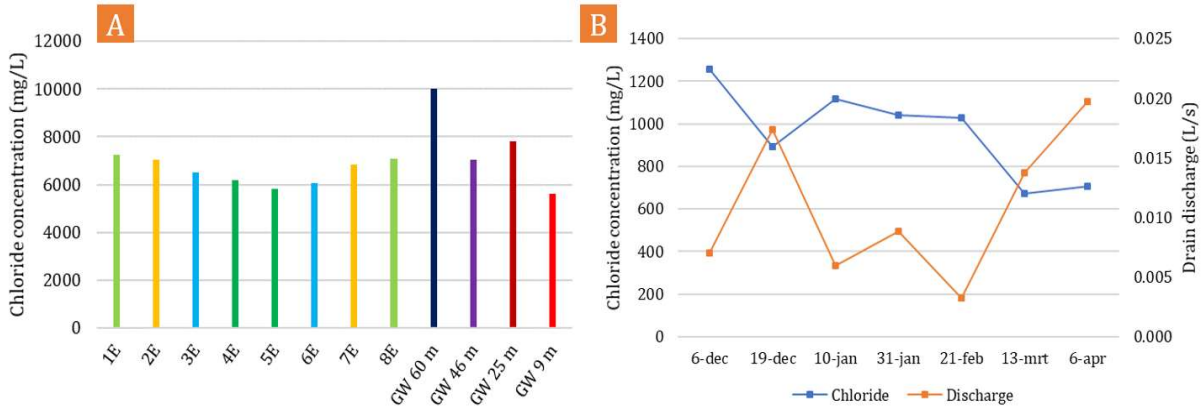

Figure 4.3: Left (A): Comparison between deep pore water (4 m) and groundwater chloride concentrations. The same colors were used for the boreholes located in parallel, evidencing the similarity of chloride concentrations for these boreholes. Right (B): Average discharge and chloride concentration per day of sampling.

4.2.1.2. Drains discharge

Drain discharge varied from 0.003 L/s to 0.035 L/s, with an average of 0.011 L/s. Spatially, discharge seemed to decrease in the drains located at the end of the ditch (see Table 4.4): from drains 1 to 5, the mean discharge was 0.013 L/s, whilst for drains 6 to 10, this value was 0.008 L/s. This decrease may be caused by a reduction in infiltration rate near the farm, where soil composition is presumably more clayish. In terms of temporal variations, the lowest average discharge was recorded in February (0.003 L/s), whereas the highest average happened in April (0.020 L/s) (see Table 4.5).

Table 4.4: Average discharge per drain.

	Drains										
	1	2	3	4	5	6	7	8	9	10	All
Average Discharge (L/s)	0.011	0.012	0.015	0.013	0.011	0.007	0.008	0.008	0.009	0.008	0.011

Table 4.5: Average discharge per day of sampling.

	Average Discharge (L/s)							
	6-dec	19-dec	10-jan	31-jan	21-feb	13-mrt	6-apr	3-mei
Drains	0.007	0.017	0.006	0.009	0.003	0.014	0.020	- *

* Discharge could not be measured this day.

Figure 4.4 compares the drain discharge and the total rainfall (mm) obtained for the Heiloo rainfall station, which is located 3.5 km from the study area. Noticeably the high discharges in December and April followed high precipitation rates, and other measurements also seem to correlate well with the rainfall pattern in the area. The only exception is perhaps the measurement of March, in which the discharge was very high, whilst rainfall was very low.

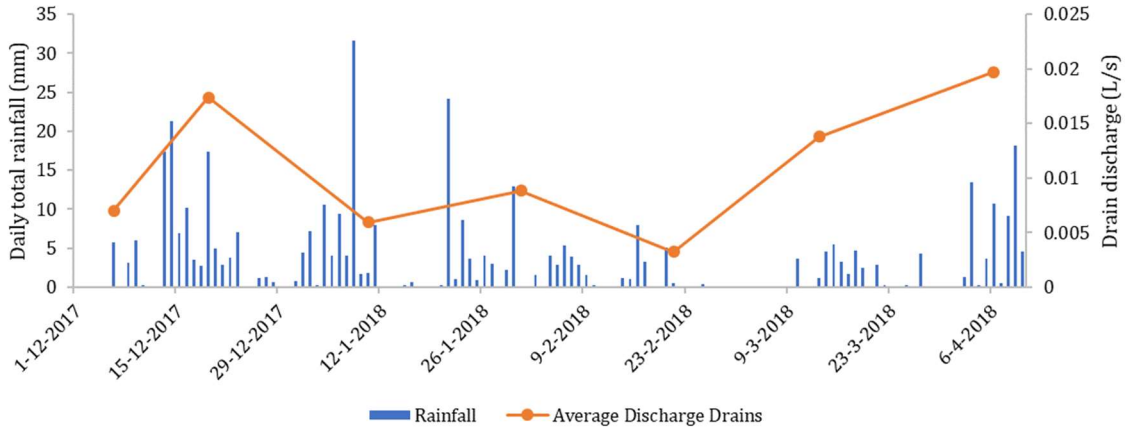

Figure 4.4: Total rainfall (mm) and average drain discharge for the study area. The graph ends in April since no discharge could be measured in May. Rainfall data were obtained from the website of the KNMI (Koninklijk Nederlands Meteorologisch Instituut).

4.2.1.3. Oxygen concentration

Oxygen was measured for the drains, ditch and groundwater samples. In the shallow groundwater, oxygen concentrations averaged 8.5 ± 0.8 mg/L. At B1 and B6, however, lower values as 3.1 mg/L and 5.1 mg/L were recorded. Overall, these were relatively high values, and are presumably attributed to the bubbling that occurred during the pumping. For the deep groundwater, as expected, oxygen was negligible (<0.1 mg/L), indicating anoxic conditions.

Oxygen concentrations in the drains varied from 1.7 mg/L to 7.1 mg/L, with an average of 3.9 mg/L. Spatially, oxygen in drain water seemed to increase towards the end of the ditch, with the lowest value found in drain 1 (2.8 mg/L) and the highest in drain 10 (5.0 mg/L) (see Table 4.6). In terms of sampling period, the lowest averages were found in December and January (3.5 mg/L) and the highest found in March (4.7 mg/L). In May, the actual lowest value was found, but as it refers to only one drain, we cannot use as a representative value, since the concentrations in the other drains are unknown. The results of modelling calculations with PHREEQC show that, the average oxygen partial pressure in the drains is below the atmospheric levels, indicating ongoing oxygen consumption in the drains (see Table 4.9).

For the ditch water samples, the O_2 concentrations were much higher, varying from 2.7 to 22.0 mg/L, with an average of 9.6 mg/L. Opposite to the drains, an expressive difference was found between the sampling dates (see Table 4.7). Whilst at the 10th of January, the average concentration was 2.8 mg/L, in February oxygen averaged 21.9 mg/L. In February, the water was partially frozen, and an excessive amount of algae was presence below the ice layer. This may be the reason why oxygen levels were extremely high on this day. In the spring concentrations were also relatively high, which may be attributed to the extensive growth of grasses and reeds inside the ditch. Oxygen was slightly lower in the middle of the ditch than at the end of it, with mean values of 9.4 mg/L and 9.8 mg/L, respectively.

Table 4.6: Average oxygen concentration per drain.

	Drains											Ditch Middle	Ditch End	Ditch Total
	1	2	3	4	5	6	7	8	9	10	All			
Average oxygen concentration (mg/L)	2.8	3.4	3.3	3.7	4.5	4.6	4.3	4.2	4.2	5.0	3.9	9.4	9.8	9.6

Table 4.7: Average oxygen concentration in drains and ditch samples according to sampling date.

	Average oxygen concentration (mg/L)							
	6-dec	19-dec	10-jan	31-jan	21-feb	13-mrt	6-apr	3-mei
Drains	3.5**	3.5	3.5	4.1	4.4	4.7	3.7	1.7**
Ditch	- *	3.9	2.8	9.0	21.9	7.0	15.7	7.3

* Except for drain 1, temperature and oxygen were measured later this day and, therefore, these values are not reliable.
** Value representative of only one drain (drain 1 in 06/12 and 03/5).

4.2.1.4. Temperature

Temperature was also measured for the groundwater and the surface water samples. For the deep groundwater samples, the temperature was rather constant, ranging between 10.5°C and 11.0°C, with an average of 10.7°C. The shallow groundwater samples, as expected, showed more variability. The temperature range for these samples was 11.6°C to 16.5°C, with an average of 14.0°C.

The temperature in the drains was slightly below that in the ditch water (see Table 4.8), with exception of the sampling in February, when the average drain water temperature was higher than the average ditch one: 5.0^{0}C and 3.6^{0}C, respectively. In April and May, the highest average temperatures were found: 7.6^{0}C and 12.8 ^{0}C in the drains and 10.7^{0}C and 18.5^{0}C in the ditch water samples. Overall, the temperature did not vary much among the drains in a certain sampling day.

Table 4.8: Average temperature in drains and ditch samples according to sampling date.

	Average Temperature (^{0}C)							
	6-dec	19-dec	10-jan	31-jan	21-feb	13-mrt	6-apr	3-mei
Drains	8.9**	10.1	7.4	6.8**	5.0	5.8	7.6	12.8**
Ditch	- *	11.5	7.5	- ***	3.6	5.8	10.7	18.5

* Except for drain 1, temperature and oxygen were measured later this day and, therefore, these values are not reliable.
** Value representative of only one drain (drain 1 in 06/12 and 03/5 and drain 10 in 31/01).
***Ditch water temperature was not measured this day.

4.2.1.5. Carbonate chemistry

Since, pH, alkalinity and Ca are intrinsically related due to carbonate chemistry, they will be presented together in this section. The (calculated) values of alkalinity (as HCO_3^-) for the pore water samples increased with depth, varying from 238.3 ± 37.6 mg/L at 0.75 m and 1182.8 ± 336.6 mg/L at 4 m. The pH values for these samples were much higher than for all the other water types: 8.4 ± 0.2. Such high pH values are not expected for pore water and can be attributed to the excessive CO_2 degassing (Appelo & Postma, 2005) due to the long time between the extraction and preparation of the samples (about 2 weeks). This is evidenced by the high CO_2 partial pressures, with an average of Log P_{CO_2} equal to -2.68 ± 0.33 (see Table 4.9). Upon CO_2 degassing and consequent increase in pH, the speciation of carbonic and phosphoric acid is shifted and there is a tenfold increase of CO_3^{2-} and PO_4^{3-} in solution for each unit of pH rise (Appelo &

Postma, 2005). As a result, the Saturation Index (SI) of some minerals such as vivianite, OH-apatite, calcite, dolomite, and siderite rises, favoring their precipitation. Ultimately the concentrations of phosphate, calcium, and iron, which are elements of main interest in this thesis, are altered and not reliable anymore. This could possibly have affected also the alkalinity calculations, which may be underestimated.

Calcite was supersaturated in pore water, with an average SI of 1.43 ± 0.33. Here, saturated conditions will be referred to when SI is between -0.3 and 0.3, whereas supersaturated to SI above 0.3 and undersaturated when SI is below -0.3 (Griffioen et al., 2013). This value is not reliable given the altered carbonic acid speciation in solution, due to degassing. As a consequence of calcite precipitation, Ca^{2+} concentrations in solution were lowered, especially for the deep pore water samples, where degassing of such an extent is not likely to occur. The average calcium concentration at 0.75 m depth was 115.4 mg/L (60.4 – 162.2 mg/L), whilst at 4 m it was 125.3 mg/L (83.1 – 207.4 mg/L). Despite the similarity between the shallowest and deepest layer, the depth profiles differed notably among the boreholes. For B1, B6, B7, and B8, calcium concentrations increased from 1.25/2 m to 3 m, decreasing at 4 m. Oppositely, in B4 and B5, a drop was observed at 2 m depth, slightly increasing again from 3 m to 4 m. Concentrations in B2 and B3 were sort of constant until 3 m, gently increasing at 4 m depth.

Table 4.9: Saturation Index (SI) for calcite and partial pressures of CO_2 and oxygen for all the water sources, obtained through modelling calculations made with PHREEQC. Reference CO_2 and O_2 partial pressure in equilibrium with the atmosphere are $10^{-3.5}$ and $10^{-0.7}$ atm., respectively.

	SI (Calcite)	Log P_{CO_2}	Log P_{O_2}
Deep groundwater	0.87 ± 0.11	-1.43 ± 0.13	-
Shallow Groundwater	0.19 ± 0.28	-1.77 ± 0.26	-0.74 ± 0.16
Pore water	*1.43 ± 0.33*	*-2.68 ± 0.33*	-
Drains	0.35 ± 0.22	-1.48 ± 0.21	-1.04 ± 0.11
Ditch	0.64 ± 0.20	-1.70 ± 0.23	-0.74 ± 0.30

In the shallow groundwater samples, pH was near neutral, varying from 6.9 to 7.3. Alkalinity (as HCO_3^-) ranged from 518.5 mg/L to 795.4 mg/L, with an average of 641.4 mg/L. For B2, however, a pH of 7.7 and alkalinity of 1287.1 mg/L was registered. B2 also registered the lowest Log P_{CO_2} (-2.2) and the highest SI for calcite (0.81). The average Log P_{CO_2} and calcite SI were -1.77 ± 0.26 and 0.19 ± 0.28, respectively, indicating non-equilibrium CO_2 degassing for the shallow groundwater samples. In terms of calcium concentrations, the range was between 197.9 mg/L to 284.0 mg/L, with an average of 224.9 mg/L. Outside this range, B1 and B7 showed exceptionally high values: 420.0 mg/L and 441.3 mg/L, respectively. For both boreholes, Log P_{CO_2} was also relatively high: -1.65 and -1.47.

In the deep groundwater samples, pH varied between 7.4 and 7.6, being within the range expected for this region (Griffioen et al., 2013). Alkalinity for these samples was the highest among all the water samples, varying from 1671.4 mg/L to 2135.0 mg/L, with an average of 1913.9 mg/L. As such, Log P_{CO_2} was also high (-1.43 ± 0.13), and calcite was supersaturated with an average SI of 0.87 ± 0.11. Such high CO_2 pressures are expected for the Holocene coastal lowlands – where the parcel is located – due to the extensive degradation of marine sedimentary organic matter (Griffioen et al., 2013). Calcium concentrations were lower than those found in the shallow samples and slightly higher than those found in deep pore water, varying between 146 mg/L and 263.3 mg/L, with an average of 200.3 mg/L.

The pH of the drains and ditch water samples was mostly in the neutral range, being slightly higher for the ditch ones (see Table 4.10): pH varied between 6.8 and 7.7 in the drains, with an average of 7.1, whereas the range was between 7.0 to 7.8 in the ditch, with a mean of 7.4. When plotted together with the average discharge per day of sampling, it seems that pH is inversely correlated to discharge (Figure 4.5). This is somehow reasonable: the lower the discharge, the higher is the transient time of water in the drains, and hence, more CO_2 degassing may occur, resulting in higher pH values (Van der Grift et al., 2014). The average alkalinity in the drains varied from 561.9 mg/L to 787.0 mg/L, increasing towards the drains located at the

end of the ditch. A similar trend was observed for the ditch, where alkalinity averaged 730.8 mg/L in the middle and 791.7 mg/L at the end of it. The highest average values for alkalinity were mostly registered during the colder months (see Table 4.10). According to the SI calculations in PHREEQC (see Table 4.9), the average Log P_{CO_2} in the drains was -1.48 ± 0.21, which is far above atmospheric values, indicating non-equilibrium conditions and ongoing CO_2 degassing. As such, calcite SI was also relatively low, with an average of 0.35 ± 0.22. In the ditch, slightly higher values of SI for calcite and lower Log P_{CO_2} were calculated, suggesting that, despite more advanced, CO_2 degassing was still not complete in the ditch. It is worth to mention that, for both drains and ditch water samples, OH-apatite SI was highly variable but mostly saturated to supersaturated, with an average of 0.48 ± 1.44 for the drains and 1.53 ± 1.03 for the ditch.

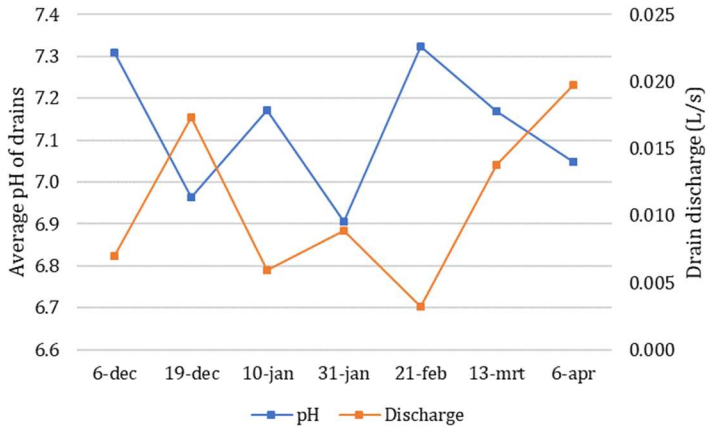

Figure 4.5: Average pH and discharge from drains. As discharge could not be measured in May, the pH results of this sampling date were not included in the graph.

Due to degassing, the pore water concentrations of calcium are not reliable. For comparison purposes, Figure 4.6 shows the mixing lines for calcium and chloride based on (1) shallow pore water and deep groundwater and (2) shallow and deep groundwater. For B2 and B7, as the shallow groundwater samples have high chloride concentrations, only the shallow pore water values were considered. Notably, calcium concentrations in the shallow groundwater are higher than in the pore water, creating a flatter mixing line, in which some of the drain samples are below and some are above it. When considering the mixing line with the pore water concentrations, basically all the drains are above the line, suggesting an increase of Ca^{2+} in water before entering the drains, likely due to dissolution of calcium carbonates. However, this may also be a consequence of the $CaCO_3$ precipitation in the glovebox, resulting in lower Ca^{2+} in the pore water, placing the majority of the drains to be above the mixing line. Calcium levels did not seem to differ significantly between the drains and ditch water samples, averaging 235.0 mg/L (142.9 – 343.8 mg/L) for the drains and 234.3 mg/L (201.7 – 277.8 mg/L) for the ditch ones. This suggests little $CaCO_3$ precipitation, despite supersaturation for calcite. Due to the non-equilibrium conditions in the drains, no correlation between Ca^{2+} and HCO_3^- could be found.

Table 4.10: Left (A): Average pH and alkalinity values for individual drains and ditch. Right (B): Average pH and alkalinity values for drains and ditch samples per day of sampling.

A

	pH	Alkalinity as HCO_3^- (mg/L)
Drain 1	7.0	609.2
Drain 2	7.2	561.9
Drain 3	7.1	608.6
Drain 4	7.1	621.0
Drain 5	7.2	592.7
Drain 6	7.1	605.6
Drain 7	7.1	733.9
Drain 8	7.2	787.0
Drain 9	7.1	728.9
Drain 10	7.2	745.7
Ditch Middle	7.4	730.8
Ditch End	7.4	791.7

B

	pH		Alkalinity as HCO_3^- (mg/L)	
	All drains	Ditch	All drains	Ditch
6-dec	7.3	7.6	752.7	592.4
19-dec	7.0	7.1	635.8	689.3
10-jan	7.2	7.4	730.2	896.7
31-jan	6.9	7.3	682.0	805.2
21-feb	7.3	7.5	659.6	894.3
13-mrt	7.2	7.7	568.5	850.3
6-apr	7.0	7.3	588.0	732.0
3-mei	7.0*	7.1	555.1*	629.5

* Value representative of only one drain (drain 1).

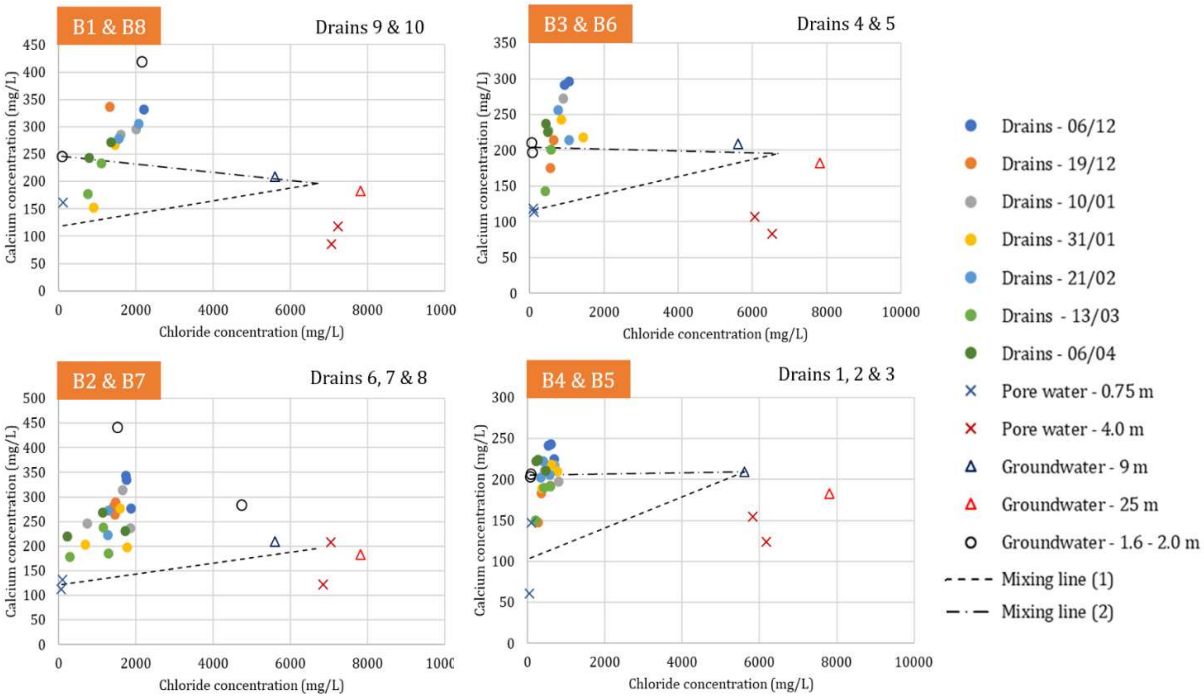

Figure 4.6: Mixing lines for calcium and chloride concentrations. For both mixing lines the average concentrations of groundwater samples collected at 9 m and 25 m depth was used as the endpoint. For B4 and B5, only the concentrations of groundwater at 9 m depth were used, due to flow estimation. The initial point of the mixing line (1) was the shallow pore water concentrations, whereas for the mixing line (2), the shallow groundwater values were used.

4.2.2. Chemical analysis

4.2.2.1. Phosphate

None of the shallowest pore water samples analyzed showed significant concentrations of phosphate (<0.02 mg/L), which is attributed to the degassing of the samples. At different depths, however, some sporadic high concentrations were found. In total, 7 out of 40 samples had PO_4 concentrations between 5 mg/L and 10.7 mg/L. Since some phosphate was lost due to precipitation of phosphate minerals such as OH-apatite and vivianite, as a consequence of CO_2 degassing, we can infer that the initial concentrations for some of these pore water samples could have been even higher than the aforementioned values. Despite the unreliable pore water results, very little phosphate was also found in the fresh shallow groundwater samples (0.08 – 1.2 mg/L) (see Figure 4.7). Higher concentrations were obtained for B1, B2 and B7, where PO_4 varied from 1.1 mg/L to 7.0 mg/L. However, these samples also showed high chloride concentrations and, therefore, are not comparable to the pore water ones. As such, the shallow pore water concentrations of phosphate were still used as the initial point for the mixing line. For the endpoint, however, the concentrations of the groundwater were used, due to the variability and uncertainty regarding the deep pore water values. As illustrated in Figure 4.7, the mixing line traced for phosphate and chloride is very steep and phosphate concentrations in the drains are mostly above the mixing line for the sampling days of January and February. Near the end of the ditch, however, PO_4 concentrations in the drains 9 and 10 are below the mixing line even for those sampling days.

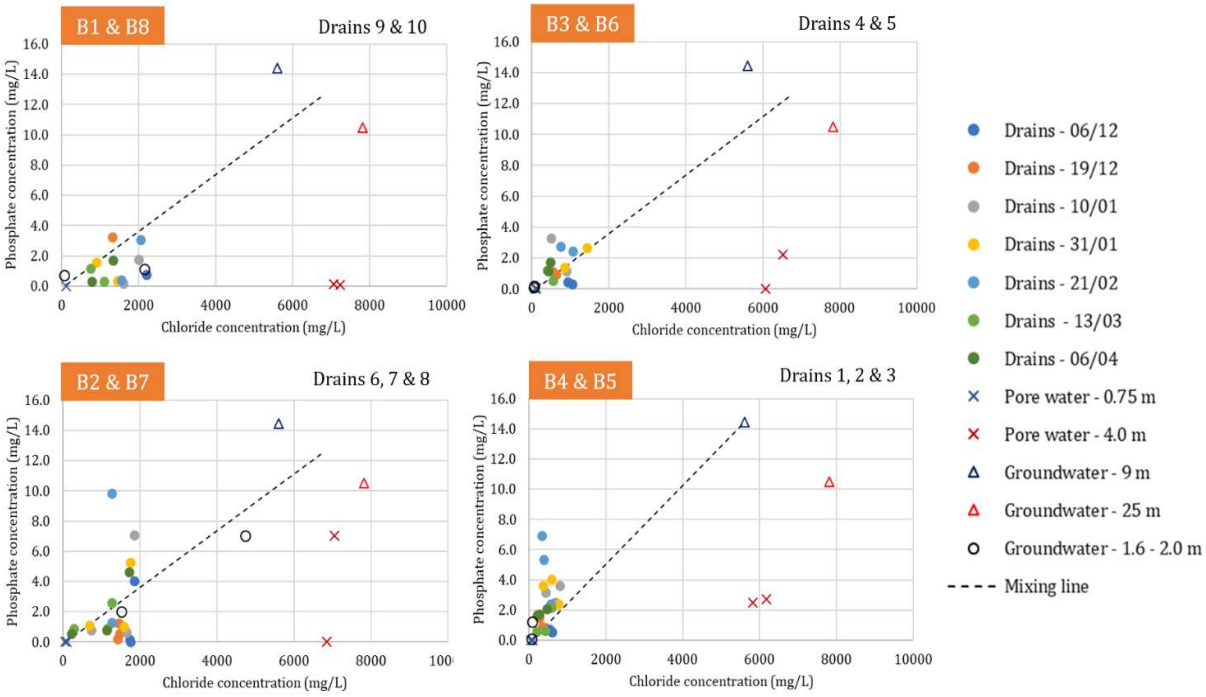

Figure 4.7: Mixing line between shallow pore water (initial point) and the average of groundwater from 9 m and 25 m depth (endpoint) for phosphate and chloride concentrations. For B4 and B5, only the concentrations of groundwater at 9 m depth were used, due to flow estimation.

Different from the pore water, phosphate concentrations in groundwater were much higher. The larger concentrations were found for the samples collected at 9 m and 25 m depth – 14.4 mg/L and 10.5 mg/L – lowering to 6.2 mg/L and 7.2 mg/L at 46 m and 60 m. These results are expected due to the extensive degradation of subterranean marine organic matter, present in the Holocene layer where the study area is located (Griffioen et al., 2013). In this area, according to Griffioen et al. (2013) – who performed an

extensive characterization of the groundwater composition of The Netherlands – the 82.5-percentile of PO_4 is 16 mg/L, indicating nutrient-rich groundwater.

Interestingly, all the phosphorus found in the ditch, drain and shallow groundwater correspond to ortho-PO_4, as indicated by the perfect correlation with an R^2 higher than 0.99 shown in Figure 4.8. The exclusive presence of inorganic soluble phosphorus discards the contribution of organic P from, i.e., manure application. Overall, total P concentrations averaged 0.6 mg/L in the drains and 0.5 mg/L in the ditch. These values are above the suggested limit of 0.15 mg/L for total P established for the Good Ecological Potential (GEP) in the Zuid Schermer (Jaarsma & Van Ee, 2014), in order to accomplish with the good ecological status of the regional water bodies aimed by the Water Framework Directive.

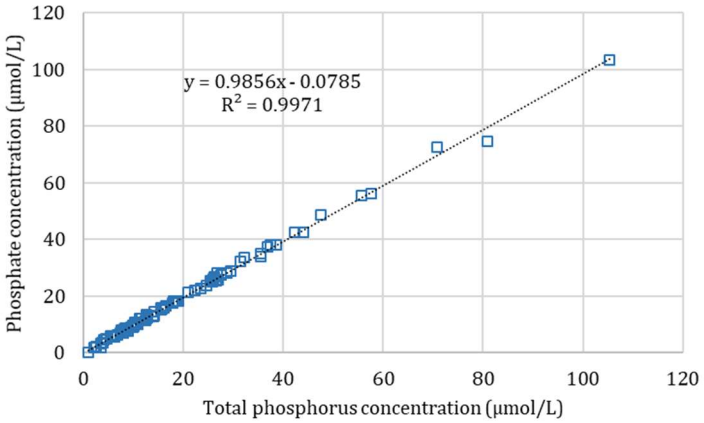

Figure 4.8: Correlation between total P and PO_4 in drains, ditch and shallow groundwater.

Phosphate concentrations in the surface water samples were, for the majority of the sampling days, much lower than those found in the groundwater. Concentrations in the drains were highly variable, with a range from 0.02 mg/L to 9.8 mg/L, and an average of 1.9 mg/L. Interestingly, drain 1 was the only drain where phosphate concentrations were relatively stable. In the ditch, this range was a bit lower, from 0.5 mg/L to 3.6 mg/L, and a mean of 1.6 mg/L. The samples collected in February showed the highest concentrations of PO_4 in drain water, averaging 3.8 mg/L (see Table 4.11). High concentrations were also found in the two samples from January, with mean values of 2.3 mg/L and 2.4 mg/L. For ditch samples, the highest PO_4 concentrations were registered in January and December, with 3.1 mg/L and 2.0 mg/L. For both drains and ditch samples, the lowest phosphate concentrations were found in March.

In terms of spatial differences, the drains with the highest and lowest phosphate concentrations were drains 8 and 6, with 4.4 mg/L and 0.7 mg/L, respectively (see Table 4.12). Low concentrations were also found in drain 9, where average PO_4 was 0.8 mg/L. Phosphate concentrations did not follow a clear spatial pattern but seemed to be higher for the drains located at the beginning of the ditch where the average concentration was 2.4 mg/L. Similarly, the water samples collected in the middle of the ditch showed, on average, almost twice the phosphate concentration of samples collected at the end of it: 2.0 mg/L and 1.1 mg/L, respectively.

Table 4.11: Average PO_4 concentration per sampling day.

	Average PO_4 concentration (mg/L)							
	6-dec	19-dec	10-jan	31-jan	21-feb	13-mrt	6-apr	3-mei
Drains	1.1	1.3	2.4	2.3	3.8	1.1	1.6	1.4*
Ditch	1.5	2.0	3.1	1.5	1.1	1.1	1.2	1.0

* Value representative of only one drain (drain 1).

Table 4.12: Average PO_4 concentration per drain and ditch water samples.

	Drains											Ditch Middle	Ditch End	Ditch Total
	1	2	3	4	5	6	7	8	9	10	All			
Average PO_4 concentration (mg/L)	2.4	2.5	2.4	1.5	1.5	0.7	1.3	4.4	0.8	1.9	1.9	2.0	1.1	1.6

4.2.2.2. Iron

Similar to phosphate, iron concentrations in pore water are also not reliable, due to the likely precipitation of Fe(II) minerals. Basically, no iron was found in none of the pore water samples, where concentrations were majorly below 0.1 mg/L. Nevertheless, the concentrations of Fe in the shallow groundwater were also low (0.03 – 1.2 mg/L), supporting the use of pore water concentrations as the initial point of the mixing line. The only exception was B6, where an exceptional value of 28.5 mg/L was registered. The endpoint of the mixing line was formed by the average concentrations of Fe found in groundwater at 9 m and 25 m depth (see Figure 4.9). For all the cases, the concentrations of Fe in the drain water were higher than the ones represented by the mixing line. For some of the sampling days, these concentrations were even higher than those found in the groundwater, suggesting an additional source of iron in water exfiltrating via the drains.

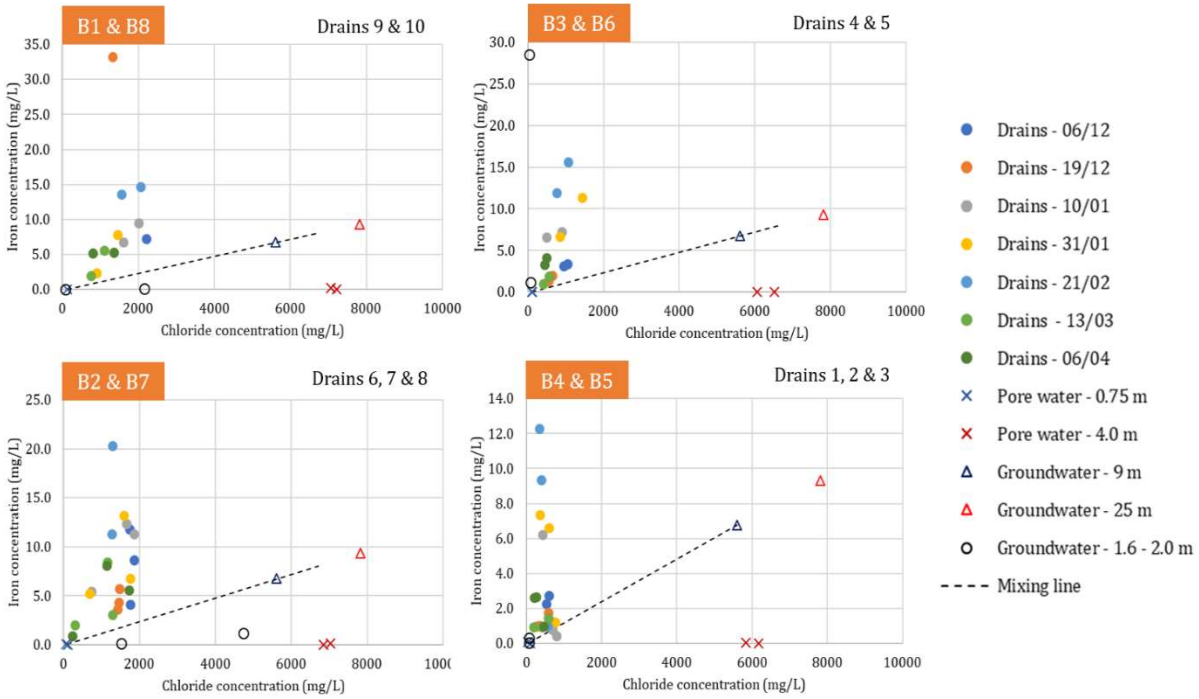

Figure 4.9: Mixing line between shallow pore water (initial point) and the average of groundwater from 9 m and 25 m depth (endpoint) for iron and chloride concentrations. For B4 and B5, only the concentrations of groundwater at 9 m depth were used, due to flow estimation.

In the groundwater samples, however, iron concentrations averaged 6.5 mg/L. At 9 m, Fe concentration was 6.8 mg/L, increasing to 9.3 mg/L at 25 m depth. At greater depths, Fe concentrations were slightly lower, registering 4.6 mg/L at 46 m, and 5.2 mg/L at 60 m.

The concentrations of iron in the drain water samples had a very broad range of values, oscillating between 0.4 mg/L and 33.3 mg/L, with an average of 6.1 mg/L. As observed for phosphate, the concentrations were highly variable in space and time, with exception of drain 1, where Fe concentrations were more stable

among the sampling dates. Despite the great variability, a trend with higher concentrations towards the end of the ditch (see Table 4.13) could be observed. Drain 9 was the one with the highest average concentration, due to the exceptional value of 33.3 mg/L found in December. Despite showing the second highest average, drain 7 had the largest Fe concentrations throughout all the sampling days. In these two drains, the average Fe concentrations were higher than Fe found in any of the groundwater samples. Oppositely, drain 1 showed the lowest average value, only 1.4 mg/L. Another pattern was also observed among the sampling dates: the highest levels of iron in drain water were found for the coldest months, averaging 6.9 mg/L in January and 12.2 mg/L in February (see Table 4.14). In February, with exception of drain 1, all the other drains showed Fe concentrations above those found in groundwater samples of both 9 m and 25 m depth. The lowest concentrations were found during the spring, with 2.7 mg/L in March and May, and 3.9 mg/L in April.

The ditch water samples showed considerably less iron, with a range from 0.1 mg/L to 2.7 mg/L and an average of 0.9 mg/L. Iron concentrations were slightly lower in the middle of the ditch than at the end of it: 0.8 mg/L and 1.1 mg/L, respectively. The lowest concentrations in the ditch were found in February and April, with 0.3 mg/L and 0.2 mg/L.

Table 4.13: Average Fe concentration per drain and ditch sample.

	Drains											Ditch Middle	Ditch End	Ditch Total
	1	2	3	4	5	6	7	8	9	10	All			
Average Fe concentration (mg/L)	1.4	4.0	4.2	5.0	6.4	5.2	10.7	6.6	11.4	6.8	6.1	0.8	1.1	0.9

Table 4.14: Average Fe concentration per sampling day.

	Average Fe concentration (mg/L)							
	6-dec	19-dec	10-jan	31-jan	21-feb	13-mrt	6-apr	3-mei
Drains	4.9	6.0	6.7	6.9	12.2	2.7	3.9	2.7*
Ditch	1.2	1.3	2.3	0.3	0.3	1.1	0.2	0.7

* Value representative of only one drain (drain 1).

The water samples of the 21st of February were also analyzed regarding its percentage of Fe^{2+}. The results pointed out that, on average, 96.3% of the total Fe of the drain water was Fe^{2+}. For the ditch water, this percentage was slightly lower: 69.8%. These results were used as an input in PHREEQC to better estimate the redox potential based on the redox couple Fe(II)/Fe(III) for the calculations of the SI of the main minerals prone to precipitation in the drains and ditch.

4.2.2.3. Dissolved Organic Carbon (DOC)

As illustrated in Figure 4.10, DOC concentrations did not vary significantly among the shallowest and deepest pore water samples, which resulted in a mixing line with a very flat slope. In general, the concentrations at 4 m were also very similar to those found in the groundwater at 9 m and 25 m depth. Both the drain water and the shallow groundwater samples showed DOC concentrations below the mixing line, indicating the possible consumption of organic matter between the surface and 2 m depth. The only exception occurred in the 10th of January, when DOC concentrations in the drains were extremely high, being above the values found for both pore water and groundwater samples.

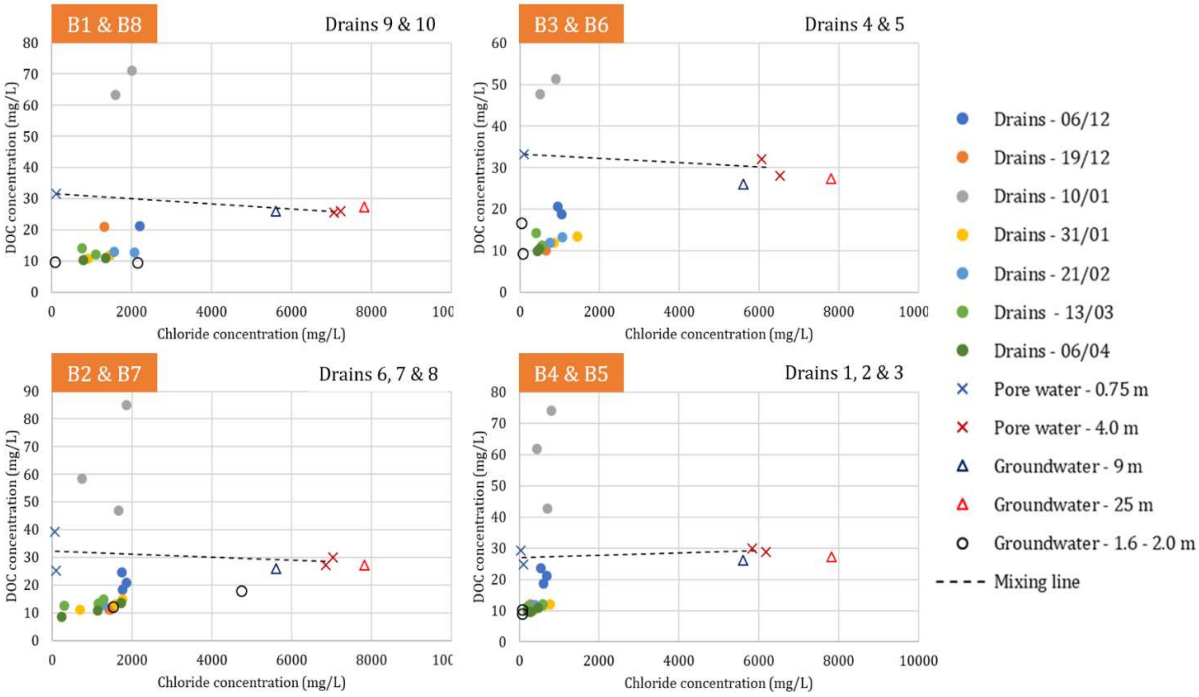

Figure 4.10: Mixing line between the average of shallow and deep pore water samples for DOC and chloride concentrations.

For most of the pore water samples, the average concentration of DOC was high at 0.75 m depth and decreased until 2 m depth, averaging 30.6 ± 5.5 mg/L and 25.8 ± 4.6 mg/L, respectively. For B6 this decrease was the most evident, which may indicate the degradation of DOC during downward transport. Even though the shallowest and deepest pore water samples showed similar concentrations, the depth profiles of DOC varied considerably between 2 m and 4 m depth, and a single pattern was not identified. In general, DOC concentrations slightly increased down to 4 m depth, where the average concentration was 28.4 ± 2.2 mg/L (see Figure 4.11).

In the shallow groundwater samples, DOC concentrations were similar to those found in the drains, varying from 9.1 to 17.9 mg/L, with a mean of 11.9 mg/L. In deep groundwater, these values were higher and decreased with depth, showing an average of 24.2 mg/L (19.2 – 27.3 mg/L).

No major differences were found between drains and ditch water, with DOC values of 13.6 ± 3.8 mg/L and 15.1 ± 3.4 mg/L, respectively (see Figure 4.11). As said before, DOC concentrations were exceptionally high at the 10th of January, with an average of 60.4 mg/L in the drains and 55.9 mg/L in the ditch samples.

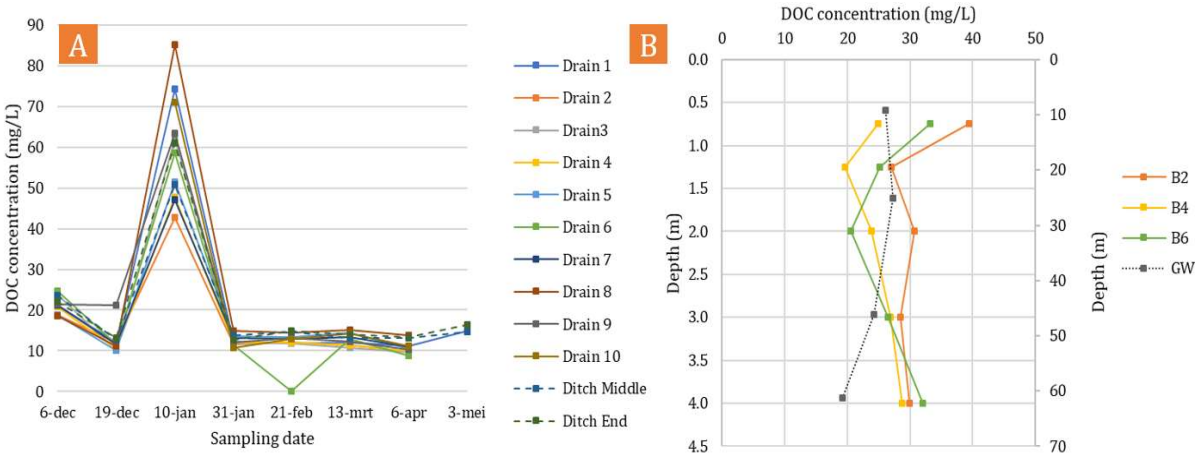

Figure 4.11: Left (A): Temporal data set of DOC concentration in drains and ditch water. Right (B): DOC depth profile for selected boreholes and for groundwater (GW).

4.2.2.4. Ammonium and nitrate

Different from DOC, ammonium (NH_4) concentrations varied significantly among the shallow and deep pore water samples, indicated by the steep slope of the mixing line (see Figure 4.12). Besides, higher ammonium concentrations were found at 4 m depth, than at 9 m and 25 m in groundwater. The shallow groundwater and drain samples collected near the beginning of the ditch are pretty much on the mixing line, suggesting a conservative behavior of NH_4 in this zone of the parcel. For the drains 6 to 10, however, NH_4 concentrations are slightly below the mixing line, indicating possible ammonium consumption prior to entering the drains.

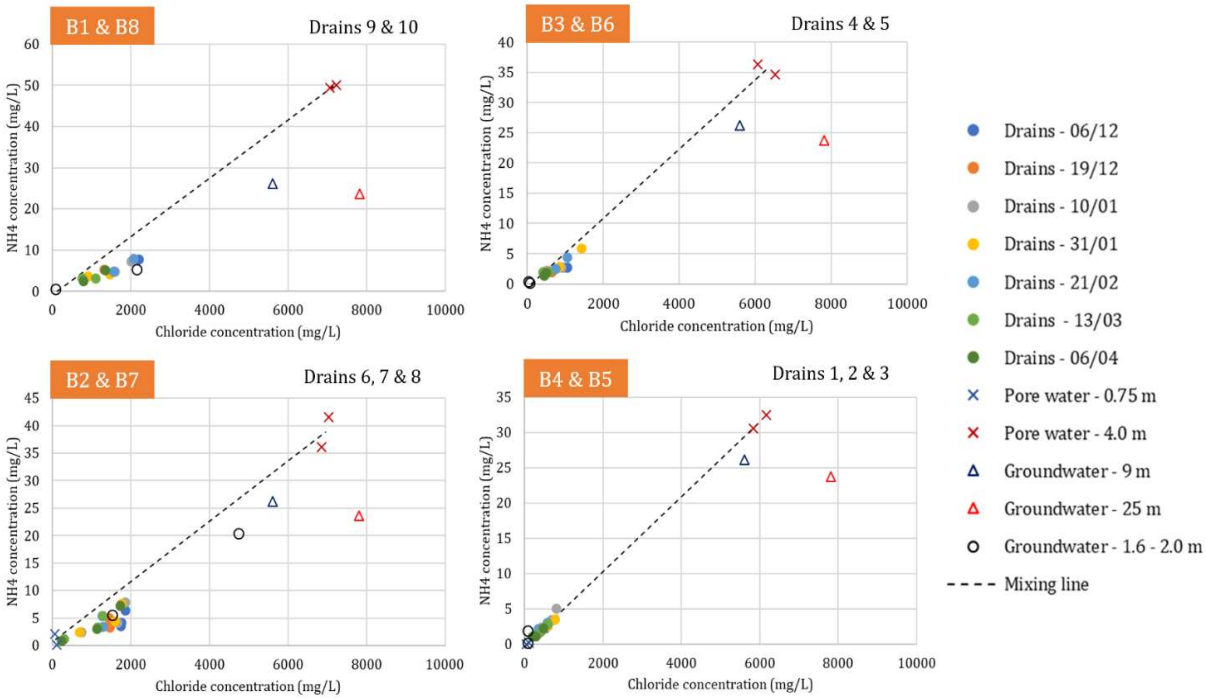

Figure 4.12: Mixing line between the average of shallow and deep pore water samples for NH_4 and chloride concentrations.

The NH_4 and chloride depth profiles were very similar, with very low concentrations near the surface and increasing concentrations with depth. In fact, ammonium and chloride are very well correlated, with an R^2 equal to 0.94 (Figure 4.13). These results suggest that NH_4 likely originated from deep, natural sources, instead of agricultural practices. At 0.75 m depth, NH_4 concentrations varied from 0 to 2.1 mg/L, with an average of 0.6 mg/L. At 4 m, these concentrations increased to a mean value of 38.9 mg/L, and a range between 30.6 mg/L to 50 mg/L. Overall, ammonium concentrations in B1, B2, and B8 were higher than those found in other boreholes. The high concentrations of ammonium in the pore water samples indicate reduced conditions (Christensen et al., 2000), thereby, discarding the chances of oxidation of the samples and reinforcing the suspects of CO_2 degassing.

Opposite to NH_4, nitrate concentrations in pore water were, overall, very low, remaining near 0 for the majority of the samples. Nevertheless, few exceptions are recognizable. For B4, B7, and B8, nitrate concentrations were relatively high at 0.75 m: 6.3 mg/L, 10.1 mg/L, and 8.9 mg/L, respectively. B6 and B7 also registered some nitrate at 1.25 m depth, with 2.3 mg/L and 1.7 mg/L. Concentrations close to 1 mg/L were also found between 3 m and 4 m depth for B2, B6, B7, and B8. As these samples were not acidified for analysis, it is possible that some ammonium had oxidized after the samples were taken out of the glovebox.

In the groundwater samples, ammonium concentrations seem to be more constant, oscillating between 23.7 mg/L and 29.2 mg/L (see Figure 4.13). These are high values, indicating nutrient-rich groundwater, which is expected for the region of the study area (Griffioen et al., 2013). In the shallow groundwater, NH_4 was relatively high for the boreholes where chloride concentrations were also high, varying from 5.3 mg/L to 20.4 mg/L. For the other boreholes, ammonium concentrations were much lower, varying between 0.2 mg/L and 1.9 mg/L, with an average of 0.6 mg/L. No nitrate was found at any depth in the deep groundwater samples. Equally, no nitrate was found in the shallow groundwater collected from B3, B6, and B7. For the remaining boreholes, nitrate concentrations varied from 0.3 mg/L to 1.9 mg/L.

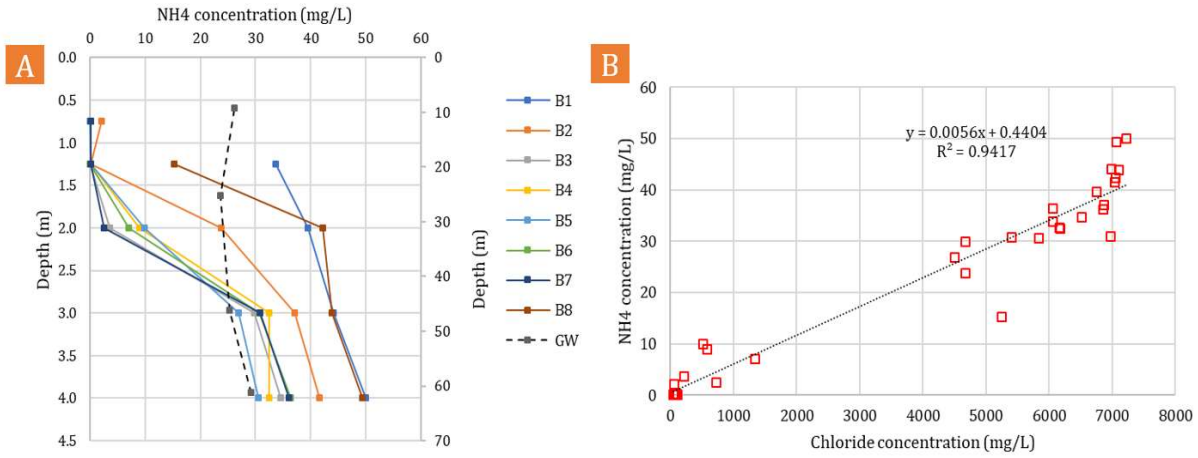

Figure 4.13: Left(A): NH_4 depth profile for pore water and groundwater (GW). B1 and B8 have no measurements at 0.75 m, due to lack of sample volume. Right(B): Correlation between chloride and NH_4 concentrations in pore water samples.

Among the surface water samples, the highest NH_4 concentrations were found in the ditch water, with a range from 1.2 mg/L to 9.3 mg/L, and an average of 6.2 mg/L. The results also show that these concentrations increased when approaching the farm (see Figure 4.14). The same pattern could be observed for the drains: the ones located closest to the end of the ditch showed higher NH_4 concentrations. Ammonium concentrations in the drains varied from 0.9 to 7.9 mg/L, with an average of 3.5 mg/L. Since ammonium seems to originate from deep, natural sources, there will be a greater load of NH_4 into the ditch, which has a larger contribution of groundwater if compared to the drains. Besides that, the shallower fresh-saline groundwater boundary near the farm is likely to be responsible for more NH_4 present at the end of

the ditch and also in the drains located in this zone of the parcel. These suspects are supported by the high correlation between Cl and NH_4 (R^2=0.79) in the drains (see Figure 4.14). Regarding nitrate, concentrations were mostly below 1 mg/L in the drains for all the sampling days, except the 19th of December, the 13th of March and the 3rd of May. For the first two, the average NO_3 concentrations in the drains were 1.2 mg/L and 3.1 mg/L. In May, drain 1 showed 10.4 mg/L of nitrate. Only in May, $NO_3$was also high in the ditch, averaging 6.3 mg/L. For the other dates, the average nitrate concentrations in the ditch remained low (<1 mg/L). Even though some nitrate was found in the drains and ditch, these values were, overall, much lower than the limit of 50 mg/L established by the European Nitrate Directive (1991).

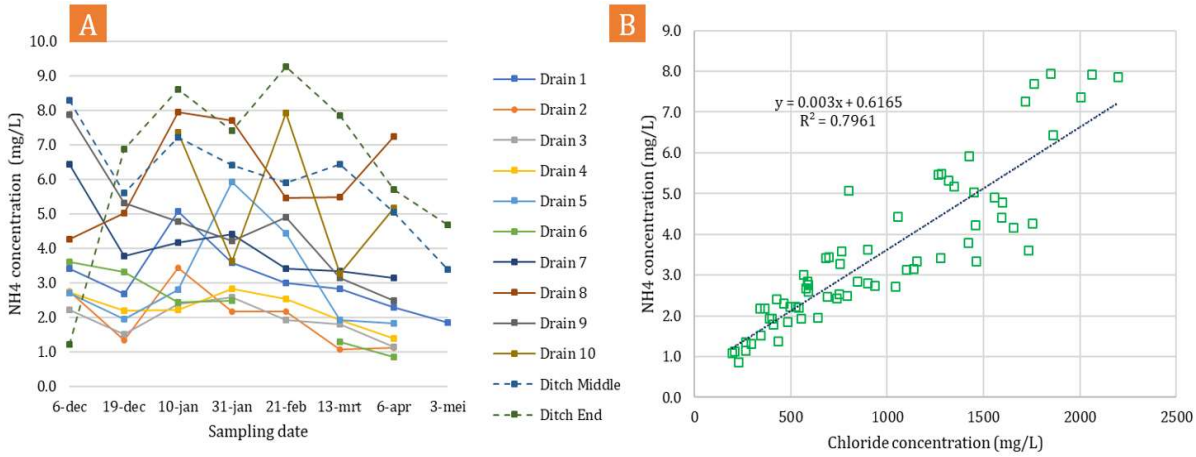

Figure 4.14: Left (A): Temporal data set of NH_4 concentration in drains and ditch water. Right (B): Correlation between chloride and NH_4 concentrations in drain samples.

4.2.2.5. Sulfate

Sulfate concentrations varied considerably for the pore water samples, both in the shallow and deep layers (see Figure 4.15). As this variability was larger for the deep pore water samples, the SO_4 concentrations in groundwater were used as the reference to create the endpoint of the mixing lines. However, basically no SO_4 was observed in groundwater from 9 and 25 m depth, which suggests that the sulfate present in drains and pore water may be originated from processes occurring in the shallow subsurface, such as pyrite oxidation. The sulfate concentration in the shallow pore water of B8 was much higher than for the other boreholes, resulting in a steeper mixing line. Consequently, this was the only case in which the majority of the drain water samples were positioned below the mixing line, possibly indicating SO_4 reduction conditions prior to the exfiltration via the drains. For the remaining boreholes, the concentration of SO_4 in the drains was majorly above the mixing line, suggesting the release of sulfate into drain water. The shallow groundwater samples were either above or below it, varying according to each case.

Several unusual features were observed for the sulfate results in the pore water depth profile (see Figure 4.16). The first of them was the discrepancy of the values found at 0.75 m depth. As an example, whilst SO_4 concentration was 18.4 mg/L in B5, in B8 it was 212.7 mg/L. For the remaining boreholes, at this depth, sulfate averaged 82.3 mg/L (56.5 – 105.9 mg/L). From 1.25 m to 4 m, SO_4 profile differed markedly among the samples. For B1, B8, and B6, sulfate concentrations decreased until 3 m, and increased to above 100 mg/L at 4 m, indicating possibly incomplete sulfate reduction. For the remaining boreholes, SO_4 increased until 2 m depth and decreased from 3 m to 4 m, except for B7, where it increased again. A different case happened at B2, where SO_4 gently increased at 1.25 m, further decreasing almost linearly with depth. The average SO_4 concentration at 4 m was 91.2 mg/L, with high variability between the samples, ranging from 2.7 mg/L to 302.6 mg/L.

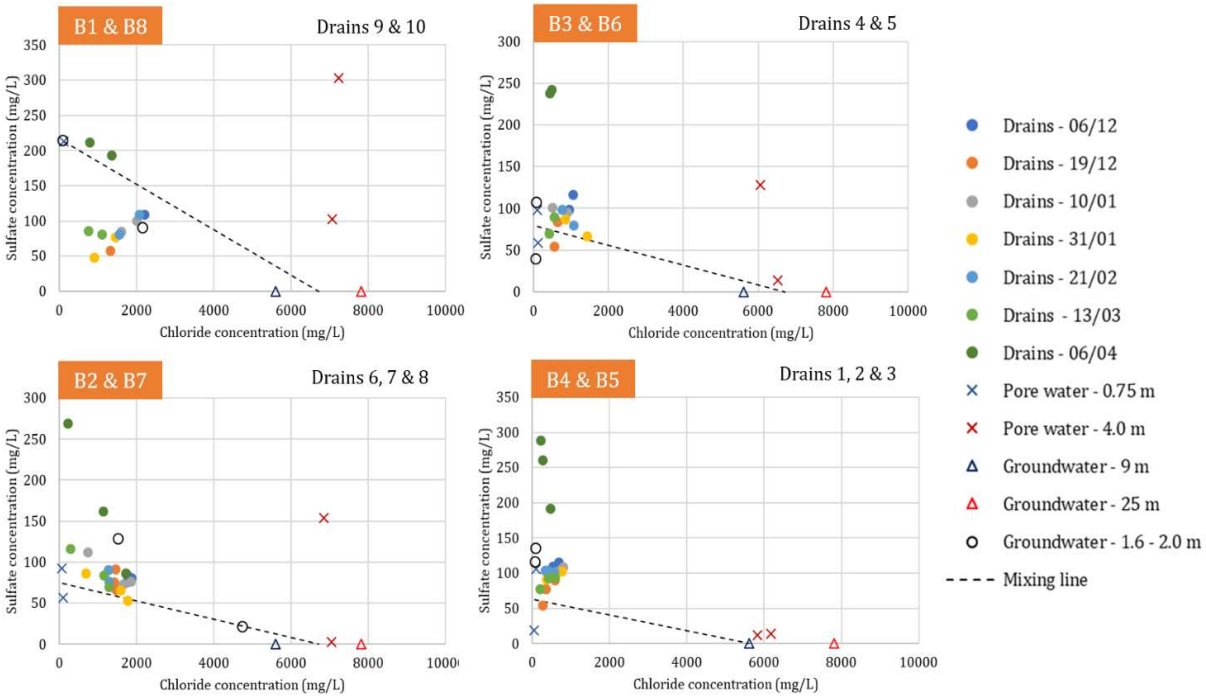

Figure 4.15: Mixing line between shallow pore water (initial point) and the average of groundwater from 9 m and 25 m depth (endpoint) for sulfate and chloride concentrations. For B4 and B5, only the concentrations of groundwater at 9 m depth were used, due to flow estimation.

As said before, groundwater from 9 m to 46 m depth showed no sulfate (<0.2 mg/L). At 60 m depth, however, the sulfate concentration was 169.9 mg/L. At such depth, groundwater is very old, and the SO_4 present presumably originates from seawater (Griffioen et al., 2013). In the shallow groundwater, most of the samples showed high sulfate concentrations, which ranged from 90.8 mg/L to 215.2 mg/L. At B2 and B6, however, SO_4 concentrations were lower with 22.1 mg/L and 39.6 mg/L, respectively.

Sulfate concentrations were usually higher and more variable in the drains than in the ditch, with a range of 47.9 to 117.0 mg/L and 62.2 to 78.8 mg/L, respectively. Overall, sulfate concentrations in drain water appeared to decrease towards the end of the ditch direction. Apart from this range, unusual high SO_4 was registered in the samples of April and May (see Figure 4.16), where concentrations went up to 289.1 mg/L in the drains and 147.6 mg/L in the ditch.

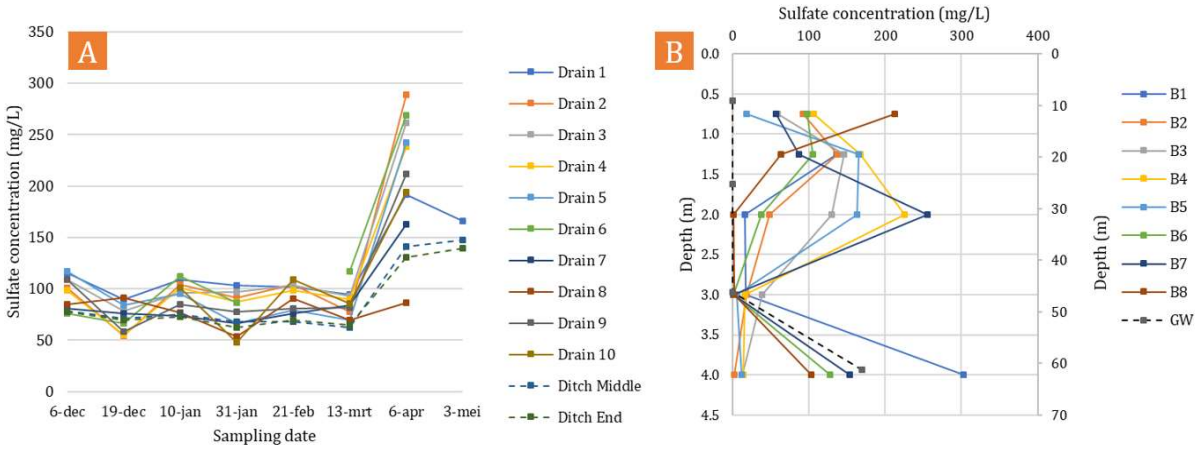

Figure 4.16: Left (A): Temporal data set of sulfate concentration in drains and ditch water. Right (B): Sulfate depth profile of all pore water and groundwater samples.

4.2.2.6. Magnesium, sodium and potassium

Magnesium, sodium, and potassium concentrations were closely related to chloride concentrations in all the water samples analyzed, which is evidenced by the high correlation coefficients (R^2>0.9) as shown in Figure 4.17. Given that high Cl, Na, K, and Mg concentrations are typical of seawater (Frapporti et al., 1993), the results indicate that these elements are coming from upward flows of salt water originally infiltrated in the coastal dune area and exfiltrating in the polder (Delsman et al., 2014), and cation-exchange processes due to saline/fresh groundwater displacement in the parcel area (Griffioen et al., 2013).

In the pore water samples, the concentrations of all three elements increased with depth, following the pattern observed for chloride. At 0.75 m, Mg, K, and Na concentrations were, on average, 8.7 ± 3.2 mg/L, 1.8 ± 1.4 mg/L and 39.1 ± 6.9 mg/L, respectively. At 4 m depth, these concentrations increased to 395.4 ± 26.4 mg/L, 164.1 ± 24.1 mg/L and 3731.3 ± 249.2 mg/L, respectively. Similarly, in groundwater these element concentrations also increased with depth. The concentrations of Mg, K, and Na at 9 m were similar to those found in pore water at 4 m depth. At 60 m, these concentrations increased considerably, registering 616.2 mg/L for Mg, 186.3 mg/L for K, and 5718 mg/L for Na.

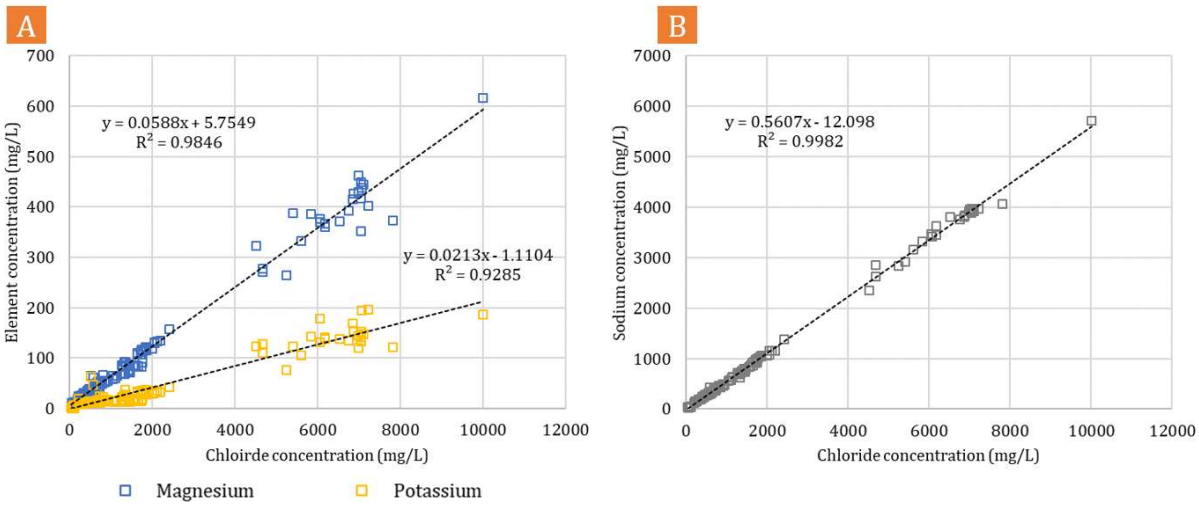

Figure 4.17: Correlation between the concentrations of chloride and the concentrations of magnesium, potassium, and sodium in all the water samples analyzed.

In the shallow groundwater samples with low chloride, Mg, K, and Na concentrations were, on average, 19.5 ± 7.9 mg/L, 6.6 ± 5.6 mg/L, and 43.6 ± 11.1 mg/L, respectively. For the ones with high chloride, these concentrations increased to 150.9 ± 107.6 mg/L, 41.0 ± 20.1 mg/L, and 1493.6 ± 987.9 mg/L.

In the drains, the average concentration of these elements was nearly half of those found in ditch water. In the drains, the concentrations of Mg, K, and Na averaged 59.5 ± 28.7 mg/L, 16.1 ± 5.9 mg/L, and 525.9 ± 293.8 mg/L, respectively. In the ditch, these concentrations were 112.0 ± 22.3 mg/L, 32.7 ± 5.2 mg/L, and 958.4 ± 217.8 mg/L. The higher concentrations of Mg, K, Na, and also Cl in the ditch can be ascribed to the larger contribution of groundwater exfiltration in the ditch than in the drains, as previously discussed (see Section 4.2.1.1.).

4.3. Sediment analysis

4.3.1. Phosphorus

4.3.1.1. Validity of the SEDEX extraction

Total P (TP) was measured via SEDEX extraction and aqua regia destruction. Overall, the SEDEX extraction results were higher than those found via aqua regia as observed in Figure 4.18. Nevertheless, the results from both procedures were well correlated, with an R^2 of 0.99.

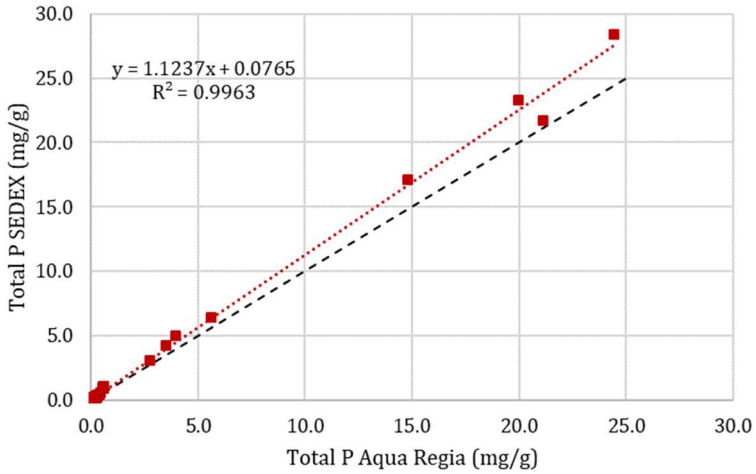

Figure 4.18: Correlation of total P extracted via SEDEX and via aqua regia destruction for all the solid samples analyzed.

In the sediment depth profile, the average total phosphorus content between 0.75 m and 4 m was 0.27 mg/g via SEDEX and 0.23 mg/g via aqua regia, accounting for a difference of 13%. For the topsoil, however, a systematic difference of up to 50% was found for all the samples analyzed. For these samples, total phosphorus extracted via aqua regia and SEDEX were 0.57 mg/g and 1.0 mg/g, respectively.

For the ditch sediment samples, total P extracted via SEDEX and aqua regia destruction averaged 4.7 mg/g and 3.9 mg/g, respectively. This gives a difference of nearly 17% between the extractions. For the drain samples, TP averaged 22.6 mg/g for the SEDEX method and 20.1 mg/g for aqua regia, resulting in a difference of 11.8%.

Despite the large differences between the methods for the shallow soil samples, the SEDEX results seem to be reliable and appropriate for determining the phosphorus fractionation in the sediment samples and, therefore, the results from this method will be used for the next sections of this thesis.

4.3.1.2. Soil profile

Total P content of the soil profile was, in general, low and with little variations between 0.75 m to 4 m depth. The only exception was B2, where a peak was registered at 1.25 m (see Figure 4.19). The average TP was the highest at the topsoil, with 1.0 ± 0.06 mg/g, decreasing to 0.20 ± 0.03 mg/g at 4 m depth.

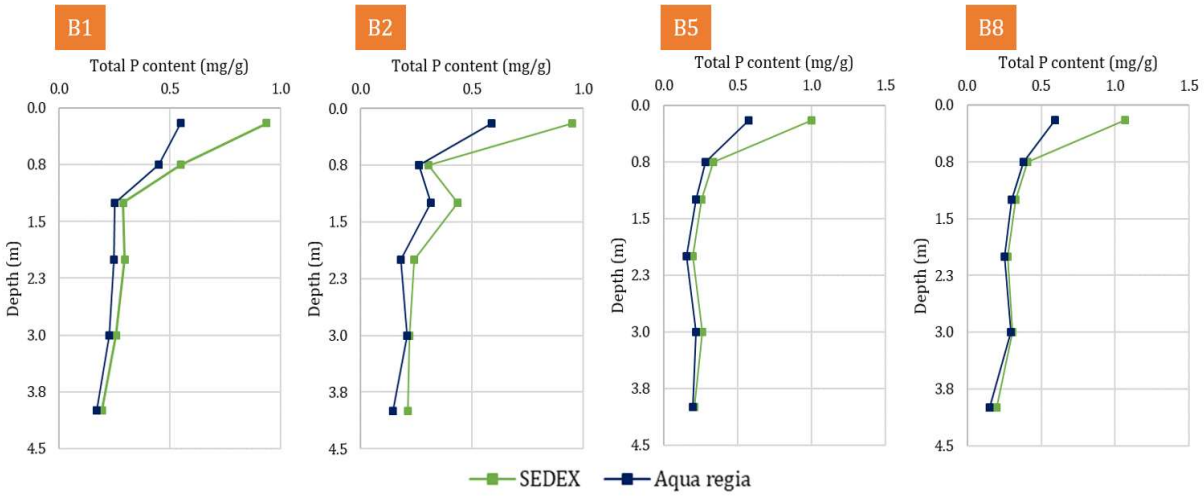

Figure 4.19: Depth profile of total P content from SEDEX and aqua regia for selected boreholes.

Figure 4.20 depicts the different P fractions found in the sediment via the SEDEX analysis and Figure 4.21, the TP based on the average percentage of each fraction extracted. Even though the results vary among different boreholes, some general patterns could be observed. In the shallow soil samples, the Fe-P was the dominant fraction (0.43 mg/g – 0.58 mg/g), comprising 50.7% of total P. On average, Org-P (0.16 – 0.18 mg/g) constituted 17.1% of TP in the topsoil, followed by Ca-P (0.13 – 0.20 mg/g) which accounted for 16.5%. Detr-P (0.11 – 0.13 mg/g) corresponded to 11.8% of total P, whilst Exch-P (0.03 – 0.05 mg/g) accounted for solely 3.9% of the total P extracted in the shallow soil samples.

From 0.75 to 4 m depth, Detr-P (0.08 – 0.20 mg/g) was the dominant form of phosphorus. The only exceptions were B1, in which Fe-P was still the prevailing P form at 0.75 m, and B2, where Fe-P peaked at 1.25 m depth. Comprising on average, 50.6% of the TP, Detr-P was nearly constant throughout the sediment column. Calcium-bound P (0.03 – 0.13 mg/g) and Fe-P (0.03 – 0.17 mg/g) were the second and third main P forms, accounting for, on average, 23.1% and 20.3% of the total P extracted, respectively. The Org-P fraction (0.004 – 0.11 mg/g) accounted for only 4.5% of total P, and decreased in all boreholes from 0.17 mg/g, on average in the topsoil, to 0.03 mg/g at 0.75 m depth. At B1, exceptionally, Org-P content was still relatively high at 0.75 m depth (0.11 mg/g). In general, at 0.75 m, B1 showed higher P content than other boreholes. Constituting only 1.5% of total P, Exch-P content was negligible throughout the entire depth profile (0.0007 – 0.01 mg/g).

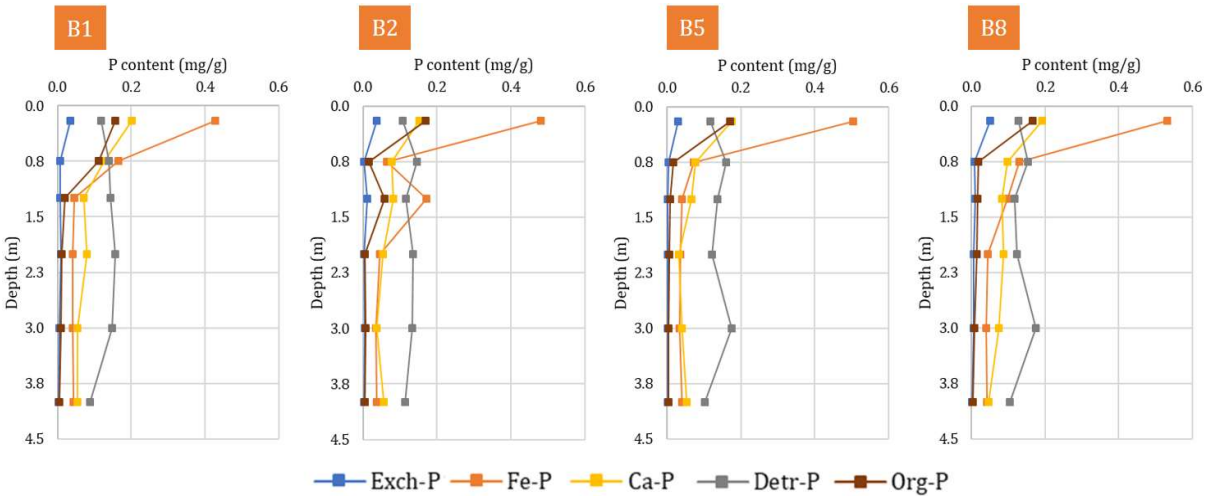

Figure 4.20: Depth profile of P content of all the fractions extracted with SEDEX for selected boreholes.

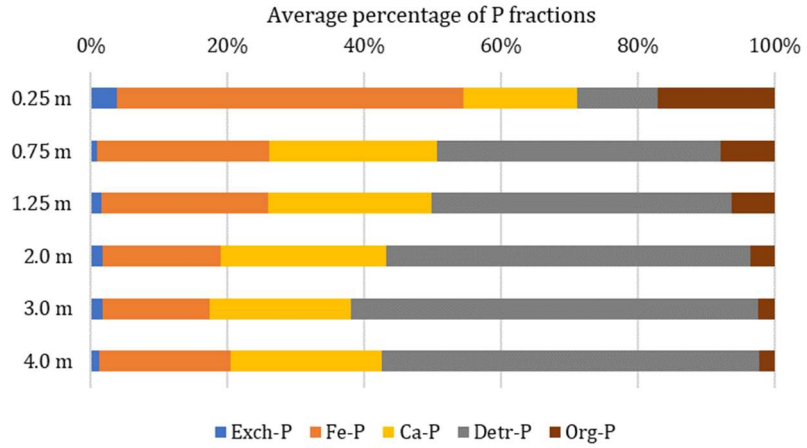

Figure 4.21: Total P composition as the average percentage of each fraction extracted from the soil samples.

4.3.1.3. Ditch bottom sediments

With an average of 4.67 mg/g (3.05 – 6.41 mg/g), the content of phosphorus in the ditch sediments was approximately 17 times higher than those found throughout the soil profile (0.75 – 4 m). The Fe-P fraction (2.33 – 5.44 mg/g) dominated the ditch sediments phosphorus, accounting for 80.8% of the TP extracted (see Figure 4.22). Next to it, Org-P (0.35 – 0.46 mg/g) constituted 9.4% of the total P. Calcium-bound P (0.20 – 0.27 mg/g) contributed to 5.5% of TP, whilst Detr-P (0.10 – 0.11 mg/g) was 2.4% of TP. Again, the lowest fraction was Exch-P (0.05 – 0.13 mg/g), which accounted for only 1.9% of the total P extracted. For TP and all the fractions extracted, with exception of Detr-P, concentrations were higher in the sediments obtained in February and collected at the end of the ditch (see Figure 4.22).

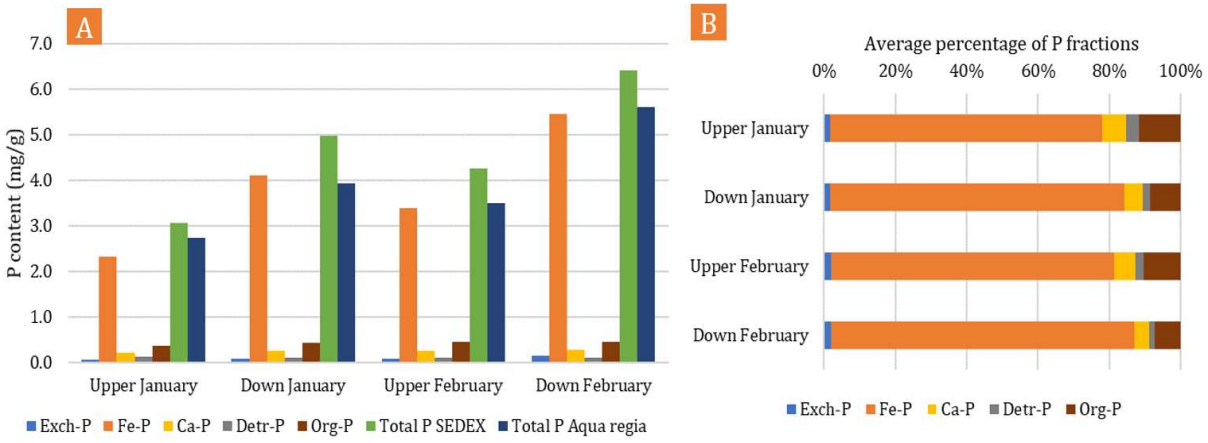

Figure 4.22: Left (A): TP and P content in all the fractions extracted with SEDEX and aqua regia for all ditch samples. Right (B): Total P composition as the average percentage of each fraction extracted from the ditch samples.

4.3.1.4. Drain particulates

With an average of 22.6 mg/g (17.13 – 28.38 mg/g), TP content in the drain slurry was nearly 5 times higher than in the ditch sediments and more than 80 times higher than in the soil column (0.75 – 4 m). Total P content decreased from drain 2 to drain 7, increasing again in drain 10. Accounting for 96.2% of the total phosphorus extracted in the drains, the Fe-P fraction (16.34 – 27.26 mg/g) was by far the prevailing P form (see Figure 4.23). The highest and lowest Fe-P concentrations were found for drains 2 and 7, whereas

drains 4 and 10 had similar results. Org-P (0.27 – 0.52 mg/g) and Ca-P (0.20 – 0.53 mg/g) constituted 2.0% and 1.5% of the total P, respectively. Ca-P contents decreased from drain 2 to drain 10, and Org-P was similar for all drains, except drain 10, in which Org-P content was nearly half of that for the other drains. Detrital P (0.03 – 0.06 mg/g) and Exch-P (0.01 – 0.07 mg/g) were the lowest phosphorus forms found in the drain particulate material, accounting each for 0.2% of TP.

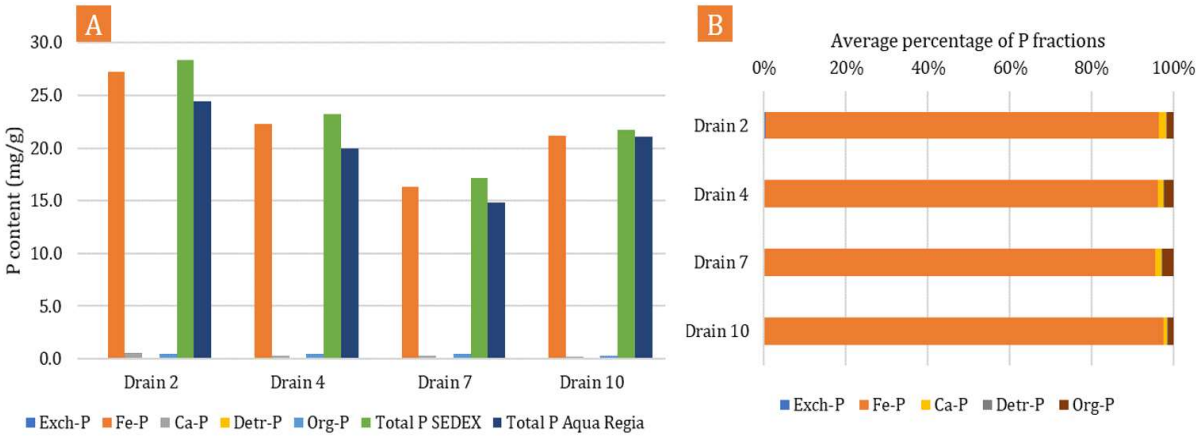

Figure 4.23: Left (A): TP and P content in various fractions extracted with SEDEX and aqua regia for all drain samples. Right (B): Total P composition as the average percentage of each fraction extracted from the drain samples.

4.3.2. Iron

Iron was extracted from the sediment via both the extraction procedure described in Claff et al. (2010) and aqua regia destruction. As only three out of the six steps described at Claff et al. (2010) were performed (see Section 3.2.5), it was not possible to validate the total Fe concentrations as it was done for the P extraction. However, it was possible to estimate the equivalent proportion of the extracted phases in the total Fe content of the samples.

4.3.2.1. Soil profile

For all the boreholes analyzed, total Fe was the highest at the topsoil, varying between 24.0 mg/g to 30.6 mg/g, with an average of 28.4 mg/g (see Figure 4.24). For the majority of the boreholes, total Fe rapidly decreased to 10.0 ± 0.7 mg/g at 0.75 m, with exception of B1, where 20.4 mg/g was registered at this depth. Overall, from 0.75 m to 4 m, Fe content was lower and less variable, averaging 4.6 ± 0.5 mg/g at 4 m. A slightly different pattern was observed for boreholes B2 and B7, where a peak of Fe was found at 1.25 m depth.

Throughout the depth profile, the majority of total Fe was constituted by fractions not extracted during the Fe extraction, such as Fe attached to organic matter and clay minerals, or Fe bound as pyrite (see Figure 4.25). Besides the undetermined Fe fractions, the prevailing form of iron varied significantly throughout the depth profiles (see Figure 4.26). In the shallow soil samples, Fe(III) from crystalline (8.3 – 9.7 mg/g) and amorphous (5.2 – 6.0 mg/g) iron oxides were the prevailing Fe form, accounting for 31.8% and 19.8% of the total Fe. Iron(II) originating from iron mono-sulfides and iron carbonates (0.18 – 0.24 mg/g) comprised only 0.7% of the total Fe. No significant exchangeable Fe was found neither at this depth nor in any other depth of the sediment profile (<0.001 mg/g).

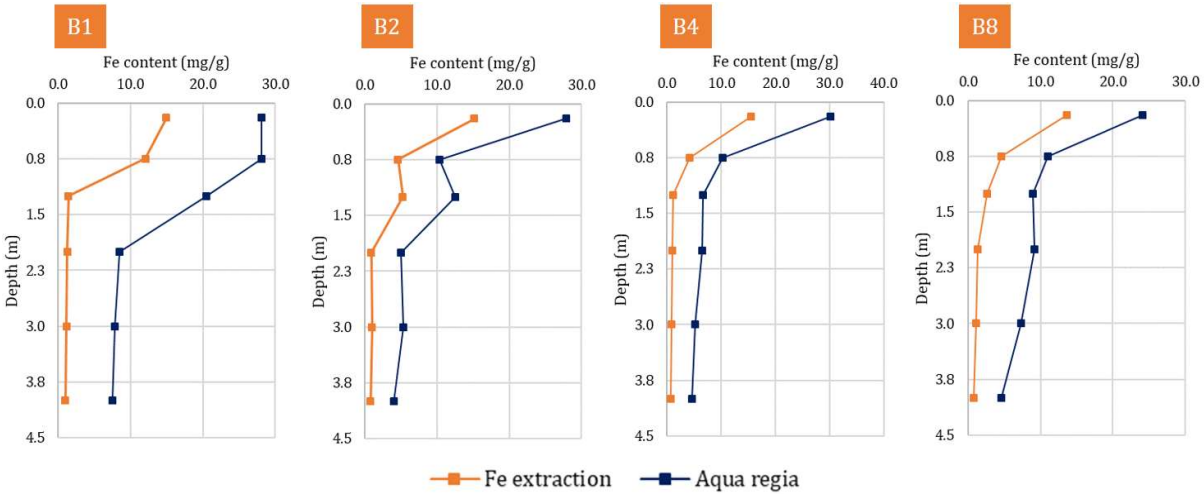

Figure 4.24: Depth profile of total Fe content from aqua regia and sum of extracted Fe content from Fe extraction for selected boreholes.

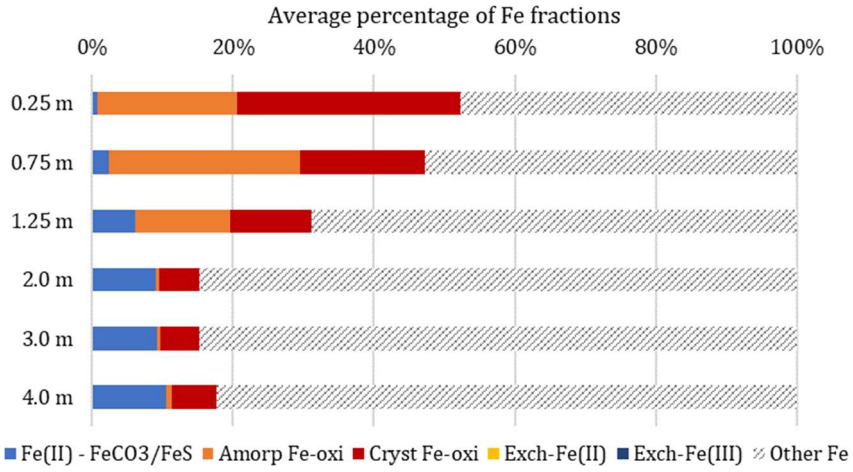

Figure 4.25: Total Fe composition as the average percentage of each fraction extracted from the soil samples.

From 0.75 m to 1.25 m depth, Fe(III) was still the prevailing form, constituting from 80-90% of the extracted Fe. At these depths, amorphous Fe-oxides slightly predominated in relation to crystalline Fe(III) forms. For B6 and B7, a peak of amorphous Fe-oxides occurred at 1.25 m, whereas at B2 a peak of crystalline Fe(III) occurred at the same depth. The contents of Fe(II) from FeS and $FeCO_3$ increased to 6.2% of total Fe at 1.25 m, varying from 0.3 mg/g to 0.9 mg/g at this depth.

From 2 m to 4 m, Fe(II) (0.4 – 0.8 mg/g) comprised nearly 50% of the Fe extracted and about 9.6% of total Fe. The other 50% was composed mostly by crystalline Fe(III) (0.2 – 0.5 mg/), whereas Fe(III) from amorphous Fe-oxides was very low (<0.1 mg/g) in all the boreholes analyzed, representing only 0.6% of total Fe.

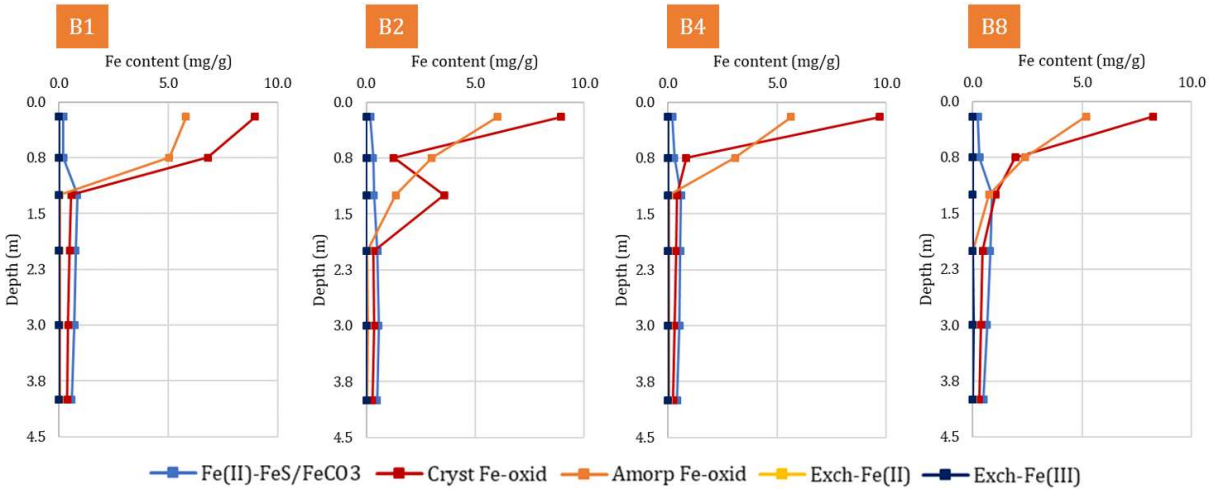

Figure 4.26: Depth profile of Fe content of various fractions extracted for selected boreholes.

4.3.2.2. Ditch bottom sediments

Total Fe contents in the ditch sediments varied from 31.1 to 44.4 mg/g, with an average of 36.3 mg/g. This average is about 5 times higher than the one found for the soil samples between 0.75 and 4 m depth. Iron content in ditch sediments increased for the samples taken in February and collected near the end of the ditch (see Figure 4.27). The fraction corresponding to the other Fe forms not analyzed via the extraction constituted, on average, 36.5% of the total Fe obtained via aqua regia.

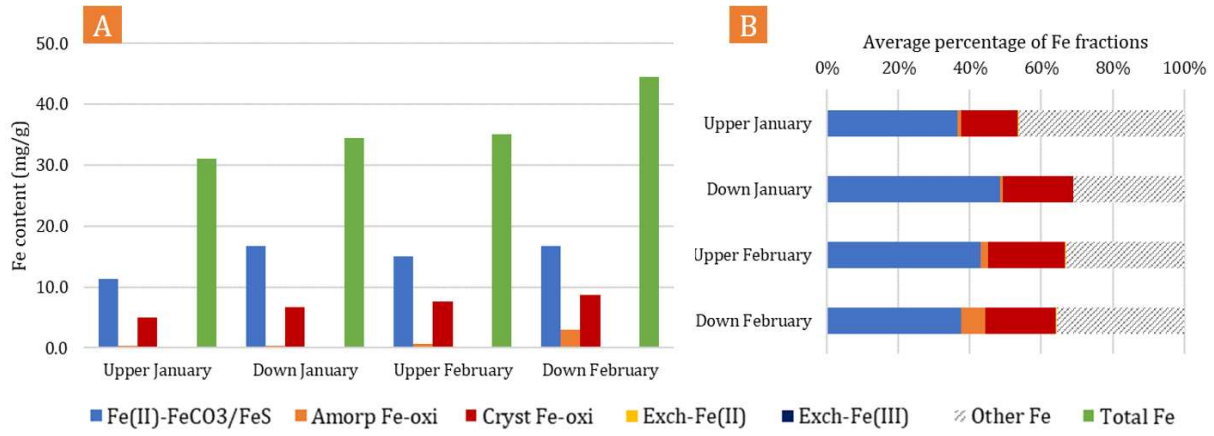

Figure 4.27: Left (A): Fe content in various fractions extracted in all ditch samples. Right (B): Total Fe composition as the average percentage of each fraction extracted from the ditch samples.

Different from what was observed for the soil samples, the predominant Fe phase in the ditches particulate material was the Fe(II) originated from iron mono-sulfides and iron carbonates (11.4 – 16.7 mg/g), which accounted to 41.4% of total Fe (see Figure 4.27). Iron(III) from crystalline (5.0 – 8.8 mg/g) and amorphous (0.3 – 3.0 mg/g) iron oxides were, on average, 19.2% and 2.7% of the total Fe present in the ditch sediments. Amorphous Fe-oxide content in the sample "Down February" was 4 to 9 times higher than for the other samples. Concentrations of exchangeable iron were low, but were the highest among all the sediments analyzed (0.03 – 0.10 mg/g), comprising 0.1% of total Fe. From the total exchangeable Fe, approximately 70% was Fe(II).

The results of SI calculations with PHREEQC pointed out that siderite and vivianite were undersaturated in the ditch with average SI values of -0.74 ± 0.19 and -4.83 ± 0.87. By discarding $FeCO_3$, the Fe(II) content found can be attributed to FeS. The remaining unknown Fe content is likely to belong to clay minerals, given the sluggish precipitation kinetics of pyrite (Appelo & Postma, 2005) and the high clay content of these samples (see Section 4.3.4).

4.3.2.3. Drain particulates

Total Fe concentrations in the drain sediments were, on average, 6 times higher than those found in the ditch material and 30 times higher those found in the soil samples, varying between 167.4 mg/g and 292.7 mg/g, with a mean of 240.2 mg/g. For the drains, the unknown Fe fractions averaged 34.2%, which is pretty similar among all the samples (see Figure 4.28).

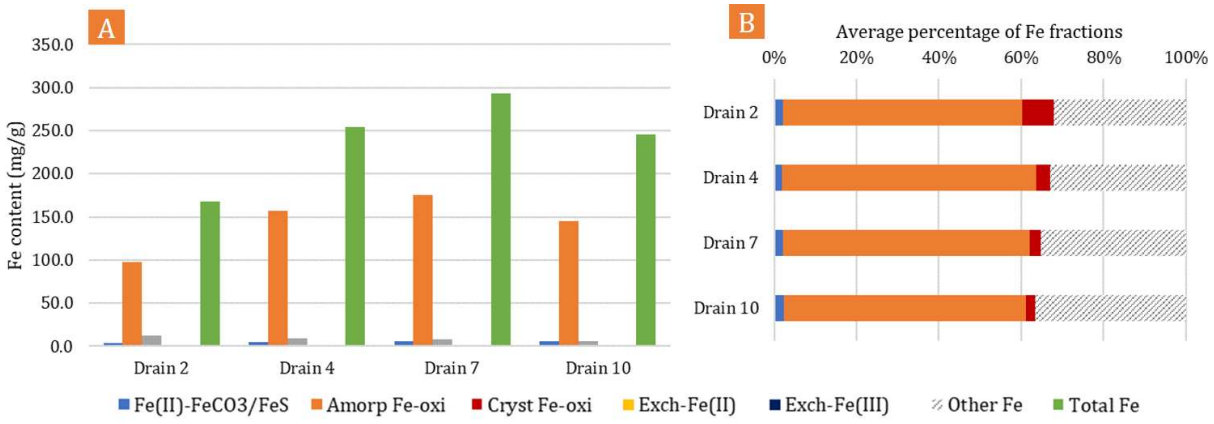

Figure 4.28: Left (A): Fe content in various fractions extracted in all drain samples. Right (B): Total Fe composition as the average percentage of each fraction extracted from the drain samples.

The majority of the Fe extracted originated from amorphous Fe-oxides (97.4 – 175.5 mg/g), comprising 59.6% of total Fe (see Figure 4.28). Crystalline iron oxides were the second major Fe form extracted (5.9 – 12.8 mg/g), accounting for 4.0% of total Fe. The sum of Fe(III) from amorphous and crystalline Fe-oxides constitute, on average, 29.2% of the total weight of the drain particulate material. The lowest (21.1%) and the highest (35.1%) percentages were found for drain 2 and drain 7, respectively. Iron(II) from iron mono-sulfides and iron carbonate was the least present fraction in the drains (3.7 – 6.0 mg/g), representing only 2.1% of the total Fe. Despite siderite and vivianite were supersaturated, with SI values of 1.12 ± 0.43 and 2.11 ± 1.48, respectively, it is unlikely that these minerals would precipitate in the drains, given their slow precipitation kinetics (Wajon et al., 1985; Walpersdorf et al., 2013).

4.3.3. Sulfur

As expected, sulfur content was very low at the topsoil and at 0.75 m, averaging 0.6 ± 0.02 mg/g and 0.2 ± 0.1 mg/g, respectively (see Figure 4.29). At 1.25 m, sulfur content increased markedly in B1, B4, B5, and B8 remaining low in the other locations. Overall, sulfur content was the highest between 2 m and 3 m for the majority of the boreholes, averaging 2.7 ± 1.1 mg/g and 2.0 ± 0.6 mg/g, respectively. From 3 to 4 m, values either became nearly constant or decreased, averaging 1.1 ± 0.2 mg/g. Sulfur content in the ditch samples was higher than in soil ones and basically constant among the samples analyzed, averaging 4.5 ± 0.1 mg/g. Such high S content supports the Fe observations for the large presence of FeS in the ditch sediments and it is also an indication of reducing environments. In the drains material, these values were less than half of the ditch ones: 1.7 ± 0.2 mg/g, pointing at more oxic conditions.

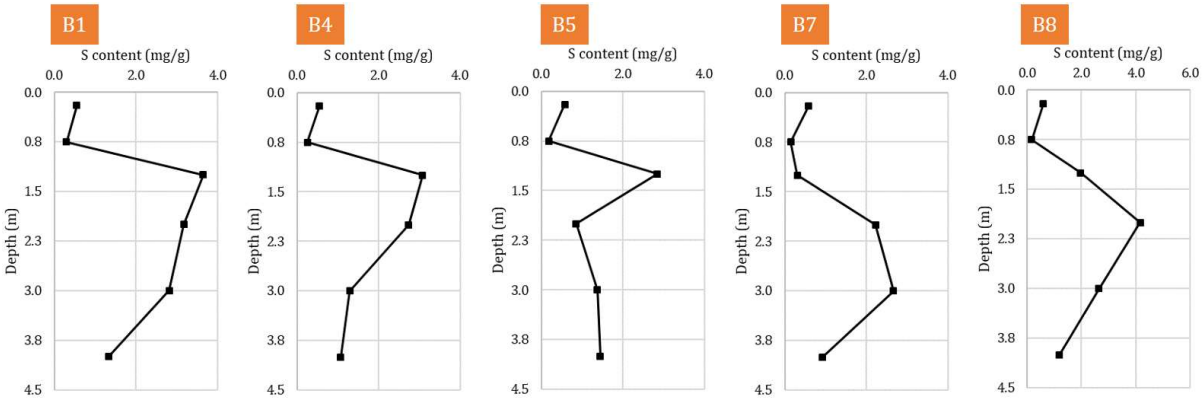

Figure 4.29: Sulfur depth profile for selected boreholes.

4.3.4. Other elements

Aluminum content in the soil samples had essentially the same distribution as Fe throughout the depth profile. The highest Al contents were observed in the shallow surface, averaging 26.1 ± 2.5 mg/g. These values markedly decreased at 0.75 m (8.9 ± 1.1 mg/g), with exception of B1, where 15.8 mg/g was registered. From 0.75 to 4 m, Al content slightly decreased, showing very little variation among the depths and averaging 4.6 ± 0.6 mg/g at 4 m. Very similar to Al, K contents in the soil depth profile were the highest at the surface (8.7 ± 1.0 mg/g) and decreased with depth becoming nearly constant at 4 m (1.7 ± 0.3 mg/g). Magnesium followed a similar pattern, varying from 6.5 ± 0.3 mg/g in the shallow surface to 3.1 ± 0.2 mg/g at 4 m. Opposite to these elements, Ca content was the lowest at the topsoil (16.8 ± 3.8 mg/g), markedly increasing at 0.75 m (44.2 ± 6.2 mg/g) (see Figure 4.30). Overall, from 0.75 m to 4 m, calcium content slightly decreased to an average of 38.3 ± 2.6 mg/g at 4 m depth. If we assume that all Ca is present as $CaCO_3$ – which is likely the case, as described later in this chapter – about 10% of the sediment is composed by calcium carbonate in the sediment profile from 0.75 m to 4 m depth. This can be ascribed to the large amounts of shells and marine sediments found in the parcel area. In the shallow surface, this percentage is much lower (about 4%) and may be attributed to decalcification as a result of pyrite oxidation (Appelo & Postma, 2005). Sodium content was less abundant than the other elements in the soil profile and varied little among depths. The lowest values were found at 0.75 m (0.3 ± 0.1 mg/g) and the highest at 3 m depth (0.6 ± 0.2 mg/g).

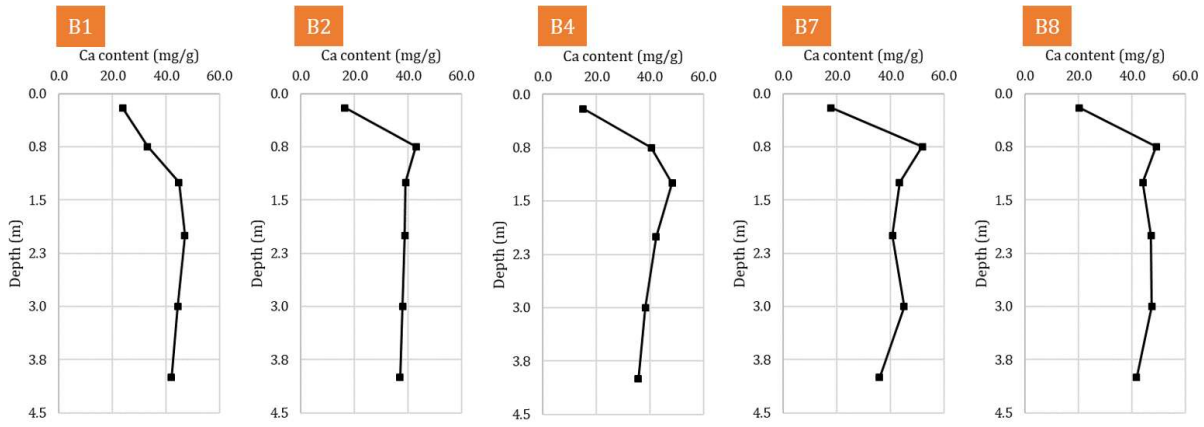

Figure 4.30: Calcium depth profile for selected boreholes.

In the ditch settled material, Al content was as high as in the shallow soil samples, whilst K and Mg contents were slightly higher, averaging 28.4 ± 1.9 mg/g, 10.6 ± 0.9 mg/g, and 8.4 ± 0.5 mg/g, respectively. Sodium content was much larger than in the soil, with a mean of 3.5 ± 0.6 mg/g. Calcium, however, was somewhat similar, with an average of 41.3 ± 2.4 mg/g. Aluminum, Na, K, and Mg contents were the highest in the samples from February, whereas Ca contents were larger in the ones collected in January, but both with little differences between the locations.

The contents of Al, K, and Mg were slightly lower in the drains if compared to the ditch and soil, but still substantial, showing an average of 22.5 ± 5.5 mg/g, 7.3 ± 2.0 mg/g and 5.8 ± 1.1 mg/g, respectively. The mean sodium content was the same as in the ditch (3.5 ± 1.6 mg/g), whilst Ca was slightly higher (43.4 ± 5.3 mg/g). Aluminum and potassium contents decreased from drains 2 to 10, whereas Na showed an opposite pattern and Mg did not follow a pattern. Calcium content was pretty similar from drain 2 to 7 but was higher at drain 10, which registered 51.2 mg/g. Assuming that all Ca is present as $CaCO_3$, about 10% of the ditch and drain sediments are composed of calcium carbonate.

Among the sediments analyzed, Al was very well correlated with K and Mg, with an R^2 equal to 0.99 and 0.90, respectively (see Table 4.15 and Figure 4.31). These and all the other correlations did not include the drain samples, since their Fe content was extremely high, and may also have influenced the other elements. A good correlation was also found for Al and Fe, with an R^2 equal to 0.97. Consequently, K and Mg were also well correlated with iron. A weak negative correlation was found between Ca and Al (R^2=0.43) and between Ca and Mg (R^2=0.19). Aluminum and sodium also do not correlate well, with an R^2 of 0.29. In fact, several scattered groups were present when plotting Al and Na together, indicating that a linear regression as shown in Figure 4.31 may be misleading in this case. Basically, no correlation was obtained between Al and Si (R^2=0.09). In fact, silicon did not seem to correlate with any of the other elements analyzed. This was somehow expected, given that silicates as K-feldspars do not dissolve completely in aqua regia, and quartz (SiO_2) is only fully dissolved by total destruction with HF. This could be evidenced by a much higher error associated with Si extraction in aqua regia if compared to other elements (53.3%). The values of Si, therefore, are not indicative and are not considered any further.

Table 4.15: R^2 values for correlation between several elements. Drain sediments were not included in the correlation analysis, since they had much higher Fe content, affecting thereby the content of the other elements.

	Na	Mg	Si	K	Al	Fe	Ca
Na	-	0.48	0.04	0.38	0.29	0.38	0.01
Mg		-	0.11	0.93	0.90	0.94	0.19
Si			-	0.09	0.09	0.11	0.04
K				-	0.99	0.97	0.36
Al					-	0.97	0.43
Fe						-	0.35
Ca							-

The good correlation between Al, K, and Mg indicates the presence of clay minerals and feldspars. The strong correlation of Al and Fe, however, suggests that they may represent clay minerals (smectite, illite, chlorite) (Koenen & Griffioen, 2014) but also olivine and pyroxene that contain Fe and Al (Johnsen, 2002). This is reasonable, since 85% of the <2 μm fraction of Dutch clay soils is constituted by clay minerals, and the rest is composed by quartz, feldspars, and oxides of Si, Al, and Fe (Griffioen et al., 2016). The weak correlation with sodium, in this case, may be attributed to the presence of Na^+ and other ions that might compete for the negative sorption sites in the clay minerals. This is also plausible since high sodium concentrations in pore water were only observed at larger depths, where Al contents were usually low. In the ditch, where both Al and Na contents were high, a good correlation between Al and Na could be found (R^2=0.92). The poor correlation of Ca with all these other elements suggests that Ca in sediment is predominantly present as calcium carbonate, which was somehow expected, since marine sediments, such as shells, are abundantly found in the study area. This is also evidenced by the saturated state of calcite in all the water types analyzed (see Table 4.9). Even though dolomite ($CaMg(CO_3)_2$) was also saturated for

the drains and ditch samples, it may not be formed extensively since dolomite precipitation is slow at low temperatures, whilst calcite precipitation is not and occurs rapidly given even slight oversaturation (Arvidson & Mackenzie, 1999). The lack of correlation between Ca and Mg also indicates that dolomite is of minor importance in the sediments analyzed.

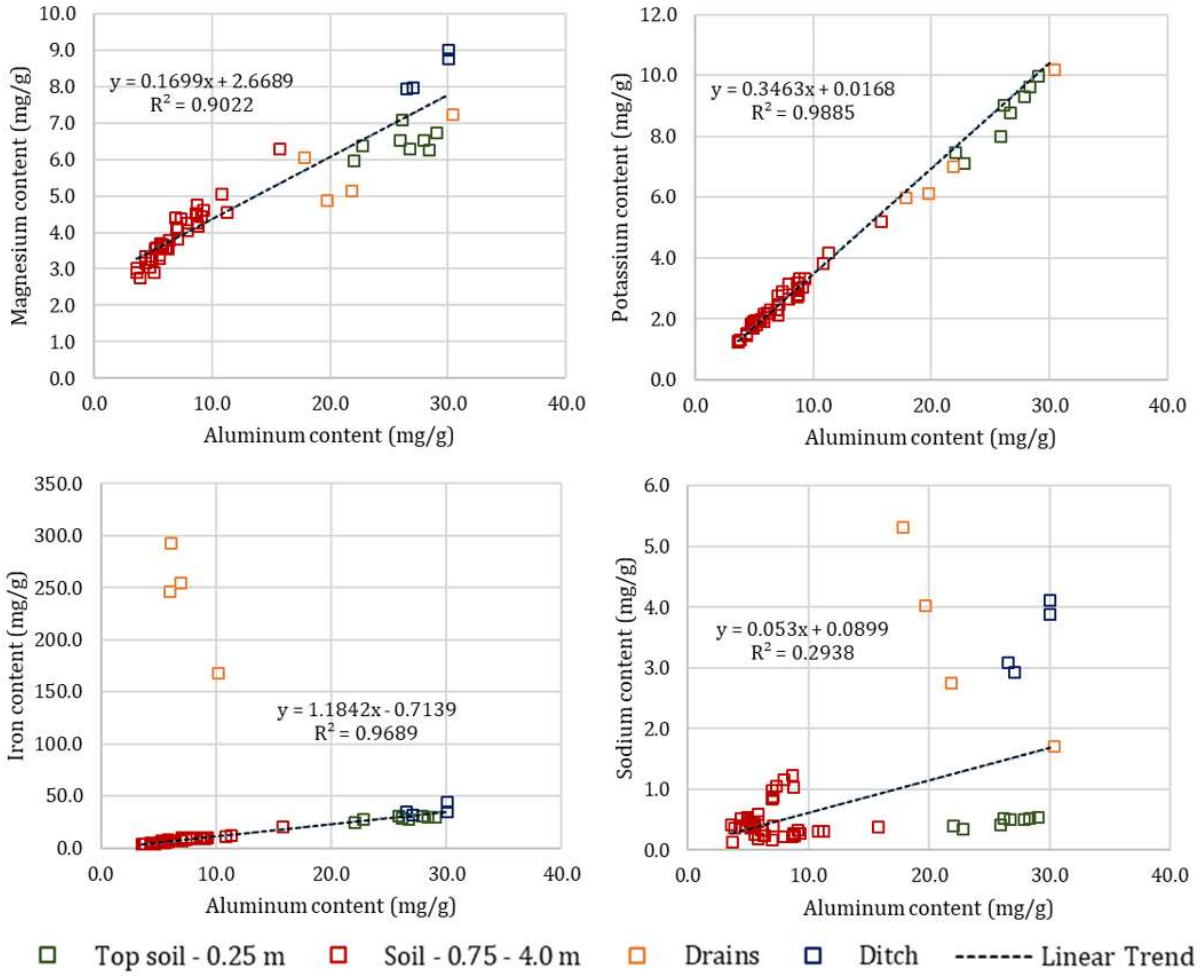

Figure 4.31: Correlation between Al content and Mg, K, Fe and Na contents. Note that, even though the drain sediments were not included in the trend line, they are shown in the graphs for illustration purposes.

5. Discussion

5.1. Results and methods reliability

In order to answer the main research question and test the hypotheses made, an extensive field work was performed together with several analytical procedures, followed by geochemical modelling simulations. The field work and laboratory analysis comprised a series of activities, which were realized under the supervision of technicians from both TNO and the University of Utrecht. These activities proceeded according to several protocols, as described in Chapter 2, and were, overall, successfully performed. Among all the methods used, the error was below 10%, which is an acceptable level of precision. The only exception occurred with the pore water analysis, in which some of the results were not reliable due to extensive CO_2 degassing of the samples, as discussed in Sections 4.2.1 and 4.2.2. In order to minimize the effects of this problem, additional data sampling was realized, which consisted of the collection of shallow groundwater samples. This extra data provided a better insight into the water composition at the shallow subsurface, which was partially affected by the degassing of the pore water. Reliable data relative to the water composition at 4 m depth, however, is still lacking for some of the major elements such as PO_4 and Fe. As a result, it is not possible to address the contribution of, i.e., iron and phosphorus, in the drain water composition to specific processes occurring in the subsurface and we can only discuss it in terms of hypothesis as presented in Section 5.2. Nevertheless, this did not interfere with the calculation of the retention of P in the drains, which was performed by geochemical modelling with PHREEQC using the data obtained for the drain water composition. Therefore, the methods employed in this research and the results obtained were, overall, reliable and sufficient to answer the main research question and test the hypotheses made.

5.2. Fe and PO_4 spatial variability

In terms of spatial variability, two opposite trends were observed: PO_4 concentrations in the drains appear to decrease towards the end of the ditch, whereas Fe seems to increase in the same direction. Despite the fact that the drains primarily transport water of meteoric origin, the results suggest that the groundwater is likely to be the major source of Fe and PO_4 in the drains, given the large concentrations of these elements found in the groundwater samples analyzed. Additionally, the chloride concentrations in the pore water samples indicate that a shallower fresh-saline groundwater boundary occurs near the farm when compared to the beginning of the ditch (see Section 4.2.1.1). As such, in the beginning of the ditch, where the groundwater table is lower, Fe(II) originated from groundwater is likely to be oxidized deeper in the soil profile (Van der Grift et al., 2014). Consequently, less Fe is transported to the drains located in this zone of the parcel, resulting in higher mobilization of PO_4. Oppositely, near the farm, where a shallower redoxcline occurs, more Fe is mobilized to the drains that can bind P and, hence, less PO_4 is available in solution. In addition to that, the deeper groundwater exfiltrating near the farm is composed by less PO_4 and more Fe than the groundwater feeding the drains in the beginning of the ditch, which could be an additional explanation for the large-scale trend observed for iron and phosphate in the drains.

Despite this major trend, both phosphate and iron concentrations were highly variable among the drains analyzed. This small-scale differences could be attributed to the heterogeneity of the parcel area and the particularities of each drain. As an example, even though the maximum Fe concentration in groundwater was 9.3 mg/L, some of the drains showed concentrations of iron up to 33 mg/L. Similarly occurred for the shallow groundwater samples, where a Fe concentration of 28 mg/L was registered in borehole B6, suggesting an extra mobilization of Fe. Given the absence of Fe concentrations in pore water, it is not possible to determine whether this additional Fe flux is coming from reactions occurring between the shallow subsurface, or from deeper in the soil profile. However, some hypotheses can be made. The first one relies on the incomplete pyrite oxidation, resulting in SO_4 and Fe(II) release (Appelo & Postma, 2005), which ultimately would end up in the drains (see Section 2.3.1). Overall, the sulfur content in the soil column seemed to increase from 0.75 m to 3 m depth, possibly indicating the presence of pyrite.

Additionally, all the drains – except drains 9 and 10 – were above the mixing line for sulfate (see Figure 4.15), indicating that more SO_4 is entering the drains than expected by the mixing. Since groundwater from 9 m to 46 m depth had no sulfate, these concentrations can only advent from processes occurring in the shallow subsurface. Pyrite oxidation would be favorable far from the farm, where there is a deeper redoxcline, and gaseous diffusion may convey a much larger flux of oxygen. As a consequence of pyrite oxidation, some acidification could be locally generated, resulting in the dissolution of Ca-P phases (Appelo & Postma, 2005; Sas et al., 2001), potentially increasing the PO_4 in solution in the drains. This is also reasonable, given that some of the Ca concentrations in the drains were above the mixing line, suggesting dissolution of Ca minerals (see Figure 4.6). Near the farm, where the fresh-saline groundwater interface is shallower, advective transport of dissolved O_2 is the only mode of O_2 transport and, given the constraints of dissolved oxygen in groundwater, pyrite oxidation would be limited in this zone of the parcel (Appelo & Postma, 2005). Besides, the shift in the redox gradient would promote sulfate reduction, which could lead to the precipitation of FeS in the drains located in that region (Smolders et al., 2006). This could explain why only drains 9 and 10 – which are the closest to the farm – were below the mixing line for sulfate.

Besides that, higher Fe concentrations in the drains could be originating from the reductive dissolution of iron oxyhydroxides through degradation of organic matter (Baken et al., 2015b). The first supportive evidence for this hypothesis is the presence of both amorphous and crystalline iron oxides, at least, until 1.25 m depth as evidenced by the results of the Fe extraction (see Figure 4.26). Another evidence could be the sharp decline of DOC from 0.75 m to 1.25 m found for most of the pore water samples, indicating that organic matter may be quite reactive and is being degraded conform it leaches through the soil column. This is more evident for B6, where DOC decreases steeply until 2 m, and also where the high Fe concentration of 28.5 mg/L was found in the shallow groundwater. Additionally, DOC concentrations were below the mixing line for all the drains analyzed for the majority of the sampling days (see Figure 4.10). However, DOC can be decomposed by a series of electron acceptors (i.e. O_2, NO_3, Fe^{3+}, SO_4, CO_2), and Fe^{3+} is unlikely to be reduced if O_2 and NO_3 are still present, since they are energetically favorable electron acceptors (Appelo & Postma, 2005). Nevertheless, in reality, systems rarely show strict redox zone boundaries, as several redox reactions may occur simultaneously (McGuire et al., 2002 cited in Rivett et al., 2008; Postma & Jakobsen, 1996). Furthermore, O_2 penetration in clay soil is likely to be limited, and a gradual decrease of the oxygen diffusion rate is expected to occur with depth (Wiersum, 1960). In addition to that, nitrate was often present in low concentrations and, mostly, in the shallowest depths. In this sense, the content of Fe^{3+} in sediment likely exceeds that of other electron acceptors such as oxygen and nitrate, and thus the mineralization of organic matter with Fe^{3+} as the electron acceptor is not an unrealistic hypothesis (Lovley & Phillips, 1986).

Individual features of the drains could also play a role in their water composition. During the field campaign, we noticed that not all the drains were buried at the same depth, as some were usually more submerged than others. This was the case, for example, of drain 8, in which discharge could not be measured in April. This drain also appears to have higher PO_4, DOC, and NH_4 than the two surrounding drains, but less Fe. Assuming that this drain was buried deeper in the soil (>1 m), it may be closer to the redoxcline, which favors the reduction of, i.e., Fe(III)-P minerals in the soil surrounding the drain and, hence, increasing the mobilization of PO_4. Another possibility is that the deeper location of the drain may also have resulted in a source with more DOC, which may enhance reduction processes in the drain, decreasing Fe by FeS formation and increasing PO_4 release due to less retention (Hyacinthe & Van Cappellen, 2004). Asides that, during the sampling period, some of the drains seemed to be partially clogged, as a large amount of sediment was released upon cleaning and flushing of the drains in March. If clogging occurs, i.e., due to precipitation of Fe oxyhydroxides in combination with the growth of microbial mass, less atmospheric oxygen penetrates in the tube drain and in the surrounding soil. As a consequence, Fe oxidation would be limited and more Fe could be present in solution inside the drain (Van der Grift et al., 2014). In this sense, the clogged state of the drains may also have played a role in their water composition and could also contribute to the ongoing oxidation of Fe(II) in the drains.

On top of that, the study area comprises an agricultural field which is often subject to management practices that affect soil crusting and compaction, vegetative cover, and soil porosity which can alter the infiltration rate of water and oxygen penetration in the soil column (Evanylo & McGuinn, 2000; Wiersum, 1960).

Considering that drain water is mainly constituted by infiltrated rainwater and that oxygen primarily governs redox potential by being the main redox-sensitive compound (Christensen et al., 2000) – affecting thereby most of the aforementioned processes – these practices in association with the heterogeneity of the parcel could ultimately exert a large influence in drain water composition.

5.3. Fe and PO_4 temporal variability

Besides spatial differences, PO_4 and Fe concentrations were also largely variable among the sampling days. Nevertheless, a certain trend could be observed: the highest PO_4 and Fe concentrations were found in the winter, whereas the lowest ones were obtained in the early spring season. Seasonal changes in Fe(II) oxidation rate were reported by Van der Grift et al. (2014) and Baken et al. (2015a), who observed lower rates during winter when compared to summer time. However, for both studies P immobilization did not seem to follow a seasonal trend as Fe did and was at all times highly efficient, being removed from solution much faster than Fe. According to them, the lower oxidation kinetics of Fe in the winter can be attributed to: 1) lower pH, 2) lower temperatures, and 3) lower residence time of water. In both studies, higher discharges were observed during the winter, resulting in less CO_2 degassing and lower pH values. This was not the case in the Schermer Polder. Despite an also inversed correlation occurred between pH and discharge (see Figure 4.5), the winter period was characterized by low discharges and relatively high pH values. When plotting the average drains discharge per sampling period together with the PO_4 and Fe concentrations, it appears that discharge is inversely correlated with these elements (see Figure 5.1). However, this correlation is weak, showing an R^2 equal to 0.40 for PO_4 and 0.45 for Fe. This correlation is even weaker for pH (R^2<0.1). Even though the highest PO_4 and Fe concentrations were found when the coldest temperatures were also registered, these elements do not correlate much better with temperature than the previous variables, showing an R^2 near the value of 0.3. Although the high concentrations in winter may, in fact, be associated with low oxidation kinetics of Fe, it is not possible to confirm or rule out that the PO_4 and Fe concentrations in the drains are primarily governed by seasonal changes in climatic conditions based on the available data of this research. A proper assessment of the seasonal influence on PO_4 and Fe immobilization would require a continuous measurement all year round.

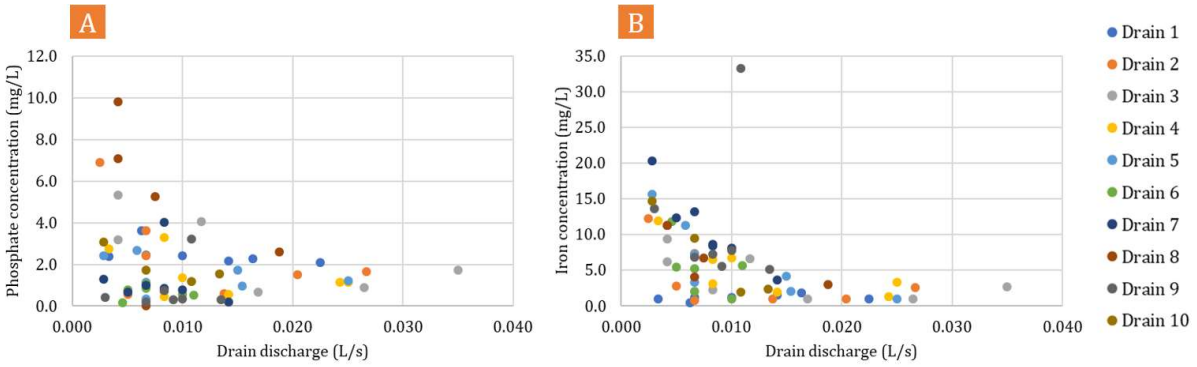

Figure 5.1: Left (A): Correlation between drain discharge and phosphate concentration in the drains. Right (B): Correlation between drain discharge and iron concentration in the drains.

Nevertheless, given the large spatial variability in phosphate and iron concentrations, it is more likely that the parcel heterogeneity and the associated geochemical processes are prevailing over seasonal trends. This could be evidenced by the fact that, among all drains analyzed, PO_4 and Fe seemed to vary less for drain 1, which showed a certain stability regarding these elements concentrations over time. As drain 1 is located at the extreme edge of the parcel, less tillage practices as ploughing, occurs on the soil close to the drain. With less disturbance of the soil, oxygen penetration and water infiltration is less variable, and so will be drain water composition, since these factors are expected to influence the geochemical reaction as

discussed in Section 5.2. In addition to the poor correlation found between PO_4 and Fe and the main temporal variables, this suggests that temporal trends in drain water composition may be, in fact, overshadowed by the large spatial variability caused by the heterogeneity of the parcel and tillage practices.

5.4. Phosphorus retention

5.4.1. Sediment analysis

The results of the P extraction analysis point out that the total phosphorus content was fairly low for the soil samples when compared to the results obtained for the ditch and drain samples. Approximately 20 times more P was found in the ditch material and nearly 80 times more in the drain sediments. These results support the theory that a great part of phosphorus is expected to be immobilized upon groundwater exfiltration due to the strong tendency for biogeochemical transformation of dissolved P to PP at redox gradients, such as in the drains and ditch, where the groundwater exfiltrates (Griffioen et al., 2006; Van der Grift et al., 2014; Baken et al., 2015a). In the recently published study of Van der Grift et al. (2018), suspended particulate matter (SPM) from six agriculture-dominated lowland catchments in the Netherlands were studied regarding the particulate phosphorus (PP) content. Their results revealed an average of 8.8 mg of phosphorus per gram of SPM analyzed. This value is higher than the average found in the ditch material (4.7 mg/g), and much lower than the average found in the drains particulate (22.6 mg/g). In the work of Owens & Walling (2002), a table with several references for total phosphorus content in the USA and Europe is presented. The values range from 0.1 mg/g to 4.5 mg/g for SPM – with an exceptional case of 13.5 mg/g for a study made in France. For channel bed sediment, which would be comparable to the ditch settled material, these values oscillated between 0.2 mg/g and 5.1 mg/g. Nguyen & Sukias (2002) found similar results for TP in ditch bottom sediments from four major New Zealand pastoral catchments, with ranges from 2.2 mg/g to 4.2 mg/g. Van der Grift et al. (2018) also compiled a series of results from other researches regarding the total P content of SPM, where average TP content did not surpass 5.7 mg/g and ranges were mostly between 0.1 and 4.2 mg/g. When comparing the results with these reference values, the P content obtained for the soil and ditch samples were within the average international values found for SPM. The average P content found in the drain particulates, however, was unquestionably larger than the highest values found in the literature.

The drain sediments showed, overall, nearly 5 times more phosphorus than the ditch material, which may be ascribed to several hypotheses. The first of them consists of a possible remobilization of phosphorus once the particulate form reaches the bottom of the ditch, in the transition zone from groundwater to surface water. There, anoxic conditions may be present – which is evidenced by the Fe(II) as the largest Fe fraction found in the settled ditch material – and PP may be remobilized to dissolved P by reductive dissolution of Fe-P minerals or aging of Fe(III) precipitates and increased state of crystallization (Van der Grift et al., 2014; Shenker et al., 2005; Mayer & Jarrell, 2000). Such remobilization may also occur due to flow-induced resuspension of sediments and associated particulate P during storm flow events (Van der Grift, 2017). Another explanation could be related to the settling properties of the particles. Van der Grift et al. (2018) found the highest P content in particles with low SPM concentrations, which are usually finer and have lower fall velocities, thereby remaining for longer periods in the water column. Oppositely, the ditch sediments likely comprise coarser particles with much tendency to settle down. As such, it is possible that the particulate matter enriched with P originating from the drains mostly became SPM during the turbulence caused by the water flow from the drains to the ditch. Asides from that, a third hypothesis is that the ditch settled particulates of authigenic origin may be diluted by other materials, and possibly adsorb more dissolved constituents present in the ditch water (Baken, 2015). In this sense, the ditch material has a higher degree of mixing with other types of sediment, such as eroded clay particles and plants debris. It is plausible, therefore, that the total phosphorus content in the ditch sediments might be 'diluted', being lower than in the drains, which is presumably mainly composed by authigenic particles.

Among the total phosphorus extracted, Fe-P was by far the major PP form in the topsoil and in the ditch and drain sediments, constituting on average 80.8% and 96.2% of TP, respectively. Likewise, Van der Grift et al. (2018) also reported the prevailing Fe-P among SPM, comprising between 38% to 95% of TP. Similar

results were also verified by Jordan et al. (2008), where about 50 – 90% of the PP from SPM collected along the salinity gradient of an estuary in the US was phosphate bound to iron oxides. These results reinforce the theory that iron-bearing particles exert a major influence on the fate of P in natural waters (Baken, 2015). The prevalence of Fe-P fraction indicates the presence of Fe(III) precipitates in the sediments analyzed. Such material has an authigenic origin and is formed upon the exfiltration of anoxic Fe-bearing groundwater, in which dissolved Fe(II) oxidizes to Fe(III) due to changes in the redox conditions (Baken et al., 2013). Dissolved phosphate present upon Fe(II) oxidation will be immobilized by these iron particles. Overall, the main binding mechanisms are via surface complexation to ferrihydrite or co-precipitation as Fe hydroxyphosphate (Griffioen, 2006). Van der Grift et al. (2016b) suggest that precipitation of a Fe hydroxyphosphate phase with a stoichiometry of $Fe_{1.67}PO_4(OH)_{2.01}$ and a molar P/Fe ratio of precipitate ($(P/Fe)_{ppt}$) of 0.6 can be used for predictive modelling of PO_4 immobilization upon aeration of pH-neutral natural groundwater with an initial molar ratio in solution ($(P/Fe)_{ini}$) up to 1.5. Binding by surface complexation is restricted by the sorption capacity of the mineral, which depends on its specific area (Griffioen, 2006) and, therefore, a lower $(P/Fe)_{ppt}$ is expected. For ferrihydrite, with a specific surface area of 600 m^2/g, the maximum theoretical density is 0.2 moles/mol Fe (Davis & Kent, 1990, cited in Griffioen, 2006). For crystalline iron oxides, such as goethite [α-FeO(OH)], the specific area reduces to a range between 50 and 94 m^2/g (Villalobos et al., 2009). Consequently, the sorption capacity is reduced to values between 0.02 and 0.03 moles/mol Fe.

The results of the Fe extraction point out that the prevailing Fe(III) form in the drains is amorphous iron oxides, whereas in the ditch and soil sediments, Fe(III) mainly originates from crystalline iron oxides. Assuming, therefore, immobilization by co-precipitation as Fe hydroxyphosphate with a $(P/Fe)_{ppt}$ ratio of 0.6 and surface complexation to ferrihydrite for the drains and to goethite for the ditch and soil sediments, we can estimate what sort of Fe-bind P mechanism is present in the sediment analyzed. Figure 5.2 shows the $(P/Fe)_{ppt}$ ratio obtained for all the sediments, with the y-axis representing the Fe-P fraction extracted via SEDEX, and the x-axis representing the sum of the Fe(III) from amorphous and crystalline iron oxides extracted. It is possible to observe that the settled ditch particles have a ratio above 0.6, varying between 0.7 and 1.0. In ditch water, the average P/Fe molar ratio in solution is 1.9, indicating an excess of PO_4 in relation to Fe. In such conditions, it is expected that Fe(II) oxidation will primarily result in the precipitation of a Fe hydroxyphosphate phase until phosphate is virtually depleted (Van der Grift et al., 2016b). The higher $(P/Fe)_{ppt}$ ratio reveals, however, the formation of a Fe hydroxyphosphate phase with other stoichiometry than the one suggested by Van der Grift et al. (2016b). Senn et al. (2015) observed the formation of amorphous Fe(III)-phosphate of Ca-Fe(III)-phosphate with maximum $(P/Fe)_{ppt}$ ratios of 0.7 and 1.1 upon aeration of initial solutions contained $(P/Fe)_{ini}$ above critical ratios of 0.5 in 8 mM $NaHCO_3$ and 0.8 in 4 mM $Ca(HCO_3)_2$ electrolytes, which could explain the high $(P/Fe)_{pp}$ ratio in the ditch sediments. Either than that, precipitation of pure strengite ($FePO_4 \cdot 2H_2O$) with a ratio of 1 is also a possibility (Griffioen, 2006). Given the semi-anoxic conditions of the ditch sediments, one might suggest the formation of vivianite ($Fe_3(PO_4)_2 \cdot 8H_2O$). Nevertheless, besides the precipitation kinetics of vivianite being very slow (Walpersdorf et al., 2013), the brackish to saline water conditions together with the high sulfate present in the ditch would promote a preferential precipitation of iron sulfides (Roden & Edmonds, 1997; Hyacinthe & Van Cappellen, 2004). Additionally, vivianite changes from white to blue after air exposure (Griffioen et al., 2016), which was not observed during the laboratory analysis. The undersaturated state of vivianite obtained with PHREEQC reinforces the suspects of the absence of the mineral in the ditch settled material. For the soil samples, as expected, a good correlation is seen with the ratio of surface complexation. Since most of the soils contain iron oxides (Schwertmann & Taylor, 1989), any input of PO_4 – originating from i.e. inorganic fertilizers – will encounter already formed Fe oxyhydroxides and, hence, surface complexation is likely to be the only mechanism possible to occur (Van der Grift et al., 2016b). Furthermore, in the soil column, it is likely that the crystalline Fe oxides are the main form binding P. This is evidenced by the simultaneous peak of Fe-P and crystalline Fe(III) observed at 1.25 m depth in borehole B2. For B6 and B7 a peak in amorphous Fe hydroxides was registered at the same depth, whilst Fe-P was absent of peaks for these boreholes, suggesting that the Fe-P fraction is better correlated to the crystalline Fe forms.

For the drains, however, the results varied conform the sample analyzed. Whilst for drain 2, the Fe-P phase seems to be constituted by a mix between P bound by surface complexation and co-precipitation, for the remaining drains Fe-P is likely to be mainly a result of surface complexation. The $(P/Fe)_{ppt}$ ratios varied

between 0.16 and 0.43, in which the lowest value was found for drain 7 and the highest for drain 2. Drains 4 and 10 had similar results: 0.23 and 0.25, respectively. The lowest ratios can be attributed to the also low P/Fe molar ratio found in solution in drains 4 and 10, which averaged 0.2, indicating that Fe is mostly in excess to PO_4 in these drains. For drain 7, the P/Fe ratio was even lower, averaging 0.1. In this sense, upon mixing of rainwater and groundwater in the drains, Fe(II) will precipitate Fe hydroxyphosphates as long as PO_4 is present. However, due to the lower ratio, PO_4 will be soon depleted and the remaining Fe(II) will precipitate as Fe oxyhydroxides (Van der Grift, 2016b). As a result, both Fe-bound PP will form and the $(P/Fe)_{ppt}$ ratio will be somewhere in between 0.2 and 0.6. Voegelin et al. (2013) observed that for low initial P/Fe ratios (<0.2), initially formed ferric phosphates were fully converted into hydrous ferric oxides with surface-adsorbed P upon continuing Fe(II) oxidation. In this sense, it is possible that most of the Fe-P phases from drains 4 to 10 will consist of P bound to Fe-oxyhydroxides. For drain 2, the average P/Fe molar ratio is 0.6, but ratios up to 1.9 were also found and, hence, a higher $(P/Fe)_{ppt}$ ratio was also expected in this drain.

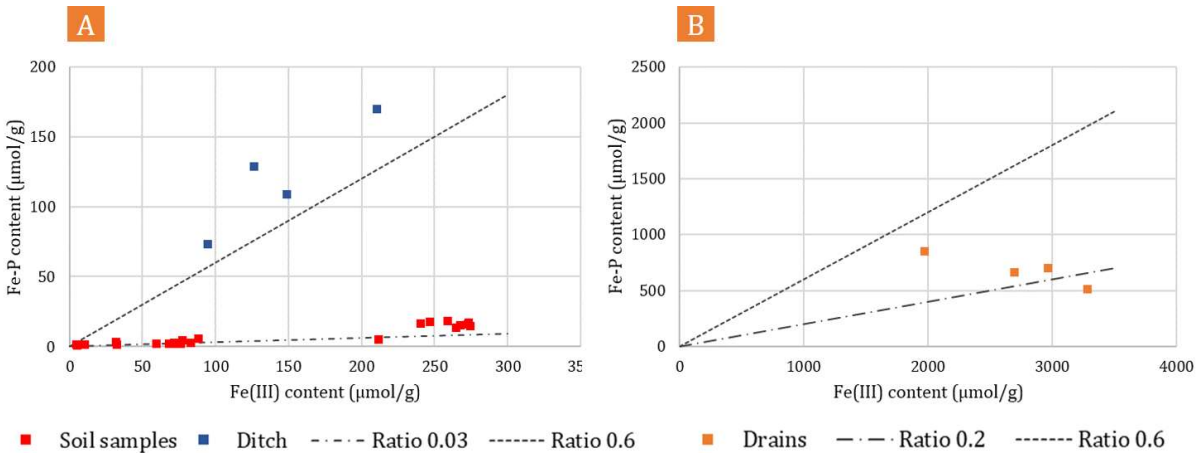

Figure 5.2: Left (A): P/Fe ratio of precipitates collected in the soil and ditch sediments. Right (B): P/Fe ratio of precipitates collected in the drains.

Organic-bound P was the second largest PP form for all the ditch and drain sediments and shallow soil samples. Similar results were also found by Van der Grift et al. (2018), who suggestively attributed the high Org-P content of the SPM to recent manure application. This hypothesis, however, may not hold for the case of the Schermer catchment. Given that all total P found in the drains, ditch, and shallow groundwater comprises ortho-PO_4, it is unlikely that the origin of the phosphate in the surface water is related to manure application and, as such, the Org-P fraction cannot be attributed to that as well. Possibly, the Org-P fraction in the sediments analyzed is originated from P adsorbed in organic molecules, forming coatings on clays (Poulenard et al., 2008), or phosphorus associated with humic and fulvic acids (Turner et al., 2005). This theory is more plausible since Org-P was only high in the shallow soil samples – where a 20 – 40 cm think tillage clay layer is present (Delsman et al., 2014) – and decreased with depth, where sand became the predominant material. In borehole B1, the soil at 0.75 m depth was the only one characterized as clay (see Table 4.1) and, accordingly, was the only borehole where Org-P fraction was relatively high at this depth. In drains and ditch, clay minerals were also present in relatively high amounts, providing a substrate for P fixation.

The Ca-P content of the samples was overall very small. However, proportionally, it comprised the third largest form throughout the sediment column from 0.75 m to 4 m depth. This high percentage of Ca-P in the soil column might be explained by the high content of Holocene marine sediments under the form of Ca-carbonate material in both sand, loam, and clay present in the polder catchment area (Griffioen et al., 2013). As such, the Ca-P fraction in the soil could have been formed upon fixation of P released from reductive dissolution of Fe-hydroxides due to changes in redox gradient in the soil profile (Shenker et al., 2005). Despite Ca-P content being 3 to 4 times higher in the drains and ditch than in the soil, it represented

a very small fraction of TP from these sediments. Griffioen (2006) suggests that the uptake of PO_4 by Ca phosphates and/or Ca carbonates might play a role upon oxygenation and degassing of nutrient-rich groundwater. For the majority of drains and ditch water samples, OH-apatite was mostly saturated or supersaturated, with an average of 0.48 ± 1.44 and 1.53 ± 1.03, respectively. However, the high CO_2 partial pressures calculated for both water types indicates that CO_2 degassing was unfinished in the drains and ditch. Since Ca-P minerals precipitation is dependent on CO_2 degassing (Griffioen, 2006) and is unlikely to occur significantly when pH is under 8 (Diaz et al., 1994), little Ca-P is expected to precipitate, playing a minor role in P retention in drains and ditch.

The Detr-P content was not significant in terms of total concentration for none of the sediment samples analyzed but was the prevailing form in the soil column. Detr-P comprises the poorly soluble (crystalline) apatite minerals, being largely composed of fluorapatite derived from igneous or metamorphic rocks (Ruttenberg, 1992). As such, detrital phosphorus in sediment has basically the same chemical and mineralogical forms as in rocks, soils and the unconsolidated surface deposits from which the sediments were derived (Bostan et al., 2000) and, therefore, it is reasonable to compose the majority of TP found in the soil sediment profile. However, given that this fraction comprises the aged form of Ca-P minerals, and the Ca-P fraction was not relevant in the drains and ditch, it is plausible Detr-P was also low. Exchangeable P was basically negligible in all the sediments analyzed. Since Exch-P represents the loosely sorbed P fraction (Ruttenberg, 1992), the low contents of this fraction in the sediments represent a lower risk of P release from the sediment to the overlying waters (Nguyen & Sukias, 2002).

5.4.2. Water analysis – unfinished Fe oxidation and P immobilization in the drains

Despite the great content of phosphorus bound to iron in drain sediments, concentrations of phosphate and iron were detectable and sometimes relatively high in drain water. This was somewhat more evident for Fe than for PO_4. With an average of 1.9 mg/L, phosphate concentrations in the drains were from 5 to 7 times lower than the ones found in groundwater from 25 m (10.5 mg/L) and 9 m depth (14.4 mg/L), respectively. The average Fe concentration of 6.1 mg/L, however, was very similar to the 6.8 mg/L found at 9 m, and slightly below to the 9.3 mg/L found at 25 m depth. Concentrations of Fe in the drain water were remarkably higher than those found in the ditch water samples. Additionally, Fe(II) constituted the majority of Fe in solution in drain water (96.3%), whereas this percentage reduced to 69.8% for the ditch water. This suggests that Fe is not completely oxidized prior to the inflow to the ditch, and the Fe oxidation mostly occurs during the transport of water in the ditch. This is also evidenced by the low Log P_{O_2} values calculated with PHREEQC for the drains, in which more than 80% of the samples showed Log P_{O_2} values inferior to -0.95, indicating partial O_2 pressure below that of air. Even though iron concentrations are expected to decrease upon the exposure to oxic conditions, the oxidation of Fe(II) to Fe oxyhydroxides is a kinetically controlled process and, hence, the transient time of water exerts a large influence on the final Fe concentrations. As such, the longer the residence time of water, the lower will be the concentration of dissolved Fe(II) due to the greater exposure time of water to oxic environments (Baken et al., 2015a). Considering the average discharge of the drains as 0.01 L/s, together with a length of 100 m and a diameter of 7 cm, and taking into account that in neither of the sampling days the water level in the drains was above 1 cm, we can estimate the flow cross-sectional area and, hence, calculate the maximum residence time of the drain water (see Figure 5.3), which turns out to be near 1 hour. This is much lower than the median hydraulic residence time of water in streams, which is about 27 h (Baken et al., 2015a). Van der Grift et al. (2014) showed that the complete oxidation of Fe(II) may vary between a couple of days to more than a week in winter conditions for an average pH of 6.17 and temperature of 5^0C. The oxidation kinetics of ferrous iron follows the rate law (Stumm & Lee, 1961):

$$-\frac{\mathrm{dFe(II)}}{\mathrm{dt}} = \mathrm{k[Fe(II)][OH^-]^2P_{O_2}} \qquad (5.1)$$

The rate of oxidation is highly dependent on pH and temperature (Stumm & Lee, 1961): a drop of half pH unit for pH around 6-7 results theoretically in a 9-fold increase in the half-life time of Fe(II) (Van der Grift et al., 2014), and for a given pH, the rate increases about 10-fold for a 15ºC temperature increase (Stumm

& Lee, 1961). The pH in the drains was mostly near neutral, and average temperatures varied between 5.0 ºC and 12.8 ºC. At such conditions, the complete oxidation of Fe(II) is likely to occur faster than under the conditions studied by Van der Grift et al. (2014), but presumably slower than the estimated residence time of the water in the drains, otherwise no Fe(II) would be observed in the drain water as we did. It is, therefore, reasonable that Fe is still found in large concentrations in the drains, and much less in the ditch water. Likewise, the presence of PO_4 in relatively high concentrations in the drains may be also attributed to the unfinished Fe oxidation process.

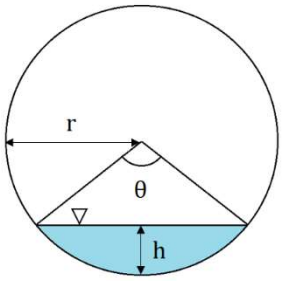

$$\theta = 2\cos^{-1}\left(\frac{r-h}{r}\right)$$

$$A = \frac{r^2(\theta - \sin\theta)}{2}$$

$$T = \frac{V}{d} = \frac{A.L}{d}$$

Figure 5.3: Equations used to calculate the cross-sectional area of the flow and the residence time of water in the drains. In the equations, h is the water level in the drain (m), r is the radius of the drain (m), A is the cross-sectional area (m^2), V is the volume of water in the drain (m^3), L is the drain length (m) and d is the average discharge of the drain (m^3/s).

5.4.3. Modeling analysis

The P retention was simulated for three different scenarios (see Section 3.3). The first one comprised the aeration of the theoretical initial solution entering the drains, as a mixture of shallow and deep groundwater. In the second, the real drain water composition was aerated for the two more extreme conditions, when Fe and PO_4 were the highest and the lowest found in solution. Lastly, the complete aeration of the solution composition of groundwater from 9 m and 25 m depth was simulated, as a representative scenario for the groundwater exfiltration in the ditch. The results from all the simulations are shown in Tables 5.1, 5.2 and 5.3.

By analyzing the first simulation, we observe that the mixing with groundwater from 25 m instead of 9 m, increases the number of boreholes where P immobilization is complete. This is a reasonable outcome, given that the water from 25 m depth is less rich in PO_4 and more rich in Fe, favoring P retention. Noticeably the degree of immobilization of phosphorus was larger for B8 than for B5 after mixing with the deepest groundwater. This is attributed to the larger transport of groundwater by B8, which is located near the farm, where presumably a shallower fresh-saline groundwater interface occurs. In both scenarios, the solution composition referring to B3 and B6 did not contain any phosphate anymore after aeration, which can be ascribed to the relatively high Fe concentrations found in the shallow groundwater from these boreholes. As previously discussed, this extra Fe load in B6 may be the result of the reductive dissolution of iron oxyhydroxides via organic matter mineralization. Since B3 is located in parallel to B6, reactive DOC is likely to be present in this region of the parcel.

Table 5.1: Results of simulation 1 - Aeration of the theoretical initial solution entering the drains, composed by the mixture of shallow and groundwater sample from 9 m depth. The last column represents the P/Fe ratio obtained from the measured content of the drain sediments.

	Groundwater - 9 m							Drains	
	P/Fe ini	P final (µmol)	Fe final (µmol)	P immobilized	$Fe(OH)_3$(µmol)	Fe hydroxy (µmol)	(P/Fe)ppt	(P/Fe)pt	
B3	0.55	0.0	0.0	100.0%	2.4	17.4	**0.55**	**0.23**	D4
B4	0.81	2.8	0.0	74.3%	0.0	8.0	**0.60**	**0.43**	D2
B5	2.61	17.0	0.0	23.0%	0.0	5.1	**0.60**	**0.43**	D2
B6	0.03	0.0	0.0	100.0%	445.1	16.4	**0.03**	**0.23**	D4
B8	1.48	21.1	0.0	40.5%	0.0	14.4	**0.60**	**0.25**	D10

Table 5.2: Results of simulation 1 - Aeration of the theoretical initial solution entering the drains, composed by the mixture of shallow and groundwater sample from 25 m depth. The last column represents the P/Fe ratio obtained from the measured content of the drain sediments.

	Groundwater - 25 m							Drains	
	P/Fe ini	P final (µmol)	Fe final (µmol)	P immobilized	$Fe(OH)_3$(µmol)	Fe hydroxy (µmol)	P/Fe	(P/Fe)pt	
B3	0.37	0.0	0.0	100.0%	14.0	13.2	**0.37**	**0.23**	D4
B4	0.49	0.0	0.0	100.0%	2.9	8.0	**0.49**	**0.43**	D2
B5	1.69	12.5	0.0	35.4%	0.0	6.9	**0.60**	**0.43**	D2
B6	0.03	0.0	0.0	100.0%	456.8	12.3	**0.03**	**0.23**	D4
B8	0.84	7.9	0.0	71.3%	0.0	19.7	**0.60**	**0.25**	D10

Table 5.3: Results of simulations 2 and 3 - Aeration of the actual solution coming out of the drains (intermediate scenario) and aeration of the two groundwater samples (9 m and 25 m depth), representing the ditch exfiltration.

Aeration		P/Fe ini	P final (µmol)	Fe final (µmol)	P immobilized	$Fe(OH)_3$ (µmol)	Fe hydroxy (µmol)	(P/Fe)ppt
GW 9 m		1.25	80.1	0.0	47.9%	0.0	73.6	**0.60**
GW 25 m		0.66	10.8	0.0	90.4%	0.0	101.4	**0.60**
21-feb	Drain 1	1.40	14.5	0.0	42.9%	0.0	10.9	**0.60**
	Drain 2	0.33	0.0	0.0	100.0%	99.1	72.8	**0.33**
	Drain 3	0.33	0.0	0.0	100.0%	75.2	55.9	**0.33**
	Drain 4	0.13	0.0	0.0	100.0%	166.0	28.5	**0.13**
	Drain 5	0.09	0.0	0.0	100.0%	239.5	25.3	**0.09**
	Drain 7	0.04	0.0	0.0	100.0%	341.7	13.7	**0.04**
	Drain 8	0.51	0.0	0.0	100.0%	30.1	103.5	**0.51**
	Drain 9	0.02	0.0	0.0	100.0%	237.4	4.2	**0.02**
	Drain 10	0.12	0.0	0.0	100.0%	209.7	32.8	**0.12**
13-mrt	Drain 1	0.86	7.1	0.0	69.4%	0.0	16.1	**0.60**
	Drain 2	0.39	0.0	0.0	100.0%	5.6	6.3	**0.39**
	Drain 3	0.46	0.0	0.0	100.0%	3.8	7.4	**0.46**
	Drain 4	0.15	0.0	0.0	100.0%	25.3	5.3	**0.15**
	Drain 5	0.71	1.9	0.0	84.9%	0.0	10.7	**0.60**
	Drain 6	0.26	0.0	0.0	100.0%	20.0	9.5	**0.26**
	Drain 7	0.06	0.0	0.0	100.0%	135.0	9.5	**0.06**
	Drain 8	0.49	0.0	0.0	100.0%	9.8	27.5	**0.49**
	Drain 9	0.03	0.0	0.0	100.0%	95.3	3.2	**0.03**
	Drain 10	0.35	0.0	0.0	100.0%	14.7	12.7	**0.35**

Different from the first simulation, when aerating the real solution composition of the drains, P is completely immobilized in nearly all the samples analyzed. The only exceptions were drains 1 and 5. For the first one P was still remaining in solution after aeration in both of the extreme scenarios. This result is somewhat expected, since drain 1 was the only drain in which the average P/Fe molar ratio was above 1, indicating an excess load of PO_4 in relation to Fe and, hence, less immobilization is to be expected. In drain 5, all phosphorus could be retained in February, but 15% of P was still in its mobile phase when simulating it with the water composition from March. This could be attributed to the fact that, in March, iron

concentration in drain 5 was only 1.0 mg/L, whereas the average Fe concentration in this drain is 6.4 mg/L. The concentration of phosphate, however, was very similar to the average value (1.5 mg/L), registering 1.2 mg/L. This imbalance caused by the deficit of iron is, therefore, the likely reason for the incomplete P retention.

The comparison between the first and second simulations, however, shows that the degree of P immobilization is much higher upon aeration of the real drain water composition, which consequently shows a much lower P/Fe molar ratio in solution. Despite the fact that this ratio does not represent the initial composition of the drains, given that oxidation is already happening together with precipitation of Fe-P phases, it shows that there is an excess of Fe in relation to PO_4 for the vast majority of the drains. Given that, the solution from the first simulation considers solely the mixing between freshwater and groundwater from 9 m and 25 m depth, it completely disregards any Fe and PO_4 contribution coming from processes occurring in the shallow subsurface. Ideally, this contribution could be determined by the pore water composition of the boreholes, which unfortunately was hindered by the degassing of the samples. As such, the real subsurface flow entering the drains is unknown. Considering the high degree of immobilization, it is possible that there is an extra mobilization of Fe or precipitation of P prior to entering in the drains, lowering the P/Fe ratio, or even extra mobilization of both Fe and PO_4, but more Fe than PO_4. These results confirm the hypothesis that the conservative mixing of groundwater and rainwater is not sufficient to predict drain water composition, which is likely to be largely affected by geochemical processes occurring in the shallow subsurface, as discussed in Section 5.2. It is also noticeable that the P/Fe molar ratio is highly variable among drains, but somehow similar throughout time, even when considering the most extreme scenarios. This reinforces the suspects that temporal variability may be overshadowed by the spatial heterogeneity at the parcel scale.

Opposite to the drains, the aeration of the groundwater samples resulted in incomplete immobilization of phosphate for both the simulation scenarios. For the groundwater of 9 m depth, more than 50% of initial P would still be in solution after complete aeration, which could explain the larger concentrations of PO_4 found in the middle of the ditch. Such low retention capacity is somehow expected, given the high P/Fe molar ratio of 1.25 for this groundwater solution. This ratio, however, was nearly half for the groundwater of 25 m depth. Nevertheless, upon aeration, practically 10% of the initial P would still be in the mobile phase. As such, it is possible to infer that, even though the potential of P retention in the drains is significantly high, the complete immobilization of PO_4 in the ditch is unlikely to occur, presumably due to the excess P present in the groundwater composition from both depths and the greater contribution of groundwater exfiltration in the ditch.

Another interesting outcome from the simulations was that, whenever P was subject to incomplete immobilization, solely Fe hydroxyphosphate was formed, resulting in a $(P/Fe)_{ppt}$ ratio of 0.6. For the cases with complete P retention, $Fe(OH)_3$ also precipitated, lowering the final $(P/Fe)_{ppt}$ ratio to a range between 0.02 and 0.51. This is in accordance with the findings of Van der Grift et al. (2016b), who reported that Fe(II) oxidation would primarily result in the precipitation of a Fe hydroxyphosphate phase until complete depletion of PO_4, with a further formation of Fe oxyhydroxides from the excess Fe. Overall, the $(P/Fe)_{ppt}$ obtained from both simulations corresponded well with the ratios found in the sediment analysis. The only exception was for B6 in the first simulation, which showed a much lower $(P/Fe)_{ppt}$ ratio, presumably due to the extreme high Fe concentrations in the shallow groundwater sample from this borehole. Nevertheless, the results from the aeration of the real drain water composition seemed to correlate better with the results from sediment analysis, which is a reasonable outcome since we are comparing the actual solution responsible for the drain slurry precipitates. The discrepancies found between the simulation and the real conditions may be attributed to the fact that the modeling was based on thermodynamic equilibrium, without accounting for kinetics. Since Fe hydroxyphosphate and Fe oxyhydroxide have different precipitation rates (Van der Grift et al., (2016b)), the incorporation of kinetics in the simulations would have resulted in different $(P/Fe)_{ppt}$ ratios, depending on the stage of oxidation of the water in the drains, which is an unknown variable.

5.5. Research implications

Most of the studies regarding P immobilization upon exfiltration of anoxic-bearing groundwater in lowland catchments focus on the final mechanisms and pathways of phosphorus in surface water bodies, regardless of the heterogeneity of the surrounding landscape and the geochemical processes associated to it (Baken et al., 2015a; Van der Grift et al., 2014; Van der Grift et al., 2016b; Griffioen, 2006). Furthermore, the majority of these researches emphasize P retention in surface water bodies, such as ditches and streams, whilst tile drainage is usually of minor importance. The outcome of this thesis highlights the importance of tile drainage in P retention, by showing that drains are likely to be a major sink of P in lowland catchments, where subsurface drainage networks are applied to remove surface water ponding and drain shallow water tables (Nguyen & Sukias, 2002). This was confirmed by the results of the geochemical simulations with PHREEQC which showed that P could be completely immobilized in nearly all the drains analyzed, for the two most extreme conditions, when the highest and lowest P and Fe were found in solution. The extensive analysis of drain water composition is highly recommended for a better understanding of the spatial distribution of P immobilization in the subsurface where drainage network systems are deployed. In addition to that, the results show that P and Fe concentrations in the drains are highly variable in space and time. This large variability can be attributed to the geochemical processes occurring in the subsurface which, in turn, are associated with the heterogeneity of the landscape. Processes such as pyrite oxidation and dissolution of iron oxides are likely to be important sources of Fe exfiltrating via tile drains, exerting major influence on the P immobilization by decreasing the P/Fe molar ratio of the water. As such, the heterogeneity of the landscape and the associated geochemical processes should be taken into account when assessing phosphorus retention in lowland catchments.

Due to the CO_2 degassing of the pore water samples during lab sampling it was not possible to properly address the real contribution of subsurface fluxes of Fe and PO_4 entering the drains. As another recommendation, further researches that aim to assess P retention in lowland areas by taking into account the heterogeneity of the landscape should have a proper characterization of the pore water depth profile and extra care should be taken during sampling and analysis to avoid precipitation due to oxidation and/or degassing. Either than that, this research was carried out mostly during the winter period, when crops were not growing in the parcel area. In the growing season, when fertilizers are likely to be applied in the soil, the P leaching from the topsoil may lead to a different outcome regarding P immobilization. Besides the difference in land use, distinctive temporal conditions, such as temperature and discharge, are also likely to alter drain water composition and, hence, P retention in the drains. As such, it is recommended continuous data collection throughout the entire year, in order to address the effect of seasonality and land use on P immobilization in the drains.

6. Conclusion

The aim of this research was to assess the P retention in the drains of a marine clay polder dominated by agricultural practices. In order to address this goal, five hypotheses were established. First, we hypothesized that a large part of retention of P occurs upon the mixing of rainwater and groundwater in the drains. This was confirmed by the geochemical modelling simulations, which showed that P could be completely immobilized in nearly all the drains analyzed, for the two most extreme conditions, when the highest and lowest P and Fe were found in solution. The retention capacity of the drains was also evidenced by the remarkable P content in the drains sediments, which was larger than the references found for SPM in literature. In the second hypothesis, Fe-P would be the prevailing PP from in the sediments, which was confirmed by the fact that more than 95% of the PP extracted in the drains consisted of Fe-bound P. Accordingly, Fe-P was also the largest PP fraction found in the ditch and shallow soil samples. In the third hypothesis, calcium-bound P was assumed to be the second major fraction among PP. Nevertheless, Ca-P comprised only 5.5% and 1.5% of total P extracted from the drains and ditch sediments, respectively. Overall, it did not seem to play an important role in P retention, likely due to the limited CO_2 degassing in the drains and ditch samples. In the fourth hypothesis, P and Fe concentrations in the drains and, hence, the P immobilization would be affected by the heterogeneity of the parcel. The results from both the field campaign and the geochemical modelling showed that, despite the fact that drain water composition is mainly governed by the exfiltration of nutrient-rich groundwater, the large spatial variability of the drain water composition, i.e., regarding the Fe and P concentrations, can only be explained by the contribution of these elements originating from geochemical processes occurring in the shallow subsurface (i.e., pyrite oxidation). These processes are linked to the heterogeneity of the parcel and to tillage practices, and showed a large influence on P immobilization in the drains in the outcome of the modeling simulations, confirming the hypothesis made. In the fifth hypothesis, drain water quality was assumed to vary with drain discharge and season. In fact, drain water composition was also highly variable throughout time and inversely correlated with discharge and temperature. Nevertheless, this correlation was very weak, suggesting that temporal variability may be overshadowed by the large spatial heterogeneity.

Acknowledgments

I first would like to thank the farmer Ted for allowing the research on his property. I also would like to express my gratitude to Pr. dr. Jasper Griffioen for the opportunity to write my thesis as an internship at TNO and also for the guidance and supervision over the last seven months. I also would like to immensely thank Alwina Hoving, for the great support in all the phases of this thesis. Bas Van der Grift is also thanked for the valuable comments and suggestions regarding the modelling analysis. I also would like to thank Andrzej Alojzy for the lithological classification of the sediment samples. Gillian Schout, Thom Claessen, Rémon Saaltink, Rob van Ede, Bart Meijninger, Henco Kuiphof, Mariëlle van Vliet, and Tano Kivits are also acknowledged for their contribution to the field work and laboratory analyses.

Finally, I would like to thank and dedicate this thesis to my parents, who always believed in my potential and supported me to achieve my goals.

Erica Barbosa.

7. References

Appelo, C. A., & Postma, D. (2005). *Geochemistry, groundwater and pollution*. Second edition. ed. Balkema. Rotterdam, The Netherlands.

Arvidson, R. S., & Mackenzie, F. T. (1999). The dolomite problem: Control of precipitation kinetics by temperature and saturation state. *American Journal of Science*, 299(4), 257-288.

Baken, S., Sjöstedt, C., Gustafsson, J. P., Seuntjens, P., Desmet, N., De Schutter, J., & Smolders, E. (2013). Characterization of hydrous ferric oxides derived from iron-rich groundwater and their contribution to the suspended sediment of streams. *Applied Geochemistry*, 39, 59-68. doi:10.1016/j.apgeochem.2013.09.013.

Baken, S. (2015). *The effect of iron-rich particles on the fate and bioavailability of phosphorus in streams*. PhD thesis. KU Leuven.

Baken, S., Salaets, P., Desmet, N., Seuntjens, P., Vanlierde, E., & Smolders, E. (2015a). Oxidation of Iron Causes Removal of Phosphorus and Arsenic from Streamwater in Groundwater-Fed Lowland Catchments. *Environmental Science & Technology*, 49(5), 2886-2894. doi:10.1021/es505834y.

Baken, S., Verbeeck, M., Verheyen, D., Diels, J., & Smolders, E. (2015b). Phosphorus losses from agricultural land to natural waters are reduced by immobilization in iron-rich sediments of drainage ditches. *Water Research*, 71, 160-170. doi:10.1016/j.watres.2015.01.008.

Bosch, J. H. A. (2000). *Standaard Boor Beschrijvingsmethode, ver. 5.1*. Report no. NITG 00-141-A, 98pp.

Bostan, V., Dominik, J., Bostina, M., & Pardos, M. (2000). Forms of particulate phosphorus in suspension and in bottom sediment in the Danube Delta. *Lakes and Reservoirs: Research and Management*, 5(2), 105-110. doi:10.1046/j.1440-1770.2000.00104.x

Boyd, C. E. (2015). *Water Quality - An Introduction*. London, Springer.

Burdige, D. J. (1993). The biogeochemistry of manganese and iron reduction in marine sediments. *Earth-Science Reviews*, 35(3), 249-284.

Carpenter, S. R. (2008). Phosphorus Control is Critical to Mitigating Eutrophication. *Proc. Natl. Acad. Sci.* , 105(32), 11039-11040. doi:10.1073/pnas.0806112105.

Chardon, W. J., & Schoumans, O. F. (2002). Solubilization of phosphorus: Concepts and process description of chemical mechanisms. p. 44-52. *In*: Chardon, W. J., & Schoumans, O. F. (eds.) Phosphorus losses from agricultural soils: Processes at the field scale. COST Action 832. Alterra, Wageningen, The Netherlands.

Christensen, T. H., Bjerg, P. L., Banwart, S. A., Jakobsen, R., Heron, G., & Albrechtsen, H. (2000). Characterization of redox conditions in groundwater contaminant plumes. *Journal of Contaminant Hydrology*, 45(3-4), 165-241. doi:10.1016/s0169-7722(00)00109-1.

Claff, S. R., Sullivan, L. A., Burton, E. D., & Bush, R. T. (2010). A sequential extraction procedure for acid sulfate soils: Partitioning of iron. *Geoderma*, 155(3-4), 224-230. doi:10.1016/j.geoderma.2009.12.002.

Cordell, D. (2010). *The Story of Phosphorus: Sustainability Implications of Global Phosphorus Scarcity for Food Security*. PhD thesis. University of Technology/Linköping University.

Council Directive 91/676/EEC. (12 December 1991), concerning the protection of waters against pollution caused by nitrates from agricultural sources, OJ 1991, L 375/1-8.

Dahm, C. M., Grimm, N. B., Marmonier, P., Valett, H. M., & Vervier, P. (1998). Nutrient dynamics at the interface between surface waters and groundwater. *Freshwater Biology*, 40, 427-451.

Davis, J.A., Kent, D.B. (1990). Surface complexation modeling in aqueous geochemistry. In: Hochella Jr., M.F., White, A.F. (Eds), *Mineral-water interface geochemistry*. Reviews in Mineralogy, Miner. Soc. Am., 23. Washington, DC, 177-260.

De Klein, J. J. M. (2008). *From Ditch to Delta, Nutrient retention in running waters*. PhD thesis. Wageningen University, Wageningen, The Netherlands.

De Vries, J. J. (2007). Groundwater. p. 295-315. *In:* Wong, T., Batjes, D. A. J., De Jager, J. (eds.) Geology of the Netherlands. Royal Netherlands Academy of Arts and Sciences, The Netherlands.

Delsman, J. R. (2015). *Saline groundwater-surface water interaction in coastal lowlands*. PhD thesis. Vrije Universiteit Amsterdam, The Netherlands.

Delsman, J. R., Waterloo, M. J., Groen, M. M., Groen, J., & Stuyfzand, P. J. (2014). Investigating summer flow paths in a Dutch agricultural field using high frequency direct measurements. *Journal of Hydrology*, 519, 3069-3085. doi:10.1016/j.jhydrol.2014.10.058.

Diaz, O. A., Reddy, K. R., & Moore Jr, P. A. (1994). Solubility of inorganic phosphorus in stream water as influenced by pH and calcium concentration. *Water Research*, 28(8), 1755-1763. doi:10.1016/0043-1354(94)E0051-S.

DINOloket – Data en Informatie van de Nederlandse Ondergron. Available at: https://www.dinoloket.nl/.

Dzombak, D. A., Morel, F.M.M. (1990). *Surface Complexation Modeling: Hydrous Ferric Oxide*. Wiley-Interscience, New York.

Evanylo, G., McGuinn, R. (2000). Agricultural Management Practices and Soil Quality: Measuring, Assessing, and Comparing Laboratory and Field Test Kit Indicators of Soil Quality Attributes. Virginia Cooperative Extension, Publication 452-400.

Frapporti, G., Vriend, S. P., & Van Gaans, P. F. (1993). Hydrogeochemistry of the Shallow Dutch Groundwater: Interpretation of the National Groundwater Quality Monitoring Network. *Water Resources Research*, 29(9), 2993-3004.

Gächter, R., & Müller, B. (2003). Why the phosphorus retention of lakes does not necessarily depend on the oxygen supply to their sediment surface. *Limnol. Oceanogr.* 48(2), 929-933.

Goldberg, S., & Sposito, G. (1984). A Chemical Model of Phosphate Adsorption by Soils: 1. Reference Oxide Minerals. *Soil Science Society of America Journal*, 48, 772-778.

Griffioen, J. (1994). Uptake of Phosphate by Iron Hydroxides during Seepage in Relation to Development of Groundwater Composition in Coastal Areas. *Environmental Science & Technology*, 28(4), 675-681. doi:10.1021/es00053a022.

Griffioen, J., Buijs, E.A. & Broers, H.P. (1994). *Voorkomen en gedrag van enkele spoormetalen in ondiepe grondwater-sediment systemen. Een case-study aan de hand van vijf putten in Noord-Brabant*. TNO Grondwater en Geo-Energie. Repport no. OS 94-39A.

Griffioen, J., De Louw, P. G., Boogaard, H. L., & Hendriks, R. F. (2002). *De achtergrondbelasting van het oppervlaktewatersysteem met N, P en Cl, en enkele ecohydrologische parameters in West -Nederland*, The Netherlands. Report no. NITG 02-166-A.

Griffioen, J., Notenboom, J., Schraa, G, Stuurman, R.J., Runhaar, H. & Van Wirdum, G. (2003). *Systeemgericht grondwaterbeheer. De natuurwetenschappelijke werking van grondwatersystemen in relatie tot ecosystemen en grondwaterbeheer*. Stenfert Kroese, 189 pp.

Griffioen, J. (2006). Extent of immobilization of phosphate during aeration of nutrient-rich, anoxic groundwater. *Journal of Hydrology*, 320, 359-369. doi:10.1016/j.jhydrol.2005.07.047.

Griffioen, J., Vermooten, S., & Janssen, G. (2013). Geochemical and palaeohydrological controls on the composition of shallow groundwater in the Netherlands. *Applied Geochemistry*, 39, 129-149. doi:10.1016/j.apgeochem.2013.10.005.

Griffioen, J., Klaver, G., & Westerhoff, W. (2016). The mineralogy of suspended matter, fresh and Cenozoic sediments in the fluvio-deltaic Rhine–Meuse–Scheldt–Ems area, the Netherlands: An overview and review. *Netherlands Journal of Geosciences*, 95(1), 23-107. doi:10.1017/njg.2015.32.

Gunnars, A., Blomqvist, S., Johansson, P., & Andersson, C. (2002). Formation of Fe(III) oxyhydroxide colloids in freshwater and brackish seawater, with incorporation of phosphate and calcium. *Geochimica Et Cosmochimica Acta*, 66(5), 745-758.

Haynes, R. J. (1982). Effects of liming on phosphate availability in acid soils. *Plant and Soil*, 68(3), 289-308.

Holtan, H., Kamp-Nielsen, L., & Stuanes, A. O. (1988). Phosphorus in Soil, Water and Sediment: An Overview. *Hydrobiologia,* 170, 19-34.

Holman, I. P., Whelan, M. J., Howden, N. J., Bellamy, P. H., Willby, N. J., Rivas-Casado, M., & McConvey, P. (2008). Phosphorus in groundwater-an overlooked contributor to eutrophication? *Hydrological Processes*, 22(26), 5121-5127. doi:10.1002/hyp.7198.

Hyacinthe, C., & Van Cappellen, P. (2004). An authigenic iron phosphate phase in estuarine sediments: Composition, formation and chemical reactivity. *Marine Chemistry*, 91(1-4), 227-251. doi:10.1016/j.marchem.2004.04.006.

Jaarsma, N., Van Ee, G. (2014). *Herziening KRW doelen HHNK Ten behoeve van SGBP1 en SGBP2.* Hoogheemraadschap Hollands Noorderkwartier, Heerhugowaard, The Netherlands. Report no 14.38620.

Johnsen, O. (2002). *Minerals of the World* (Princenton Field Guides). Princenton, New Jersey: Princenton University Press.

Jordan, T. E., Cornwell, J. C., Boynton, W. R., & Anderson, J. T. (2008). Changes in phosphorus biogeochemistry along an estuarine salinity gradient: The iron conveyer belt. *Limnology and Oceanography*, 53(1), 172-184. doi:10.4319/lo.2008.53.1.0172.

Koninklijk Nederlands Meteorologisch Instituut (KNMI). (n.d.). Dagwaarden neerslagstations. Retrieved April 20, 2018, from https://www.knmi.nl/nederland-nu/klimatologie/monv/reeksen

Koenen, M., & Griffioen, J. (2014). Mineralogical and geochemical characterization of the Boom Clay in the Netherlands. Rep. No. OPERA-PU-TNO521-1.

Koppelaar, R. H., & Weikard, H. P. (2013). Assessing phosphate rock depletion and phosphorus recycling options. *Global Environmental Change*, 23(6), 1454-1466. doi:10.1016/j.gloenvcha.2013.09.002.

Ligtvoet, W., Beugelink, G. P., & Franken, R. (2008). *Evaluation of the Water Framework Directive in the Netherlands; costs and benefits Summary of PBL report 500140001 (in Dutch)*. Netherlands Environmental Assessment Agency (PBL), the Netherlands.

Lovley, D. R., & Phillips, E. J. (1986). Organic Matter Mineralization with Reduction of Ferric Iron in Anaerobic Sediments. *Applied and Environmental Microbiology*, 51(4), 683-689.

Lucassen, E. C., Smolders, A. J., Van der Salm, A. L., & Roelofs, J. G. (2004). High groundwater nitrate concentrations inhibit eutrophication of sulphate-rich freshwater wetlands. *Biogeochemistry*, 67(2), 249-267.

Mayer, T. D., & Jarrell, W. M. (2000). Phosphorus sorption during iron(II) oxidation in the presence of dissolved silica. *Water Research*, 34(16), 3949-3956. doi:10.1016/s0043-1354(00)00158-5.

McGuire, J. T., Long, D. T., Klug, M. J., Haack, S. K., Hyndman, D. W. (2002). Evaluating behavior of oxygen, nitrate and sulphate during recharge and quantifying reduction rates in a contaminated aquifer. *Environ. Sci. Technol.* 36(12), 2693-2700.

Merrington, G., Winder, L., Parkinson, R., & Redman, M. (2002). *Agricultural Pollution: Environmental Problems and Practical Solutions*. CRC Press.

Murrmann, R. P., Peech, M. (1969). Effect of pH on labile and soluble phosphate in soils. *Soil Science Society of America Proceedings.* 33, 205-210.

Neset, T. S., & Cordell, D. (2011). Global Phosphorus Scarcity: Identifying Synergies for a Sustainable Future. *J. Sci. Food Agric*, 92(1), 2-6. doi:10.1002/jsfa.4650.

Nguyen, L., & Sukias, J. (2002). Phosphorus fractions and retention in drainage ditch sediments receiving surface runoff and subsurface drainage from agricultural catchments in the North Island, New Zealand. *Agriculture, Ecosystems & Environment*, 92(1), 49-69. doi:10.1016/s0167-8809(01)00284-5.

Oenema, O., Van Liere, L., & Schoumans, O. (2005). Effects of lowering nitrogen and phosphorus surpluses in agriculture on the quality of groundwater and surface water in the Netherlands. *Journal of Hydrology*, 304, 289-301. doi:10.1016/j.jhydrol.2004.07.044.

Oude Essink, G. H. P. (2001). Salt Water Intrusion in a Three-dimensional Groundwater System in The Netherlands: A Numerical Study. Transport in Porous Media, 43, 137-158.

Owens, P. N., & Walling, D. E. (2002). The phosphorus content of fluvial sediment in rural and industrialized river basins. Water Research, 36(3), 685-701.

Parkhurst, D. L., & Appelo, C. (2013). Description of input and examples for PHREEQC version 3: a computer program for speciation, batch-reaction, one-dimensional transport, and inverse geochemical calculations US geological survey techniques and methods (Vol. 6, pp. 497): US geological survey.

Postma, D., & Jakobsen, R. (1996). Redox zonation: Equilibrium constraints on the Fe(III)/SO_4 -reduction interface. *Geochimica Et Cosmochimica Acta*, 60(17), 3169-3175. doi:10.1016/0016-7037(96)00156-1.

Poulenard, J., Dorioz, J., & Elsass, F. (2008). Analytical Electron-Microscopy Fractionation of Fine and Colloidal Particulate-Phosphorus in Riverbed and Suspended Sediments. *Aquatic Geochemistry* , 14, 193-210. doi: 0.1007/s10498-008-9032-5.

Reddy, K. R., Kadlec, R. H., Flaig, E., & Gale, P. M. (1999). Phosphorus Retention in Streams and Wetlands: A Review. *Critical Reviews in Environmental Science and Technology*, 29(1), 83-146. doi: 10.1080/10643389991259182

Reijneveld, A., & Oenema, O. (2012). Developments in soil phosphorus status in a recently reclaimed polder in the Netherlands. *Nutrient Cycling in Agroecosystems* , 94, 33-45. doi:10.1007/s10705-012-9524-y.

Reynolds, C. S., & Davies, P. S. (2001). Sources and bioavailability of phosphorus fractions in freshwaters: a British perspective. *Biological Reviews*, 76, 27-64.

Rijkswaterstaat. (2018). Normaal Amsterdams Peil (NAP). Retrieved June 28, 2018, from https://www.rijkswaterstaat.nl/zakelijk/open-data/normaal-amsterdams-peil/index.aspx

Rivett, M. O., Buss, S. R., Morgan, P., Smith, J. W. N., & Bemment, C. D. (2008). Nitrate attenuation in groundwater: A review of biogeochemical controlling processes. *Water Research*, 42(16), 4215-4232. doi:10.1016/j.watres.2008.07.020.

Robards, K., McKelvie, I. D., Benson, R. L., Worsfold, P. J., Blundell, N. J., & Casey, H. (1994). Determination of carbon, phosphorus, nitrogen and silicon species in waters. *Analytica Chimica Acta*, 287, 147-190.

Roden, E. E., & Edmonds, J. W. (1997). Phosphate mobilization in iron-rich anaerobic sediments: Microbial Fe(III) oxide reduction versus iron-sulfide formation. *Archiv Fur Hydrobiologie*, 139(3), 347-378.

Ruttenberg, K. C. (1992). Development of a sequential extraction method for different forms of phosphorus in marine sediments. *Limnology and Oceanography*, 37(7), 1460-1482. doi:10.4319/lo.1992.37.7.1460.

Sas, L., Tang, C., & Rengel, Z. (2001). Suitability of hydroxyapatite and iron phosphate as P sources for *Lupinus albus* grown in nutrient solution. *Plant and Soil*, 235, 159-166.

Schoumans, O. F. (2015). *Phosphorus leaching from soils: process description, risk assessment and mitigation*. PhD thesis. Wageningen University.

Schoumans, O. F., & Chardon, W. J. (2015). Phosphate saturation degree and accumulation of phosphate in various soil types in The Netherlands. *Geoderma,* 237-238, 325-335. doi:10.1016/j.geoderma.2014.08.015.

Schoumans, O. F., & Groenendijk, P. (2000). Modeling Soil Phosphorus Levels and Phosphorus Leaching from Agricultural Land in the Netherlands. *Journal of Environmental Quality*, 29(1), 111-116. doi:10.2134/jeq2000.00472425002900010014x

Schwertmann, U. (1991). Solubility and dissolution of iron oxides. *Plant and Soil*, 130(1-2), 1-25.

Schwertmann, U., & Taylor, R. M. (1989). Iron oxides. In: *Minerals in Soil Environments* (2nd ed.). WI: Soil Science Society of America.

Senn, A., Kaegi, R., Hug, S. J., Hering, J. G., Mangold, S., & Voegelin, A. (2015). Composition and structure of Fe(III)-precipitates formed by Fe(II) oxidation in water at near-neutral pH: Interdependent effects of phosphate, silicate and Ca. *Geochimica Et Cosmochimica Acta*, 162, 220-246. doi:10.1016/j.gca.2015.04.032.

Shenker, M., Seitelbach, S., Brand, S., Haim, A., & Litaor, M. I. (2005). Redox reactions and phosphorus release in re-flooded soils of an altered wetland. *European Journal of Soil Science*, 56, 515-525. doi:10.1111/j.1365-2389.2004.00692.x

Sinke, A. J. C. (1992). *Phosphorus dynamics in the sediment of a eutrophic lake.* PhD thesis. Agricultural University, Wageningen, The Netherlands.

Smit, A. L., Van Middelkoop, J. C., Van Dijk, W., & Van Reuler, H. (2015). A substance flow analysis of phosphorus in the food production, processing and consumption system of the Netherlands. *Nutrient Cycling in Agroecosystems* , 103(1), 1-13. doi:10.1007/s10705-015-9709-2.

Smolders, A. J. P., Lamers, L. P. M., Lucassen, E. C. H. E. T., Van der Velde, G., & Roelofs, J. G. M. (2006). Internal eutrophication: How it works and what to do about it—a review. *Chemistry and Ecology*, 22(2), 93-111. doi:10.1080/02757540600579730.

Stumm, W., & Lee, G. F. (1961). Oxygenation of Ferrous Iron. *Ind. Eng. Chem.,* 53 (2), 143-146. doi:10.1021/ie50614a030.

Torrent, J., Barrón, V., & Schwertmann, U. (1990). Phosphate Adsorption and Desorption by Goethites Differing in Crystal Morphology. *Soil Science Society of America Journal*, 54(4), 1007-1012.

Turner, B. L., Cade-Menun, B. J., Condron, L. M., & Newman, S. (2005). Extraction of soil organic phosphorus. *Talanta*, 66, 294-306. doi:10.1016/j.talanta.2004.11.012.

Van der Grift, B., Rozemeijer, J. C., Griffioen, J., & Van der Velde, Y. (2014). Iron oxidation kinetics and phosphate immobilization along the flow-path from groundwater into surface water. *Hydrology and Earth System Sciences*, 18(11), 4687-4702. doi://doi.org/10.5194/hess-18-4687-2014.

Van Der Grift, B., Broers, H. P., Berendrecht, W., Rozemeijer, J., Osté, L., & Griffioen, J. (2016a). High-frequency monitoring reveals nutrient sources and transport processes in an agriculture-dominated

lowland water system. *Hydrology and Earth System Sciences*, 20(5), 1851-1868. doi:10.5194/hess-20-1851-2016.

Van der Grift, B., Behrends, T., Osté, L. A., Schot, P. P., Wassen, M. J., & Griffioen, J. (2016b). Fe hydroxyphosphate precipitation and Fe(II) oxidation kinetics upon aeration of Fe(II) and phosphate-containing synthetic and natural solutions. *Geochimica Et Cosmochimica Acta*, 186, 71-90. doi:10.1016/j.gca.2016.04.035.

Van der Grift, B. (2017). *Geochemical and hydrodynamic phosphorus retention mechanisms in lowland catchments.* PhD thesis. Utrecht University.

Van der Grift, B., Osté, L., Schot, P., Kratz, A., Van Popta, E., Wassen, M., & Griffioen, J. (2018). Forms of phosphorus in suspended particulate matter in agriculture-dominated lowland catchments: Iron as phosphorus carrier. Science of The Total Environment, 631-632, 115-129. doi:10.1016/j.scitotenv.2018.02.266.

Van der Salm, C., Van den Toorn, A., Chardon, W. J., & Koopmans, G. F. (2012). Water and Nutrient Transport on a Heavy Clay Soil in a Fluvial Plain in The Netherlands. *Journal of Environment Quality*, 41, 229-241. doi:10.2134/jeq2011.0292.

Van der Zee, S. E. A. T. M. (1988). *Transport of Reactive Contaminants in Heterogenous Soil Systems*. PhD thesis. Agricultural University, Wageningen, The Netherlands.

Van Grinsven, H. J., Tiktak, A., & Rougoor, C. W. (2016). Evaluation of the Dutch implementation of the nitrates directive, the water framework directive and the national emission ceilings directive. *NJAS - Wageningen Journal of Life Sciences*, 78, 69-84. doi:10.1016/j.njas.2016.03.010.

Van Puijenbroek, P., Cleij, P., & Visser, H. (2014). Aggregated indices for trends in eutrophication of different types of fresh water in the Netherlands. *Ecological Indicators,* 36, 456-462. doi:10.1016/j.ecolind.2013.08.022.

Van Vuuren, D. P., Bouwman, A. F., & Beusen, A. H. (2010). Phosphorus demand for the 1970–2100 period: A scenario analysis of resource depletion. *Global Environmental Change*, 20(3), 428-439. doi:10.1016/j.gloenvcha.2010.04.004.

Villalobos, M., Cheney, M. A., & Alcaraz-Cienfuegos, J. (2009). Goethite surface reactivity: II. A microscopic site-density model that describes its surface area-normalized variability. *Journal of Colloid and Interface Science*, 336(2), 412-422. doi:10.1016/j.jcis.2009.04.052.

Viollier, E., Inglett, P. W., Hunter, K., Roychoudhury, A. N., & Van Cappellen, P. (2000). The ferrozine method revisited: Fe(II)/Fe(III) determination in natural waters. *Applied Geochemistry*, 15(6), 785-790.

Voegelin, A., Senn, A., Kaegi, R., Hug, S. J., & Mangold, S. (2013). Dynamic Fe-precipitate formation induced by Fe(II) oxidation in aerated phosphate-containing water. *Geochimica Et Cosmochimica Acta*, 117, 216-231. doi:10.1016/j.gca.2013.04.022

Wajon, J.E., Ho, G.E., Murphy, P.J. (1985). Rate of precipitation of ferrous iron and formation of mixed iron–calcium carbonates by naturally occurring carbonate materials. *Water Res*. 19 (7), 831–837.

Walpersdorf, E., Koch, C. B., Heiberg, L., O'connell, D. W., Kjaergaard, C., & Hansen, H. C. B. (2013). Does vivianite control phosphate solubility in anoxic meadow soils? *Geoderma*, 193-194, 189-199.

Wiersum, L. K. (1960). Some experiences in soil aeration measurements and relationships to depth of rooting. *Netherlands Journal of Agricultural Science*, 8(4), 245-252.

Withers, P. J., & Haygarth, P. M. (2007). Agriculture, phosphorus and eutrophication: a European perspective. *Soil Use and Management*, 23(Suppl.1), 1-4.

Withers, P. J., Neal, C., Jarvie, H. P., & Doody, D. G. (2014). Agriculture and Eutrophication: Where Do We Go from Here? *Sustainability*, 6, 5853-5875. doi:10.3390/su6095853.

Worsfold, P., McKelvie, I., & Monbet, P. (2016). Determination of phosphorus in natural waters: A historical review. *Analytica Chimica Acta*, 918, 8-20. doi:10.1016/j.aca.2016.02.047.

Appendix I

Tables A.1-A.8 show the boreholes description in terms of the percentage of clay, silt, sand, gravel and organic matter, according to Bosch (2000). Calcite was also classified under categories, in which 1 means no calcite, 2 means some calcite, and 3 holds for large presence of calcite. The M63 represents the median grain size (μm) of the sand fraction.

Table A.1: Lithological description of borehole B1.

	Soil Layer	Depth (m)	M63	% Clay	% Silt	% Sand	% Gravel	% OM	$CaCO_3$
B1	A	0.75		10	30	60	0	2	3
	B	1.25	110	0	25	75	0	1	3
	C	2.00	110	0	12	88	0	1	3
	D	3.00	120	0	8	92	0	1	3
	E	4.00	110	0	12	88	0	1	3

Table A.2: Lithological description of borehole B2.

	Soil Layer	Depth (m)	M63	% Clay	% Silt	% Sand	% Gravel	% OM	$CaCO_3$
B2	A	0.75	90	2	33	65	0	1	3
	B	1.25		3	52	45	0	1	3
	C	2.00	115	0	8	92	0	1	3
	D	3.00	120	0	6	94	0	1	3
	E	4.00	120	0	7	93	0	1	3

Table A.3: Lithological description of borehole B3

	Soil Layer	Depth (m)	M63	% Clay	% Silt	% Sand	% Gravel	% OM	$CaCO_3$
B3	A	0.75		3	52	45	0	1	3
	B	1.25	100	1	20	79	0	2	3
	C	2.00	100	0	15	85	0	1	3
	D	3.00	110	0	8	92	0	1	3
	E	4.00	115	0	8	92	0	1	3

Table A.4: Lithological description of borehole B4.

	Soil Layer	Depth (m)	M63	% Clay	% Silt	% Sand	% Gravel	% OM	$CaCO_3$
B4	A	0.75		3	52	45	0	1	3
	B	1.25	100	0	15	85	0	1	3
	C	2.00	105	0	15	85	0	1	3
	D	3.00	110	0	15	85	0	1	3
	E	4.00	110	0	8	92	0	1	3

Table A.5: Lithological description of borehole B5.

	Soil Layer	Depth (m)	M63	% Clay	% Silt	% Sand	% Gravel	% OM	$CaCO_3$
B5	A	0.75		3	52	45	0	1	3
	B	1.25		3	52	45	0	1	3
	C	2.00	110	0	8	92	0	2	3
	D	3.00	110	0	8	92	0	2	3
	E	4.00	100	0	12	88	0	2	3

Table A.6: Lithological description of borehole B6.

	Soil Layer	Depth (m)	M63	% Clay	% Silt	% Sand	% Gravel	% OM	$CaCO_3$
B6	A	0.75		3	52	45	0	1	3
	B	1.25		3	52	45	0	1	3
	C	2.00	115	0	8	92	0	2	3
	D	3.00	120	0	8	92	0	1	3
	E	4.00	110	0	8	92	0	1	3

Table A.7: Lithological description of borehole B7.

	Soil Layer	Depth (m)	M63	% Clay	% Silt	% Sand	% Gravel	% OM	$CaCO_3$
B7	A	0.75		3	52	45	0	1	3
	B	1.25		3	52	45	0	1	3
	C	2.00	100	0	12	88	0	2	3
	D	3.00	115	0	8	92	0	1	3
	E	4.00	115	0	8	92	0	1	3

Table A.8: Lithological description of borehole B8.

	Soil Layer	Depth (m)	M63	% Clay	% Silt	% Sand	% Gravel	% OM	$CaCO_3$
B8	A	0.75		3	52	45	0	1	3
	B	1.25		3	52	45	0	1	3
	C	2.00	100	0	12	88	0	2	3
	D	3.00	100	0	12	88	0	2	3
	E	4.00	100	0	12	88	0	2	3

Table A.9: Left: Coordinates of the boreholes. Right: Coordinates of the drains. The coordinates are given in the RD Dutch coordinates system.

	Coordinates	
Borehole ID	X	Y
B1	113877	512553
B2	113766	512600
B3	113682	512620
B4	113556	512670
B5	113542	512623
B6	113641	512584
B7	113752	512553
B8	113859	512518

	Coordinates	
	X	Y
Drain 1	113524	512707
Drain 2	113571	512694
Drain 3	113596	512686
Drain 4	113654	512668
Drain 5	113681	512651
Drain 6	113738	512633
Drain 7	113764	512623
Drain 8	113797	512615
Drain 9	113840	512594
Drain 10	113879	512580

Figure A.1: Soil profile down to 1.25 m depth for all the boreholes analyzed.

Appendix II

Table A.10: DOC concentrations of all the drains and ditch water samples.

	DOC (mg/L)											
Date	Drain 1	Drain 2	Drain 3	Drain 4	Drain 5	Drain 6	Drain 7	Drain 8	Drain 9	Drain 10	Ditch Middle	Ditch End
6-dec	21.3	18.9	23.8	20.8	18.8	24.7	21.1	18.5	21.4	-	23.5	22.1
19-dec	12.0	12.1	10.0	10.6	10.2	11.6	11.6	11.3	21.2	-	12.8	13.0
10-jan	74.2	42.8	62.1	47.8	51.4	58.6	47.1	85.1	63.4	71.1	50.9	60.9
31-jan	12.2	11.7	11.8	12.1	13.6	11.3	13.1	14.9	12.0	10.8	13.7	12.7
21-feb	11.8	12.0	11.9	12.0	13.3	-	13.0	14.5	13.1	12.8	14.7	14.9
13-mrt	12.1	11.5	10.8	11.4	14.4	12.8	13.4	15.0	12.2	14.3	13.2	13.9
6-apr	11.1	9.8	9.7	10.0	10.5	8.8	11.0	13.8	10.4	11.2	13.2	13.3
3-mei	14.8	-	-	-	-	-	-	-	-	-	14.6	16.4

Table A.11: Chloride concentrations of all the drains and ditch water samples.

	Chloride (mg/L)											
Date	Drain 1	Drain 2	Drain 3	Drain 4	Drain 5	Drain 6	Drain 7	Drain 8	Drain 9	Drain 10	Ditch Middle	Ditch End
6-dec	679.8	592.9	525.4	936.9	1042.5	1735.1	1861.4	1753.8	2198.9	-	1747.3	2124.9
19-dec	576.7	267.3	342.6	542.8	639.1	1463.9	1419.9	1451.6	1320.3	-	1365.6	1713.3
10-jan	800.4	698.4	425.5	495.4	900.6	738.2	1655.1	1849.7	1599.1	2004.1	1744.3	2066.0
31-jan	762.7	364.7	591.4	847.2	1427.4	689.1	1592.4	1762.9	1457.2	898.8	1650.8	1855.4
21-feb	564.7	338.3	390.9	752.5	1057.4	-	1279.5	1265.6	1558.7	2061.5	1838.3	2415.0
13-mrt	587.7	196.0	408.5	555.6	402.9	295.3	1155.4	1280.6	1100.3	754.8	1779.4	2064.7
6-apr	465.2	210.6	268.1	433.0	484.9	228.4	1137.0	1719.1	791.6	1346.3	1316.8	1632.4
3-mei	314.5	-	-	-	-	-	-	-	-	-	854.5	1271.1

Table A.12: Nitrate concentrations of all the drains and ditch water samples.

	Nitrate (mg/L)											
Date	Drain 1	Drain 2	Drain 3	Drain 4	Drain 5	Drain 6	Drain 7	Drain 8	Drain 9	Drain 10	Ditch Middle	Ditch End
6-dec	0.0	0.1	0.2	0.4	0.4	0.3	0.0	0.2	1.1	-	0.2	0.5
19-dec	0.2	0.6	1.0	0.9	3.2	1.6	1.8	1.4	0.0	-	0.4	0.5
10-jan	0.1	0.0	0.0	0.2	0.1	0.2	0.1	0.0	0.0	0.3	0.2	0.2
31-jan	0.1	0.2	0.0	0.2	0.0	0.2	0.1	0.2	0.2	0.6	0.2	0.2
21-feb	0.0	0.0	0.0	0.0	0.0	-	0.0	0.0	0.0	0.0	0.2	0.0
13-mrt	0.3	2.0	0.8	3.1	3.1	7.2	2.8	3.7	1.8	5.7	1.1	0.6
6-apr	0.7	0.2	0.2	0.2	0.2	0.5	0.0	0.0	0.2	0.4	0.2	0.3
3-mei	10.4	-	-	-	-	-	-	-	-	-	5.4	7.2

Table A.13: Sulfate concentrations of all the drains and ditch water samples.

	Sulfate (mg/L)											
Date	Drain 1	Drain 2	Drain 3	Drain 4	Drain 5	Drain 6	Drain 7	Drain 8	Drain 9	Drain 10	Ditch Middle	Ditch End
6-dec	115.4	101.3	109.3	98.7	117.0	76.0	80.8	85.0	108.9	-	78.8	77.9
19-dec	90.0	54.1	78.1	54.9	84.4	66.8	75.9	91.7	58.0	-	70.8	69.9
10-jan	108.9	104.0	95.9	100.8	95.4	112.2	73.4	76.5	84.8	100.6	75.3	73.0
31-jan	103.1	90.9	96.6	86.9	66.6	86.6	66.1	53.4	77.3	47.9	68.3	62.3
21-feb	101.7	103.8	103.5	98.8	79.6	-	76.3	90.5	80.9	109.0	68.1	69.6
13-mrt	94.2	77.9	93.0	89.5	69.8	116.6	84.3	69.6	81.5	85.7	62.2	64.6
6-apr	191.9	289.1	261.2	238.1	242.4	269.2	162.5	86.7	211.9	193.7	141.0	130.3
3-mei	166.4	-	-	-	-	-	-	-	-	-	147.6	139.2

Table A.14: Aluminum concentrations of all the drains and ditch water samples.

	Aluminum (mg/L)											
Date	Drain 1	Drain 2	Drain 3	Drain 4	Drain 5	Drain 6	Drain 7	Drain 8	Drain 9	Drain 10	Ditch Middle	Ditch End
6-dec	0.002	0.001	0.002	0.009	0.002	0.001	0.003	0.002	0.001	-	0.002	0.002
19-dec	0.004	0.002	0.002	0.002	0.002	0.001	0.001	0.002	0.002	-	0.001	0.001
10-jan	0.006	0.009	0.003	0.004	0.003	0.002	0.005	0.002	0.003	0.006	0.016	0.001
31-jan	0.005	0.002	0.003	0.003	0.000	0.000	0.000	0.002	0.001	0.001	0.012	0.000
21-feb	0.002	0.001	0.003	0.000	0.005	-	0.003	0.002	0.001	0.000	0.000	0.000
13-mrt	0.001	0.001	0.001	0.001	0.001	0.001	0.000	0.000	0.003	0.001	0.001	0.003
6-apr	0.000	0.000	0.001	0.001	0.001	0.001	0.000	0.001	0.000	0.001	0.006	0.001
3-mei	0.004	-	-	-	-	-	-	-	-	-	0.003	0.003

Table A.15: Calcium concentrations of all the drains and ditch water samples.

	Calcium (mg/L)											
Date	Drain 1	Drain 2	Drain 3	Drain 4	Drain 5	Drain 6	Drain 7	Drain 8	Drain 9	Drain 10	Ditch Middle	Ditch End
6-dec	225.4	243.9	241.7	292.3	296.6	343.8	277.2	336.0	332.7	-	245.6	277.8
19-dec	192.9	148.2	183.9	175.3	214.3	289.8	281.6	264.4	336.6	-	219.9	242.8
10-jan	197.6	217.6	211.2	228.0	273.4	246.4	314.1	237.2	286.2	295.9	236.3	254.5
31-jan	210.6	189.6	218.3	243.1	218.8	203.9	276.6	198.8	268.0	153.2	211.8	210.4
21-feb	206.0	202.7	222.6	257.0	214.9	-	272.5	223.5	279.3	306.6	201.7	240.9
13-mrt	192.4	150.9	190.0	201.1	142.9	178.8	238.5	186.3	233.5	177.6	205.3	227.0
6-apr	211.4	222.3	224.3	237.7	225.9	220.3	269.6	231.1	244.1	272.2	228.6	246.1
3-mei	180.7	-	-	-	-	-	-	-	-	-	238.1	262.8

Table A.16: Iron concentrations of all the drains and ditch water samples.

	Iron (mg/L)											
Date	Drain 1	Drain 2	Drain 3	Drain 4	Drain 5	Drain 6	Drain 7	Drain 8	Drain 9	Drain 10	Ditch Middle	Ditch End
6-dec	1.2	2.7	2.3	3.1	3.3	11.8	8.6	4.1	7.2	-	1.3	1.1
19-dec	1.8	1.0	1.0	1.3	2.0	5.7	3.7	4.3	33.3	-	1.1	1.5
10-jan	0.4	0.8	6.2	6.5	7.2	5.4	12.4	11.3	6.8	9.5	1.8	2.7
31-jan	1.2	7.3	6.6	6.7	11.3	5.3	13.2	6.7	7.8	2.3	0.3	0.3
21-feb	1.0	12.3	9.4	11.9	15.7	-	20.3	11.3	13.6	14.7	0.1	0.4
13-mrt	1.5	0.9	0.9	1.9	1.0	2.0	8.4	3.1	5.6	2.0	0.8	1.4
6-apr	1.0	2.6	2.7	3.3	4.1	0.9	8.1	5.6	5.2	5.3	0.1	0.2
3-mei	2.7	-	-	-	-	-	-	-	-	-	0.7	0.7

Table A.17: Potassium concentrations of all the drains and ditch water samples.

	Potassium (mg/L)											
Date	Drain 1	Drain 2	Drain 3	Drain 4	Drain 5	Drain 6	Drain 7	Drain 8	Drain 9	Drain 10	Ditch Middle	Ditch End
6-dec	17.2	14.8	11.6	15.4	13.9	14.8	28.1	18.9	33.1	-	35.9	36.2
19-dec	14.3	10.4	9.8	13.1	10.9	13.7	16.4	23.2	16.0	-	27.4	29.5
10-jan	22.2	17.1	13.1	11.4	15.2	11.6	15.2	29.5	19.2	30.0	34.4	36.6
31-jan	17.3	11.7	12.3	14.5	21.8	11.8	15.9	28.2	16.8	17.8	33.5	33.2
21-feb	15.4	11.2	10.1	13.8	17.1	-	12.7	23.1	18.0	31.3	37.6	42.2
13-mrt	14.7	8.9	10.5	11.7	11.0	9.1	14.1	22.2	14.3	17.3	33.0	36.5
6-apr	14.0	10.9	10.9	11.8	13.6	9.1	13.7	28.4	14.0	24.6	28.4	30.9
3-mei	12.0	-	-	-	-	-	-	-	-	-	21.3	25.7

Table A.18: Magnesium concentrations of all the drains and ditch water samples.

	Magnesium (mg/L)											
Date	Drain 1	Drain 2	Drain 3	Drain 4	Drain 5	Drain 6	Drain 7	Drain 8	Drain 9	Drain 10	Ditch Middle	Ditch End
6-dec	51.9	44.0	38.0	56.1	59.3	83.0	115.8	90.8	134.1	-	116.9	132.7
19-dec	43.1	21.7	26.2	38.7	37.2	71.1	73.8	87.5	68.6	-	90.6	107.2
10-jan	66.2	53.1	36.3	36.3	55.2	46.6	84.6	118.4	86.8	119.0	115.0	131.5
31-jan	55.4	31.7	41.0	51.6	83.8	42.7	83.1	107.3	75.6	53.3	107.7	117.3
21-feb	44.9	31.7	31.8	49.4	64.9	-	68.0	86.1	84.9	130.5	122.4	156.7
13-mrt	45.2	19.7	31.5	39.0	29.4	24.5	65.5	82.8	60.0	49.4	113.9	130.7
6-apr	38.8	25.1	25.4	34.4	39.8	23.3	64.6	112.2	49.5	92.2	92.2	110.1
3-mei	30.1	-	-	-	-	-	-	-	-	-	62.6	84.4

Table A.19: Manganese concentrations of all the drains and ditch water samples.

	Manganese (mg/L)											
Date	Drain 1	Drain 2	Drain 3	Drain 4	Drain 5	Drain 6	Drain 7	Drain 8	Drain 9	Drain 10	Ditch Middle	Ditch End
6-dec	0.8	1.0	0.8	1.1	1.2	1.5	1.1	1.4	1.4	-	0.9	1.1
19-dec	0.6	0.4	0.5	0.6	0.6	1.2	1.1	0.9	3.6	-	0.7	0.9
10-jan	0.8	0.8	0.8	0.8	1.2	1.1	1.5	1.1	1.3	1.3	0.9	1.0
31-jan	0.8	0.8	0.8	1.0	1.1	0.9	1.4	0.8	1.3	0.6	0.8	0.8
21-feb	0.8	1.0	0.9	1.3	1.1	-	1.5	0.9	1.4	1.5	0.7	1.0
13-mrt	0.7	0.4	0.6	0.7	0.3	0.6	1.0	0.6	1.0	0.5	0.8	0.9
6-apr	0.5	0.4	0.5	0.6	0.6	0.5	1.0	0.9	0.8	0.9	0.6	0.8
3-mei	0.5	-	-	-	-	-	-	-	-	-	0.6	0.7

Table A.20: Sodium concentrations of all the drains and ditch water samples.

	Sodium (mg/L)											
Date	Drain 1	Drain 2	Drain 3	Drain 4	Drain 5	Drain 6	Drain 7	Drain 8	Drain 9	Drain 10	Ditch Middle	Ditch End
6-dec	396.0	302.4	285.5	478.5	552.2	913.3	1040.0	935.1	1154.0	-	978.7	1163.0
19-dec	342.0	147.6	191.1	287.3	327.0	780.7	762.4	738.5	692.0	-	747.6	941.4
10-jan	465.6	399.3	230.7	264.7	455.6	399.0	865.7	1055.0	865.6	1065.0	983.9	1155.0
31-jan	426.0	201.8	310.5	432.6	804.1	377.4	846.5	998.1	763.5	486.2	927.7	1038.0
21-feb	327.6	181.5	208.0	393.9	575.0	-	686.3	724.1	827.5	1072.0	1045.0	1379.8
13-mrt	339.3	118.4	227.2	303.3	243.5	178.1	633.1	719.2	574.7	420.0	1010.0	1148.0
6-apr	281.4	134.5	157.3	233.7	277.1	148.6	617.9	984.2	433.6	718.7	726.1	911.0
3-mei	986.4	-	-	-	-	-	-	-	-	-	474.4	705.4

Table A.21: Total P concentrations of all the drains and ditch water samples.

	Total P (mg/L)											
Date	Drain 1	Drain 2	Drain 3	Drain 4	Drain 5	Drain 6	Drain 7	Drain 8	Drain 9	Drain 10	Ditch Middle	Ditch End
6-dec	0.8	0.2	0.2	0.1	0.1	0.1	1.4	0.0	0.3	-	0.8	0.1
19-dec	0.8	0.5	0.3	0.4	0.3	0.2	0.1	0.4	1.1	-	0.8	0.5
10-jan	1.2	0.8	1.0	1.1	0.4	0.3	0.2	2.5	0.1	0.6	1.1	0.9
31-jan	0.8	1.2	1.3	0.4	0.8	0.4	0.3	1.7	0.1	0.5	0.7	0.3
21-feb	0.8	2.2	1.8	0.9	0.8	-	0.4	3.3	0.1	1.0	0.5	0.3
13-mrt	0.7	0.2	0.2	0.2	0.4	0.3	0.3	0.9	0.1	0.4	0.4	0.3
6-apr	0.7	0.6	0.6	0.4	0.6	0.2	0.2	1.5	0.1	0.6	0.5	0.3
3-mei	0.4	-	-	-	-	-	-	-	-	-	0.4	0.3

Table A.22: Ammonium concentrations of all the drains and ditch water samples.

	Ammonium (mg/L)											
Date	Drain 1	Drain 2	Drain 3	Drain 4	Drain 5	Drain 6	Drain 7	Drain 8	Drain 9	Drain 10	Ditch Middle	Ditch End
6-dec	3.4	2.7	2.2	2.7	2.7	3.6	6.4	4.3	7.9	-	8.3	1.2
19-dec	2.7	1.3	1.5	2.2	2.0	3.3	3.8	5.0	5.3	-	5.6	6.9
10-jan	5.1	3.4	2.4	2.2	2.8	2.4	4.2	7.9	4.8	7.4	7.2	8.6
31-jan	3.6	2.2	2.6	2.8	5.9	2.5	4.4	7.7	4.2	3.6	6.4	7.4
21-feb	3.0	2.2	1.9	2.5	4.4	-	3.4	5.5	4.9	7.9	5.9	9.3
13-mrt	2.8	1.1	1.8	1.9	1.9	1.3	3.3	5.5	3.1	3.3	6.4	7.8
6-apr	2.3	1.1	1.1	1.4	1.8	0.9	3.1	7.2	2.5	5.2	5.0	5.7
3-mei	1.9	-	-	-	-	-	-	-	-	-	3.4	4.7

Table A.23: Phosphate concentrations of all the drains and ditch water samples.

	Phosphate (mg/L)											
Date	Drain 1	Drain 2	Drain 3	Drain 4	Drain 5	Drain 6	Drain 7	Drain 8	Drain 9	Drain 10	Ditch Middle	Ditch End
6-dec	2.5	0.6	0.7	0.5	0.3	0.2	4.0	0.0	0.7	-	2.4	0.5
19-dec	2.3	1.5	0.9	1.1	1.0	0.5	0.2	1.2	3.2	-	2.5	1.5
10-jan	3.6	2.4	3.2	3.3	1.2	0.8	0.7	7.1	0.2	1.7	3.6	2.7
31-jan	2.4	3.6	4.0	1.4	2.7	1.1	1.0	5.3	0.3	1.6	2.0	1.0
21-feb	2.4	6.9	5.3	2.7	2.4	-	1.3	9.8	0.4	3.1	1.4	0.8
13-mrt	2.2	0.6	0.7	0.5	1.2	0.9	0.9	2.6	0.3	1.2	1.2	0.9
6-apr	2.1	1.7	1.7	1.2	1.7	0.6	0.8	4.6	0.3	1.7	1.5	0.8
3-mei	1.4	-	-	-	-	-	-	-	-	-	1.1	1.0

Table A.24: pH values of all the drains and ditch water samples.

	pH											
Date	Drain 1	Drain 2	Drain 3	Drain 4	Drain 5	Drain 6	Drain 7	Drain 8	Drain 9	Drain 10	Ditch Middle	Ditch End
6-dec	6.9	7.4	7.4	7.4	7.4	7.2	7.4	7.4	7.3	-	7.7	7.5
19-dec	6.8	7.0	7.0	7.0	7.0	6.9	7.0	7.0	7.0	-	7.1	7.1
10-jan	7.0	7.1	7.2	7.2	7.2	7.2	7.2	7.3	7.2	7.3	7.3	7.4
31-jan	6.9	7.0	6.9	6.9	6.8	7.0	6.9	6.9	6.9	6.9	7.3	7.3
21-feb	7.3	7.2	7.2	7.2	7.7	-	7.2	7.4	7.3	7.4	7.6	7.3
13-mrt	7.2	7.3	7.1	7.1	7.1	7.1	7.1	7.1	7.1	7.4	7.7	7.8
6-apr	6.9	7.1	7.0	7.0	7.0	7.1	7.1	7.1	7.1	7.1	7.2	7.4
3-mei	7.0	-	-	-	-	-	-	-	-	-	7.2	7.0

Table A.25: Alkalinity of all the drains and ditch water samples.

	Alkalinity as HCO_3 (mg/L)											
Date	Drain 1	Drain 2	Drain 3	Drain 4	Drain 5	Drain 6	Drain 7	Drain 8	Drain 9	Drain 10	Ditch Middle	Ditch End
6-dec	660.0	623.4	955.3	912.6	719.8	743.7	800.3	708.6	650.5	-	607.6	577.3
19-dec	658.8	475.8	475.8	469.7	664.9	695.4	689.3	707.6	884.5	-	634.4	744.2
10-jan	780.8	664.9	671.0	530.7	677.1	622.2	799.1	933.3	786.9	835.7	939.4	854.0
31-jan	603.9	542.9	603.9	634.4	762.5	628.3	756.4	805.2	719.8	762.5	786.9	823.5
21-feb	546.6	561.2	595.4	661.2	270.8	-	756.4	834.5	810.1	900.4	819.8	968.7
13-mrt	605.1	473.4	531.9	583.2	456.3	468.5	658.8	678.3	683.2	546.6	822.3	878.4
6-apr	463.6	591.7	427.0	555.1	597.8	475.8	677.1	841.8	567.3	683.2	640.5	823.5
3-mei	555.1	-	-	-	-	-	-	-	-	-	595.4	663.7

Table A.26: Oxygen concentrations of all the drains and ditch water samples.

	Oxygen (mg/L)											
Date	Drain 1	Drain 2	Drain 3	Drain 4	Drain 5	Drain 6	Drain 7	Drain 8	Drain 9	Drain 10	Ditch Middle	Ditch End
6-dec	3.5	-	-	-	-	-	-	-	-	-	-	-
19-dec	2.0	3.4	3.4	5.2	3.9	4.4	3.8	3.6	2.0	-	4.2	3.5
10-jan	2.3	3.1	2.8	2.8	3.7	4.3	3.7	3.7	4.3	4.1	2.7	3.0
31-jan	2.7	3.6	4.1	4.0	3.4	5.9	3.9	4.4	3.6	5.4	9.5	8.4
21-feb	3.9	3.7	3.0	3.4	5.1	-	5.0	4.9	5.6	5.5	22.0	21.7
13-mrt	3.5	4.3	3.8	3.4	7.1	4.0	4.9	5.6	4.7	5.6	8.0	6.0
6-apr	2.6	2.5	2.7	3.6	3.7	4.5	4.7	3.4	4.9	4.2	12.6	18.8
3-mei	1.7	-	-	-	-	-	-	-	-	-	7.1	7.5

Table A.27: Temperature of all the drains and ditch water samples.

	Temperature (°C)											
Date	Drain 1	Drain 2	Drain 3	Drain 4	Drain 5	Drain 6	Drain 7	Drain 8	Drain 9	Drain 10	Ditch Middle	Ditch End
6-dec	8.9	-	-	-	-	-	-	-	-	-	-	-
19-dec	9.1	9.3	9.3	9.9	10.6	10.5	10.7	10.6	10.8	-	11.5	11.4
10-jan	7.0	7.3	7.3	7.4	7.5	7.4	7.4	7.4	7.4	7.4	7.3	7.6
31-jan	-	-	-	-	-	-	-	-	-	6.8	-	-
21-feb	5.4	4.9	5.2	5.6	4.8	-	4.7	4.9	4.6	4.7	5.3	1.8
13-mrt	6.0	5.9	5.9	6.3	5.8	5.6	5.6	5.6	5.4	5.4	5.6	5.9
6-apr	7.5	7.1	7.1	7.4	7.4	7.6	7.9	7.9	7.9	8.2	9.6	11.7
3-mei	12.8	-	-	-	-	-	-	-	-	-	18.3	18.7

Table A.28: Electrical conductivity of all the drains and ditch water samples.

	EC (µS/cm)											
Date	Drain 1	Drain 2	Drain 3	Drain 4	Drain 5	Drain 6	Drain 7	Drain 8	Drain 9	Drain 10	Ditch Middle	Ditch End
6-dec	3210	2770	2690	4000	4300	6310	6790	6390	7700	-	6570	7420
19-dec	2760	1580	2006	2540	2900	5530	5420	5500	5420	-	5360	6410
10-jan	3670	3280	2360	2610	3920	3390	6240	6920	6040	7320	6570	7550
31-jan	3270	1989	2750	3510	5280	2960	5710	6220	5350	3470	5930	6470
21-feb	2630	1740	1900	3100	3940	-	4560	4430	5160	6200	5950	7200
13-mrt	2300	1040	1610	1960	1650	1410	3400	3730	3350	2570	5090	5860
6-apr	2530	1770	1960	2470	2620	1810	4560	6370	3540	5240	5360	6280
3-mei	1896	-	-	-	-	-	-	-	-	-	3880	5030

Table A.29: Discharge of all the drains.

	Discharge (L/s)									
Date	Drain 1	Drain 2	Drain 3	Drain 4	Drain 5	Drain 6	Drain 7	Drain 8	Drain 9	Drain 10
6-dec	0.007	0.005	0.008	0.008	0.007	0.005	0.008	0.007	0.008	-
19-dec	0.016	0.020	0.026	0.024	0.015	0.011	0.014	-	0.011	-
10-jan	0.006	0.007	0.004	0.008	0.007	0.005	0.005	0.004	0.007	0.007
31-jan	0.010	0.007	0.012	0.010	0.006	0.007	0.007	0.008	0.010	0.013
21-feb	0.003	0.003	0.004	0.003	0.003	-	0.003	0.004	0.003	0.003
13-mrt	0.014	0.014	0.017	0.014	0.025	0.007	0.008	0.019	0.009	0.011
6-apr	0.023	0.027	0.035	0.025	0.015	0.010	0.010	-	0.014	-
3-mei	-	-	-	-	-	-	-	-	-	-

Table A.30: Concentration of all the elements analyzed in the pore water samples. The numbers 1-8 represent the location of the borehole, whereas the letters A-E stand for the depth of the soil layer. Note that, alkalinity, was not measured but, instead calculated as described in Section 3.2.2.

	Element concentration (mg/L)															pH
Sample	DOC	Cl	NO_3	SO_4	Al	Ca	Fe	K	Mg	Mn	Na	Total P	NH_4	PO_4	HCO_3	
1A	-	-	-	-	0.03	75.8	0.1	5.1	4.8	0.01	45.4	0.2	-	0.2	-	-
1B	35.6	6058.8	0.0	136.6	0.01	71.5	0.1	131.2	369.3	0.01	3466.4	0.5	33.7	1.4	987.7	8.9
1C	30.9	6755.1	0.0	16.4	0.01	232.4	0.0	134.2	392.4	0.48	3752.0	2.2	39.6	7.1	1320.0	8.5
1D	27.6	6993.5	0.0	17.4	0.01	236.9	0.2	145.2	429.0	0.47	3956.4	1.9	44.1	5.5	1683.8	8.3
1E	25.9	7224.5	0.0	302.6	0.01	118.4	0.0	196.1	401.4	0.00	3964.1	0.1	50.0	0.1	554.1	8.0
2A	39.4	65.0	0.0	92.3	0.02	112.9	0.1	0.9	7.9	0.00	31.3	0.0	2.1	0.0	246.4	8.3
2B	27.1	77.3	0.0	137.8	0.01	112.1	0.0	2.4	9.5	0.00	38.4	0.0	0.2	0.0	187.4	8.4
2C	30.7	4674.1	0.0	48.0	0.09	129.7	0.1	109.6	276.7	0.00	2626.1	0.1	23.8	0.0	901.1	8.1
2D	28.5	6875.2	0.0	18.7	0.00	123.6	0.0	153.5	427.0	0.00	3840.2	0.3	37.1	0.5	1220.2	8.2
2E	29.9	7040.9	0.8	2.7	0.09	207.5	0.1	152.7	416.1	0.44	3970.4	2.4	41.6	7.0	1503.8	8.6
3A	-	114.9	0.0	58.7	0.01	114.0	0.0	1.0	9.4	0.00	32.8	0.0	-	0.0	210.6	8.5
3B	24.2	61.9	0.0	146.3	0.02	121.9	0.0	2.5	11.0	0.01	34.7	0.0	0.1	0.0	230.6	8.2
3C	21.6	221.4	0.0	129.5	0.01	117.3	0.0	20.2	24.9	0.02	129.7	0.1	3.6	0.2	324.4	8.1
3D	31.7	4681.4	0.0	38.8	0.01	71.1	0.0	128.8	270.5	0.01	2847.6	0.8	29.8	2.3	1323.8	8.5
3E	28.1	6525.2	0.0	13.4	0.00	83.1	0.0	137.4	371.4	0.00	3808.0	0.7	34.6	2.2	1304.8	8.4
4A	24.9	100.7	6.3	105.9	0.01	147.4	0.0	1.7	10.7	0.00	32.8	0.0	0.1	0.0	278.4	8.4
4B	19.6	59.2	0.5	167.4	0.00	157.8	0.1	3.9	12.1	0.04	33.4	0.0	0.1	0.0	321.3	8.1
4C	23.8	581.9	0.0	225.4	0.01	89.8	0.0	46.8	61.4	0.04	434.0	0.1	9.0	0.1	549.3	8.2
4D	26.9	6169.6	0.0	16.4	0.00	100.6	0.0	138.5	366.9	0.00	3446.8	0.6	32.5	1.9	980.2	8.4
4E	28.7	6173.5	0.0	14.1	0.01	124.3	0.0	141.5	359.9	0.00	3631.6	1.0	32.5	2.7	1506.6	8.2
5A	29.3	44.5	0.0	18.4	0.04	60.5	0.1	1.7	3.5	0.00	37.2	0.1	0.0	0.0	203.2	9.0
5B	25.3	95.6	0.0	165.6	0.01	142.8	0.0	6.4	9.0	0.13	34.4	0.1	0.2	0.0	207.3	8.2
5C	27.4	514.0	1.0	163.7	0.00	89.3	0.0	63.2	65.5	0.01	296.2	0.1	9.9	0.0	426.1	8.3
5D	25.1	4509.8	0.0	5.9	0.01	128.4	0.2	122.9	322.0	0.00	2344.2	0.3	26.9	0.8	741.6	8.2
5E	30.0	5832.9	0.0	12.2	0.01	154.5	0.1	142.3	386.0	0.02	3320.8	0.9	30.6	2.5	1488.6	8.4
6A	33.2	97.7	0.0	98.2	0.02	118.8	0.0	0.8	9.4	0.00	42.3	0.0	-	0.0	230.0	8.9
6B	25.1	51.2	2.3	105.8	0.01	104.5	0.0	3.1	8.9	0.00	36.5	0.0	0.1	0.0	240.1	8.3
6C	20.5	1338.7	0.0	37.1	0.00	193.6	0.0	37.1	69.9	0.02	629.2	0.0	7.0	0.0	341.1	8.2
6D	26.5	5402.2	0.8	1.2	0.00	239.4	0.0	123.6	387.4	0.76	2914.8	2.4	30.7	7.1	1395.2	8.6
6E	32.1	6066.8	0.0	128.2	0.01	106.8	0.0	178.4	376.6	0.00	3424.4	0.1	36.3	0.0	1101.6	8.3
7A	25.1	109.4	10.1	56.5	0.01	132.0	0.0	1.2	11.3	0.00	40.1	0.0	0.1	0.0	297.1	8.5
7B	28.4	65.8	1.7	86.8	0.01	114.6	0.0	2.1	10.1	0.00	34.3	0.0	0.1	0.0	269.2	8.4
7C	21.0	726.7	0.0	256.0	0.01	260.8	0.1	24.8	31.5	0.06	355.3	0.1	2.5	0.0	367.1	7.9
7D	29.3	6980.3	0.8	1.6	0.01	301.1	0.0	120.6	462.3	0.99	3927.0	3.2	30.9	9.5	1920.7	8.6
7E	27.3	6852.7	0.0	153.6	0.00	122.2	0.0	168.8	414.7	0.00	3798.9	0.1	36.1	0.0	933.4	8.0
8A	31.6	124.6	8.9	212.7	0.00	162.2	0.0	2.4	12.6	0.00	50.8	0.0	-	0.0	202.3	8.2
8B	31.8	5252.4	0.0	63.8	0.00	260.2	0.4	76.9	264.3	0.05	2833.6	0.1	15.3	0.1	691.7	8.5
8C	30.4	7050.8	0.8	1.4	0.01	295.4	0.0	141.7	448.8	1.37	3894.8	3.5	42.3	10.7	1699.6	8.4
8D	32.3	7106.4	0.6	2.3	0.03	281.2	0.0	147.5	443.8	1.08	3919.3	3.4	43.8	10.1	1614.4	8.5
8E	25.6	7067.5	0.9	102.6	0.01	85.7	0.2	195.3	437.4	0.00	3931.9	0.1	49.4	0.1	1069.8	8.2

Table A.31: Concentration of main elements, oxygen, alkalinity, pH, temperature and electrical conductivity of the shallow groundwater samples.

		Sample ID							
		B1	B2	B3	B4	B5	B6	B7	B8
Concentration (mg/L)	DOC	9.5	17.9	9.4	10.4	9.1	16.7	12.2	9.9
	Chloride	2149.5	4734.2	69.4	69.7	75.5	41.3	1522.9	81.1
	Nitrate	1.1	1.9	0.0	0.5	0.7	0.0	0.0	0.3
	Sulfate	90.8	22.1	107.5	116.9	136.2	39.6	129.1	215.2
	Aluminum	0.004	0.003	0.001	0.001	0.001	0.001	0.002	0.001
	Calcium	420.0	284.2	197.9	203.4	206.9	210.5	441.3	246.5
	Iron	0.12	1.16	1.18	0.32	0.03	28.55	0.11	0.04
	Potassium	29.5	64.2	2.7	2.6	14.7	2.8	29.3	10.1
	Magnesium	91.5	275.1	13.7	13.8	32.8	17.0	86.1	20.2
	Manganese	2.0	1.6	0.7	0.5	0.7	1.7	1.3	1.5
	Sodium	986.4	2632.0	51.3	34.9	48.2	29.1	862.3	54.7
	Total P	0.5	2.1	0.0	0.0	0.4	0.0	0.6	0.3
	Ammonium	5.3	20.4	0.2	0.2	1.9	0.4	5.6	0.6
	Phosphate	1.1	7.0	0.2	0.1	1.2	0.1	2.0	0.7
	Oxygen	3.1	9.5	9.3	8.1	7.5	5.1	7.6	8.6
	Alkalinity as HCO_3	795.4	1287.1	555.1	518.5	640.5	664.9	793.0	522.2
	pH	7.0	7.7	7.1	7.0	7.1	7.0	6.9	7.3
	Temperature (^{0}C)	16.5	15.6	12.0	11.6	12.5	12.2	14.2	15.4
	EC (µS/cm)	6520.0	1502.0	-	1135.0	1300.0	1237.0	3880.0	1503.0
	Depth (m)	1.8	1.8	1.8	1.6	1.7	1.8	1.9	2.0

Table A.32: Concentration of main elements, oxygen, alkalinity, pH, temperature and electrical conductivity of the deep groundwater samples.

		Groundwater depth			
		60 m	46 m	25 m	9 m
Concentration (mg/L)	DOC	19.2	24.2	27.3	26.1
	Chloride	10006.0	7053.0	7814.8	5605.4
	Nitrate	0.0	0.0	0.0	0.0
	Sulfate	169.9	0.1	0.1	0.0
	Aluminum	0.008	0.002	0.022	0.066
	Calcium	263.3	146.0	182.7	209.4
	Iron	5.2	4.6	9.3	6.8
	Potassium	186.3	133.0	122.4	105.6
	Magnesium	616.3	352.2	373.6	332.4
	Manganese	0.2	0.2	1.1	1.0
	Sodium	5718.0	3971.0	4066.0	3152.5
	Total P	2.8	2.3	4.4	4.8
	Ammonium	29.2	25.3	23.7	26.2
	Phosphate	7.2	6.2	10.5	14.4
	Oxygen	0.1	0.1	0.1	0.1
	Alkalinity as HCO_3	1842.2	2135.0	2006.9	1671.4
	pH	7.4	7.5	7.4	7.6
	Temperature (^{0}C)	11.0	10.5	10.5	10.7
	EC (µS/cm)	26600	17600	16900	15800

Appendix III

Table A.33: Results of the SEDEX extraction for the sediment samples from 0.75 to 4 m depth. The numbers 1-8 represents the location of the borehole in the parcel, whereas the letters A-E stand for the depth of the sample.

	P fractions content (mg/g)					
Sample code	Exch-P	Fe-P	Ca-P	Detr-P	Org-P	Total P (mg/g)
1A	0.01	0.17	0.13	0.14	0.11	0.55
1B	0.01	0.05	0.07	0.14	0.02	0.29
1C	0.01	0.04	0.08	0.16	0.01	0.30
1D	0.01	0.04	0.05	0.15	0.01	0.26
1E	0.00	0.04	0.05	0.09	0.01	0.19
2A	0.00	0.06	0.08	0.15	0.02	0.31
2B	0.01	0.17	0.08	0.11	0.06	0.44
2C	0.00	0.04	0.05	0.13	0.00	0.24
2D	0.00	0.03	0.04	0.13	0.01	0.22
2E	0.00	0.04	0.06	0.11	0.00	0.21
3A	0.00	0.08	0.08	0.16	0.02	0.33
3B	0.00	0.05	0.05	0.14	0.01	0.25
3C	0.00	0.04	0.05	0.10	0.01	0.20
3D	0.00	0.04	0.05	0.10	0.01	0.20
3E	0.00	0.04	0.03	0.11	0.00	0.19
4A	0.00	0.06	0.09	0.12	0.02	0.28
4B	0.00	0.04	0.06	0.11	0.01	0.23
4C	0.00	0.04	0.06	0.11	0.01	0.22
4D	0.00	0.03	0.04	0.20	0.00	0.28
4E	0.00	0.04	0.04	0.17	0.00	0.25
5A	0.00	0.07	0.08	0.16	0.02	0.33
5B	0.00	0.04	0.07	0.14	0.01	0.25
5C	0.00	0.04	0.03	0.12	0.01	0.20
5D	0.00	0.03	0.04	0.18	0.00	0.26
5E	0.00	0.04	0.05	0.10	0.00	0.21
6A	0.00	0.09	0.07	0.16	0.01	0.34
6B	0.00	0.07	0.07	0.12	0.01	0.28
6C	0.01	0.04	0.05	0.14	0.01	0.25
6D	0.00	0.04	0.04	0.08	0.00	0.17
6E	0.00	0.04	0.04	0.08	0.00	0.16
7A	0.00	0.06	0.08	0.15	0.02	0.32
7B	0.00	0.06	0.08	0.15	0.02	0.31
7C	0.00	0.04	0.06	0.14	0.01	0.25
7D	0.00	0.04	0.06	0.13	0.01	0.24
7E	0.00	0.04	0.04	0.13	0.00	0.22
8A	0.01	0.13	0.10	0.15	0.02	0.41
8B	0.01	0.10	0.08	0.12	0.02	0.32
8C	0.01	0.04	0.09	0.12	0.01	0.28
8D	0.01	0.04	0.07	0.18	0.01	0.30
8E	0.00	0.04	0.05	0.10	0.00	0.20

Table A.34: Results of the SEDEX extraction for the shallow soil samples (SS), ditch and drain samples. The last two rows show the results of the duplicates.

	P fractions content (mg/g)					
Sample code	Exch-P	Fe-P	Ca-P	Detr-P	Org-P	Total P (mg/g)
SS - B1	0.04	0.43	0.20	0.12	0.16	0.94
SS - B2	0.04	0.48	0.15	0.11	0.17	0.95
SS - B3	0.04	0.53	0.15	0.11	0.18	1.00
SS - B4	0.03	0.46	0.13	0.12	0.18	0.93
SS - B5	0.03	0.50	0.18	0.12	0.17	1.00
SS - B6	0.04	0.58	0.14	0.12	0.17	1.04
SS - B7	0.05	0.55	0.18	0.13	0.18	1.10
SS - B8	0.05	0.53	0.19	0.13	0.17	1.07
Upper January	0.05	2.33	0.20	0.11	0.35	3.05
Down January	0.08	4.11	0.26	0.11	0.42	4.98
Upper February	0.08	3.38	0.25	0.10	0.44	4.26
Down February	0.13	5.44	0.27	0.10	0.46	6.41
Drain 2	0.07	27.26	0.53	0.06	0.45	28.38
Drain 4	0.03	22.33	0.34	0.03	0.52	23.25
Drain 7	0.01	16.34	0.28	0.03	0.47	17.13
Drain 10	0.03	21.15	0.20	0.05	0.27	21.69
7C (D)	0.00	0.02	0.05	0.12	0.01	0.20
Drain 7 (D)	0.01	16.53	0.28	0.03	0.44	17.29

Table A.35: Results of the Fe extraction for the sediment samples from 0.75 to 4 m depth. The numbers 1-8 represents the location of the borehole in the parcel, whereas the letters A-E stand for the depth of the sample.

	Fe fractions (mg/g)				
Sample code	Exch - Fe(II)	Exch - Fe(III)	Fe(II) - $FeCO_3$/FeS	Amorp - Fe oxides	Cryst - Fe oxides
1A	0.00	0.00	0.20	5.03	6.80
1B	0.00	0.00	0.82	0.02	0.56
1C	0.00	0.00	0.75	0.02	0.49
1D	0.00	0.00	0.70	0.03	0.42
1E	0.00	0.00	0.57	0.04	0.37
2A	0.00	0.00	0.32	3.00	1.26
2B	0.00	0.00	0.35	1.35	3.58
2C	0.00	0.00	0.51	0.03	0.33
2D	0.00	0.00	0.56	0.06	0.38
2E	0.00	0.00	0.49	0.03	0.27
3A	0.00	0.00	0.26	3.35	1.29
3B	0.00	0.00	0.57	1.24	0.57
3C	0.00	0.00	0.55	0.04	0.37
3D	0.00	0.00	0.50	0.03	0.32
3E	0.00	0.00	0.43	0.03	0.27
4A	0.00	0.00	0.28	3.07	0.83
4B	0.00	0.00	0.60	0.05	0.40
4C	0.00	0.00	0.55	0.04	0.36
4D	0.00	0.00	0.52	0.03	0.28
4E	0.00	0.00	0.41	0.03	0.24
5A	0.00	0.00	0.30	2.59	1.41
5B	0.00	0.00	0.56	0.04	0.40
5C	0.00	0.00	0.40	0.03	0.23
5D	0.00	0.00	0.49	0.03	0.26
5E	0.00	0.00	0.51	0.03	0.29
6A	0.00	0.00	0.28	2.58	1.51
6B	0.00	0.00	0.33	2.99	0.83
6C	0.00	0.00	0.59	0.03	0.38
6D	0.00	0.00	0.48	0.03	0.30
6E	0.00	0.00	0.50	0.05	0.33
7A	0.00	0.00	0.26	2.33	0.98
7B	0.00	0.00	0.30	3.12	0.80
7C	0.00	0.00	0.56	0.03	0.35
7D	0.00	0.00	0.59	0.03	0.34
7E	0.00	0.00	0.45	0.05	0.29
8A	0.00	0.00	0.31	2.38	1.94
8B	0.00	0.00	0.87	0.75	1.03
8C	0.00	0.00	0.81	0.01	0.47
8D	0.00	0.00	0.67	0.02	0.38
8E	0.00	0.00	0.49	0.03	0.30

Table A.36: Results of the Fe extraction for the shallow soil samples (SS), ditch and drain samples. The last two rows show the results of the duplicates.

	Fe fractions (mg/g)				
Sample code	Exch - Fe(II)	Exch - Fe(III)	Fe(II) - $FeCO_3$/FeS	Amorp - Fe oxides	Cryst - Fe oxides
SS - B1	0.00	0.00	0.20	5.81	8.96
SS - B2	0.00	0.00	0.19	6.02	8.93
SS - B3	0.00	0.00	0.19	5.97	9.28
SS - B4	0.00	0.00	0.19	5.63	9.68
SS - B5	0.00	0.00	0.22	5.58	9.66
SS - B6	0.00	0.00	0.18	5.56	8.90
SS - B7	0.00	0.00	0.21	5.20	8.58
SS - B8	0.00	0.00	0.24	5.19	8.25
Upper January	0.02	0.02	11.38	0.32	4.97
Down January	0.02	0.01	16.72	0.30	6.77
Upper February	0.04	0.01	15.09	0.70	7.60
Down February	0.08	0.02	16.70	2.98	8.76
Drain 2	0.00	0.00	3.67	97.39	12.76
Drain 4	0.00	0.00	4.95	156.82	8.76
Drain 7	0.00	0.00	6.02	175.47	7.90
Drain 10	0.00	0.00	5.66	144.71	5.91
7C (D)	0.00	0.00	0.53	0.08	0.35
Drain 7 (D)	0.00	0.00	5.99	174.86	7.50

Table A.37: The content of main elements obtained via Aqua regia for all the solid samples. The numbers 1-8 represents the location of the borehole in the parcel, whereas the letters A-E stand for the depth of the sample. The last six rows show the results of the duplicates.

	Element concentration (mg/L)											
Sample code	Al	As	Ca	Fe	K	Mg	Mn	Na	P	S	Si	Sr
1A	15.8	0.02	33.1	20.4	5.2	6.3	0.3	0.4	0.4	0.3	1.8	0.3
1B	7.9	0.00	44.8	8.5	3.1	4.3	0.2	1.2	0.3	3.6	2.0	3.6
1C	7.4	0.00	47.1	7.8	2.9	4.4	0.2	1.1	0.2	3.2	2.2	3.2
1D	7.0	0.00	44.4	7.5	2.7	4.1	0.2	1.0	0.2	2.8	2.2	2.8
1E	4.9	0.00	42.0	4.9	1.9	3.2	0.2	0.5	0.2	1.3	2.0	1.3
2A	9.3	0.00	43.0	10.3	3.3	4.6	0.2	0.3	0.3	0.2	2.0	0.2
2B	11.3	0.01	39.1	12.5	4.2	4.6	0.2	0.3	0.3	0.3	1.9	0.3
2C	4.8	0.00	38.9	5.0	1.8	3.4	0.2	0.4	0.2	1.6	1.9	1.6
2D	4.4	0.00	37.9	5.3	1.5	3.3	0.2	0.5	0.2	1.7	1.6	1.7
2E	3.6	0.00	37.0	4.0	1.3	2.9	0.1	0.4	0.1	1.0	1.4	1.0
3A	7.0	0.00	40.8	9.7	2.1	4.1	0.2	0.2	0.3	0.2	1.4	0.2
3B	5.9	0.00	42.2	7.8	1.9	3.7	0.2	0.2	0.2	0.9	1.4	0.9
3C	5.2	0.00	53.7	6.7	1.8	3.6	0.2	0.4	0.2	3.6	1.8	3.6
3D	5.9	0.00	41.9	5.7	2.1	3.6	0.2	0.6	0.2	1.9	2.4	1.9
3E	4.8	0.00	35.9	4.1	1.8	3.0	0.2	0.4	0.2	0.8	3.1	0.8
4A	8.9	0.00	40.5	10.2	3.3	4.2	0.2	0.2	0.2	0.2	1.8	0.2
4B	6.3	0.00	48.3	6.7	2.2	3.5	0.2	0.2	0.2	3.1	2.5	3.1
4C	6.1	0.00	42.3	6.4	2.2	3.6	0.2	0.3	0.2	2.7	2.5	2.7
4D	5.3	0.00	38.3	5.1	1.9	3.6	0.2	0.4	0.2	1.3	2.8	1.3
4E	4.4	0.00	35.6	4.6	1.4	3.1	0.2	0.4	0.2	1.1	1.7	1.1
5A	8.8	0.01	49.8	9.8	3.0	4.7	0.2	0.3	0.3	0.2	1.6	0.2
5B	6.4	0.00	47.9	7.0	2.3	3.8	0.2	0.2	0.2	2.8	2.1	2.8
5C	3.7	0.00	37.5	3.8	1.2	3.0	0.1	0.1	0.2	0.9	1.4	0.9
5D	5.6	0.00	41.2	5.3	2.0	3.7	0.2	0.4	0.2	1.4	2.5	1.4
5E	5.0	0.00	39.7	5.2	1.7	3.3	0.2	0.5	0.2	1.4	2.4	1.4
6A	8.7	0.01	45.4	10.0	2.7	4.5	0.2	0.2	0.3	0.1	1.9	0.1
6B	7.9	0.00	41.7	9.5	2.7	4.0	0.2	0.2	0.3	0.2	2.0	0.2
6C	7.1	0.00	44.2	7.1	2.5	3.8	0.2	0.4	0.2	3.1	2.8	3.1
6D	5.8	0.00	41.5	5.5	2.0	3.6	0.2	0.5	0.2	1.4	2.8	1.4
6E	5.5	0.00	38.7	5.2	1.9	3.4	0.2	0.5	0.2	1.3	2.7	1.3
7A	9.1	0.00	51.9	8.7	3.1	4.4	0.2	0.3	0.3	0.1	2.4	0.1
7B	8.7	0.00	43.5	10.3	2.8	4.3	0.2	0.2	0.3	0.3	2.2	0.3
7C	5.5	0.00	40.7	6.1	1.9	3.3	0.2	0.3	0.2	2.2	1.9	2.2
7D	7.1	0.00	45.0	7.1	2.5	4.1	0.2	0.9	0.2	2.7	2.3	2.7
7E	3.9	0.00	35.9	3.9	1.3	2.8	0.1	0.4	0.1	0.9	1.8	0.9
8A	10.8	0.01	49.1	11.0	3.8	5.0	0.2	0.3	0.4	0.2	2.0	0.2
8B	8.8	0.00	44.1	8.9	2.9	4.5	0.2	1.0	0.3	2.0	1.8	2.0
8C	8.7	0.00	47.2	9.1	3.2	4.5	0.2	1.2	0.3	4.2	2.1	4.2
8D	7.0	0.00	47.4	7.4	2.3	4.4	0.3	0.8	0.3	2.6	2.8	2.6
8E	5.1	0.00	41.8	4.6	1.9	2.9	0.2	0.5	0.1	1.2	3.5	1.2
SS1	26.2	0.03	23.8	28.1	9.0	7.1	0.4	0.5	0.8	0.5	2.3	0.5
SS2	26.7	0.03	16.4	27.8	8.8	6.3	0.4	0.5	0.8	0.6	2.3	0.6
SS3	27.9	0.03	13.4	30.6	9.3	6.5	0.5	0.5	0.9	0.5	2.0	0.5
SS4	25.9	0.03	15.1	30.1	8.0	6.5	0.3	0.4	0.8	0.6	2.0	0.6
SS5	29.1	0.03	15.3	29.8	10.0	6.7	0.3	0.5	0.8	0.6	1.0	0.6
SS6	28.4	0.03	12.1	29.2	9.6	6.3	0.4	0.5	0.9	0.6	2.3	0.6
SS7	22.8	0.02	17.8	27.4	7.1	6.4	0.4	0.4	1.0	0.6	2.0	0.6
SS8	22.1	0.02	20.3	24.0	7.5	6.0	0.4	0.4	0.9	0.6	0.8	0.6
Upper January	27.1	0.01	42.9	31.1	9.9	8.0	0.4	2.9	2.7	4.6	1.4	4.6
Down January	26.6	0.02	43.8	34.5	9.8	8.0	0.4	3.1	3.9	4.4	2.6	4.4
Upper February	30.1	0.01	39.4	35.1	11.4	8.7	0.4	3.9	3.5	4.6	1.4	4.6
Down February	30.1	0.02	39.0	44.4	11.4	9.0	0.5	4.1	5.6	4.3	1.2	4.3
Drain 2	30.4	0.44	41.5	167.4	10.2	7.2	1.1	1.7	24.4	1.7	1.9	1.7
Drain 4	21.9	0.34	42.0	254.4	7.0	5.1	0.9	2.8	20.0	2.0	1.2	2.0
Drain 7	19.8	0.27	39.1	292.7	6.1	4.9	0.5	4.0	14.8	1.8	3.3	1.8
Drain 10	17.8	0.35	51.2	246.1	6.0	6.1	0.5	5.3	21.1	1.4	2.7	1.4
3A (D)	9.9	0.00	43.7	10.0	3.2	4.4	0.2	0.2	0.3	0.1	4.5	0.1
5B (D)	7.0	0.00	50.3	6.8	2.4	3.8	0.2	0.3	0.2	2.7	3.5	2.7
6D (D)	6.1	0.00	43.1	5.3	2.2	3.4	0.2	0.5	0.2	1.3	4.6	1.3
7C (D)	7.1	0.00	42.8	6.4	2.5	3.5	0.2	0.3	0.2	2.2	5.1	2.2
8D (D)	8.8	0.00	48.5	8.2	3.0	4.5	0.2	1.0	0.3	3.1	3.1	3.1
Drain 7 (D)	20.0	0.26	37.7	288.6	6.2	4.7	0.4	3.9	14.6	1.8	2.8	1.8